UNIVERSITY OF SIENA
Department of Medical Biotechnologies

PhD Program in Medical Biotechnologies
Cycle XXXV

Design and development of a recombinant probiotic for the prevention of antibiotic-mediated dysbiosis

Supervisor:

Prof. Jean-Denis Docquier

PhD student:

Savannah R. Devente

Academic year 2021/2022

Savannah Rowane Devente
01.02.2023 23:24:09 GMT+01:00

Abstract

The human gut microbiota, consisting of a coherent mixture of commensal microorganisms, is responsible for a number of vital functions that aid in the support and protection of the human body. The disruption of the homeostasis of the microbiota, also known as dysbiosis, can therefore lead to extensive consequences, affecting the biology in the gut. Consequently, this can lead to or affect (long-lasting) metabolic, immunological, and developmental disorders, as well as infectious diseases. Although a multitude of factors may be involved in such diseases, research has supported the significant role of antibiotic use, and rather its consequences. The "collateral damage" caused by antibiotic administration has demonstrated its potential in permanently affecting the composition of the microbiota due to the antibiotic residues reaching the colon. We are therefore in urgent need of a solution that protects patients from the damage caused by antibiotic use and ensures the functionality of antibiotics themselves on the long-run. In this study, we evaluated the potential of an antibiotic degrading yeast probiotic with unique features that prevent the transfer of functional enzymes to the commensal flora. To this end, we created 25 different DNA constructs (44 different yeast strains) with five different antibiotic degrading enzymes. With *in vitro* and *ex vivo* data we demonstrate the potential of such a versatile biological system that may have clinical application as a life biotherapeutic product (LBP) in the prevention of antibiotic-mediated dysbiosis.

Contents

List of abbreviations

AAD	Antibiotic-associated diarrhea
AMP	Antimicrobial proteins
ATCC	American Type Culture Collection
CDI	*Clostridium difficile* infection
CAI	Codon adaptation index
CTX	Ceftriaxone
DC	Dendritic cell
DNA	Deoxyribonucleic Acid
DMSO	Dimethyl sulfoxide
EreB	Erythromycin esterase B
ER	Endoplasmic reticulum
ERY	Erythromycin
CDC	Centers for Disease Control and Prevention
GALT	Gut associated lymphoid tissues
HZn	HEPES supplemented with zinc
Ig	Immunoglobulin
IMP	Imipenem
IV	Intravenous
LBP	Life biotherapeutic product
MAMP	Microbe-associated molecular patterns
MBL	Metallo-β-lactamases
MCS	Multiple cloning site
MFE	RNA minimal folding energy
MHA	Müeller Hinton agar
MHB	Müeller Hinton broth
NCF	Nitrocefin
nt	Nucleotide(s)
PCR	Polymerase chain reaction
RF	Restriction free
rpm	Revolutions per minute
RT	Room temperature
SCFA	Short-chain fatty acids
S.b.	*Saccharomyces boulardii*
S.c.	*Saccharomyces cerevisiae*
Treg	Foxp3+ T regulatory
YPD	Yeast Extract–Peptone–Dextrose
WT	Wild-type

1. INTRODUCTION

1.1 The gut microbiota

1.1.1 Composition and dynamics of a healthy gut microbiota

The entire population of microorganisms that colonize a certain location is also known as the microbiota. The gastrointestinal tract, or gut, is one of these locations and gut commensals predominantly contribute in nutrient metabolism, drug metabolism, intestinal barrier function and the prevention of colonization of pathogenic microorganisms. The human gut is naturally colonized by microbes such as bacteria, fungi, archaea, viruses and protozoa (Sekirov *et al.*, 2010 and Jandhyala *et al.*, 2015). Microorganisms are generally perceived as pathogens and are, therefore, being eliminated by the host's immune system. In contrary to this perception, the majority of bacteria found in the gut are non-pathogenic and live in a symbiotic relationship with the intestinal absorptive cells, enterocytes (Jandhyala *et al.*, 2015). The human gut microbiota accounts for over 35,000 bacterial species and approximately 10^{13} bacterial cells.

The general profile of the healthy gut microbiota is dominated by the phyla Firmicutes and Bacteroidetes, followed by the Actinobacteria and Verrucomicrobia (Britton & Cani, 2018: Chapter 1). However, this profile may vary in diversity and number between individuals. Furthermore, the gut is a relatively large organ system and differences in number can already be observed depending on the location within the gut: *e.g.* the number of bacteria vary from 10^{1} per gram of contents in the esophagus and stomach to 10^{12} per gram of contents in the colon and distal gut (O'Hara & Shanahan, 2006 and Jandhyala *et al.*, 2015). Furthermore, pH levels and bacterial composition, largely defined by nutrient requirements of individual bacteria, also vary for each part of the gut and is further illustrated in Figure 1.1.1. Each part of the gut contributes to its three main functions, being transportation, digestion and absorption of food and therefore preserves a certain pH and bacterial composition to aid in those tasks. For example, the low pH of the stomach is essential for the digestion of many nutrients and for the inactivation of harmful viruses and bacteria (*e.g. Salmonella*) that cause enteric diseases.

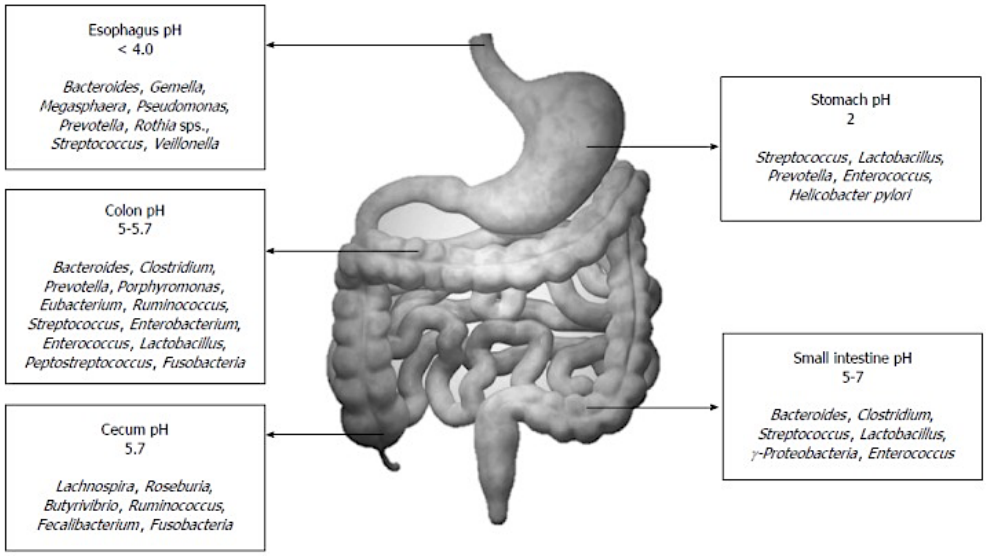

Figure 1.1.1: Distribution of pH and bacterial diversity in the healthy gut (Jandhyala et al., 2015).

Viruses are another group of prevalent microorganisms present in the microbiota. The gut virome was previously among the neglected components of the human microbiota and has now become more relevant thanks to new non-culture based metagenomic methods (Cao *et al*., 2022). The gut virome is mainly (90%) represented by intestinal bacteriophages, "viruses of bacteria" (Reyes *et al*., 2012). The virome has been described to play a critical role in the stability of other microorganisms in the gut as its composition was found to mimic the evolution of the bacterial microbiota of infants. In addition, gut viruses have been reported to be actively involved in the establishment, development and function of the human immune system. In turn, the gut bacteriome and host immunity may be responsible for the regulation of the composition and functionality of the gut virome (Cao *et al*., 2022).

1.1.2 Development of the microbiome and influencing factors

Research has suggested that the first human-microbial interaction occurs prenatal, although the effect and extent of this interaction remain to be elucidated. What is known, however, is that the first microbes that a child comes into contact with postpartum greatly influence the development of the child's microbiota. Hence the differences in microbiotas of children born vaginally or through Caesarean delivery: vaginally born infants are largely colonized with *Lactobacillus*, *Prevotella* and *Sneathia* species present in the vaginal microflora, whereas

Caesarean-born infants are mainly colonized with skin-associated microbes such as *Staphylococcus*, *Corynebacterium* and *Propionibacterium* species (Dominguez-Bello *et al*., 2010). Furthermore, during Caesarian delivery antibiotics are often administered which may also alter the composition of the newborn's microbiota. Postnatal antibiotic administration after vaginal delivery may, likewise, disrupt the microbiota irreversibly since recolonization with the vaginal microflora is unlikely. Caesarian-born infants have been additionally associated with a higher risk and frequency of infection with methicillin-resistant *Staphylococcus aureus* (MRSA), characterized by instability and low diversity of the microbiota and other long-term health problems (Centers for Disease Control and Prevention, CDC, 2006). In the early childhood, the microbiota continues to develop, resembling more that of an adult and acquiring 40-60% similarity with the adult microbiota by the age of three years (Yatsunenko *et al.*, 2012).

External factors such as breast milk, other foods, exposure to disease and the use of medications contribute to the diversification of the child's microbiome over time. For example, formula-fed infants are mainly colonized by Enterococcus, Enterobacteria, Bacteroides, Clostridia, and other anaerobic Streptococci, whereas breast-fed infants are predominantly colonized by *Bifidobacterium* and *Lactobacillus* that can easily breakdown the indigestible glycans in breast milk. Furthermore, undernutrition, especially in the early life years, may lead to devastating and long-lasting health effects that are linked to an underdeveloped microbiota. Later in life, diet continues to have a fundamental effect on the microbiota. Generally speaking, rich and diverse microbiotas are associated with diets including many fruits, vegetables and fibers. A high-calorie diet has been associated with a shift of Firmicutes/Bacteroidetes ratio in favor of Firmicutes (Jumpertz *et al*., 2011). David and colleagues (2014) even demonstrated that a four-day animal-based diet was enough to decrease the overall abundance of Firmicutes and increase that of bile-tolerant microbes in the phylum of Bacteroidetes and Proteobacteria.

1.1.3 Nutrient metabolism function

The necessary nutrients for the gut microbiota are mainly derived from carbohydrates from the host's diet. The carbohydrates that have not been digested by the gut and oligosaccharides that could not be digested are fermented by commensals residing in the colon, such as Bacteroides, Roseburia, Bifidobacterium, Fecalibacterium, and Enterobacteria. As a result, short-chain fatty acids (SCFA) like butyrate, propionate and acetate are synthesized and, in turn, provide rich

energy sources for the host (Macfarlane & Macfarlane, 2003). Furthermore, butyrate has the capability to hinder the accumulation of toxic metabolic by-products such as D-lactate through the expression of enzymes (Bourriaud *et al.*, 2002). Moreover, certain gut commensals (*e.g. Oxalobacter formigenes, Lactobacillus* species, and *Bifidobacterium* species) may reduce the risk of kidney stone formation by neutralizing oxylate that is synthesized in the intestine due to carbohydrate fermentation and bacterial metabolism (Sidhu *et al.*, 1998 & Magwira *et al.*, 2012). Lipid metabolism and lipid hydrolysis have also been reported to be positively affected by the gut microbiota through the promotion of lipoprotein lipase activity in fat cells and the increase of necessary enzyme for lipid digestion by *Bacteroides thetaiotaomicron*, respectively (Hooper *et al*., 2001). The collaboration between the human body and gut microbiota is further illustrated by the fact that proteins are metabolized via microbial proteinases and peptidases in combination with human proteinases. Furthermore, there are amino acid transporters on the bacterial cell wall that allow amino acids from the intestinal lumen to enter into bacteria, where amino acids are converted into small signaling molecules and antimicrobial peptides (bacteriocins). The conversion of L-histidine to histamine and glutamate to γ-amino butyric acid (GABA) are examples of such conversions (Jandhyala *et al.*, 2015). The gut microbiota has also been shown to be involved in the synthesis of vitamin K, several components of vitamin B and conjugated linoleic acid (CLA) of which the latter, facilitated by members of the Bacteroides genus, is known to be anti-diabetic, anti-atherogenic, anti-obesogenic, hypolipidemic and have immunomodulatory properties (Feitoza *et al.*, 2009, Devillard *et al.*, 2007 and Devillard *et al.*, 2009). Several gut commensals such as Bacteroides intestinalis also have the capability to convert primary bile acids into secondary bile acids deoxycholic and lithocolic acids in the colon (Fukiya *et al.*, 2009). Recently, the human gut microbiota has been found to also contribute in the breakdown of a variety of polyphenols (micronutrients containing multiple phenol groups) that are consumed in the diet. The secondary metabolites of polyphenols are found in a variety of plants, fruits and plant derived products (*e.g.* tea, cocoa and wine). Of these secondary metabolites, flavanoids and flavanoid sub-families are most frequently absorbed by the intestine. Furthermore, polyphenols, that usually remain inactive due to their bounded sugars, are transformed into active compounds after the removal of the sugar moiety by the gut microbiota, among other things (Marín *et al.*, 2015). Flavanones, found in citrus fruits and tomatoes are an example of polyphenols that are transformed by the Clostridium genus and *Eubacterium ramulus* (Jandhyala *et al.*, 2015).

1.1.4 Xenobiotic and drug metabolism function

The gut microbiota can use a variety of mechanisms to alter the disposition, efficacy and toxicity of xenobiotics and drugs (Carmody & Turnbaugh, 2014 and Klaassen & Cui, 2015): 1. Metabolic activation or inactivation of drugs by microbial enzymes (*e.g.* the conversion of sulfalazine, used to treat gut inflammation, to the pharmacologically active form, 5-amino 5-salicylic acid), 2. Sequestration of drugs by direct binding to the bacterial organism (*e.g.* the sequestration of L-DOPA, used in the treatment of Parkinson's disease and dopamine-responsive dystonia, by *Helicobacter pylori*), 3. Metabolic reactivation of drugs by microbial enzymes (*e.g.* the chemotherapeutic drug irinotecan or CPT-11 that is reactivated by bacterially expressed β-glucuronidase after having been metabolically inactivated in the liver (Wallace *et al.*, 2010), 4. The generation of microbiota-mediated metabolites that can act as metabolic intermediates (*e.g.* the toxicity of melanine is mainly due to its microbial formed metabolite, cyanuric acid), and 5. Direct competition of microbial and host metabolites of drugs for host enzymes (*e.g.* p-cresol and painkiller acetaminophen (paracetamol) both compete for SULT1A1). Furthermore, microbiota-mediated metabolic reactions that impact the biological activity of xenobiotics and drugs involve reduction, hydrolysis, dihydroxylation, acetylation, deacetylation, proteolysis, deconjugation, and deglycosylation processes (Sousa *et al.*, 2008 and Swanson, 2015). Broad-spectrum antibiotic chloramphenicol was one of the first drugs discovered to be a substrate of bacterial nitroreductases and thus far over 30 commonly prescribed drugs have been shown to be metabolically modified by the gut microbiota (Roldán *et al.*, 2008 and Swanson, 2015).

1.1.5 Prevention of pathogenic outgrowth function

One of the major challenges of the host's immune system is that it needs to be tolerant to the beneficial commensal microorganisms present the gut while serving its function to fight off invasive pathogens. A simple mechanism to ensure antimicrobial protection is through the presence of the two-levelled mucus layer. The mucus layer keeps luminal microbes from reaching the epithelium, predominantly in the large intestine (Jandhyala *et al.*, 2015). The inner layer of the mucus layer is denser than the outer layer and is free of organism. In contrary, the outer layer, which is more dynamic, contains organisms that feed of the provided glycans (Johansson *et al.*, 2011). Mucus is made up of different mucin glycoproteins that are secreted

by intestinal goblet cells. These cells maintain the barrier integrity by also producing factors such as trefoil-factor and the resistin-like molecule-β that can stabilize mucin polymers (Podolsky *et al.*, 1993). While the mucus layer plays an important role in the large intestine, this role is even more essential in the small intestine since its presence is scarcer here. In the small intestines, unwanted microbial protection is provided through the synthesis of antimicrobial proteins (AMPs, Jandhyala *et al.*, 2015). The synthesis of AMPs has been shown to be induced by the gut microbiota through its structural components and metabolites. An example of this is the synthesis of cathelicidins, C-type lectins, and (pro)defensins by small intestine epithelium Paneth cells though a mechanism mediated by pattern recognition receptors (PRRs, Salzman *et al.*, 2007). PRRs include the membrane associated toll-like receptors (TLR), C-type lectin receptors, and the cytosolic nucleotide-binding and oligomerisation domains like receptors. In turn, PRRs are activated by organism specific microbe-associated molecular patterns (MAMPs) such as bacterial cell wall peptidoglycan and lipopolysaccharides, lipid A, flagella, bacterial RNA/DNA and fungal cell wall β-glucans (Takeuchi & Akira, 2010 and Carvalho *et al.*, 2012). The cross-talk between PRR and MAMP results in the promotion of mucosal barrier function and the production of AMPs, mucin glycoproteins and immunoglobulin A (IgA). Furthermore, since Paneth cells are located in the crypts of the small intestinal, the concentration of AMPs is also highest over there. Despite the fact that a healthy gut microbiota is crucial for AMP production, *Bacteroides thetaiotaomicron* and *Lactobacillus innocua* have been identified as key contributors of this production (Cash *et al.*, 2006).

Commensal bacteria can also directly protect their niche through the production of antibacterial substances, *i.e.* bacteriocins. Bacteriocins are ribosomally synthesized proteinaceous toxins that specifically target members of the same or similar bacterial species (Kamada *et al*., 2013). The bacteriocin produced by *E. coli*, for example, directly inhibits the growth of the pathogenic enterohaemorrhagic *Escherichia coli* (EHEC). Human genome sequencing revealed the widespread occurrence of bacteriocins across the human gut microbiota. More specifically, Drissi and colleagues identified 175 bacteriocin-coding genes in *Firmicutes,* 79 in *Proteobacteria*, 34 in *Bacteroidetes*, and 25 in *Actinobacteria* (Drissi *et al*., 2015).

Another example of antimicrobial protection through gut microbiota-host interaction is the production of lactic acid by the Lactobacillus genus. As a result of lactic acid, the outer membrane of the bacterial cell wall gets disrupted, which allows the antimicrobial activity of

the host's lysozyme to be improved (Alakomi *et al*., 2005). The induction of local immunoglobulins is another mechanism of the gut microbiota, and especially Gram-negative organisms like Bacteroides, to prevent pathogenic outgrowth. The gut microbiota can activate intestinal dendritic cells, which in turn promotes the expression of secretory IgA. This IgA (especially sIgA2) is more resistant to bacterial degradation and can, therefore, provide a protective coat for the gut microbiota (He *et al*., 2007).

1.1.6 Immunomodulation function

Together with the innate and adaptive immune systems, the gut microbiota contributes to the changes in the body's immune system, *i.e.* immunomodulation. From the immune system, the major key players include the gut associated lymphoid tissues (GALT), effector and regulatory T lymphocytes (T cells), IgA producing B lymphocytes (B cells), Group 3 innate lymphoid cells, macrophages and dendritic cells (DCs). The involvement of the microbiota in the formation of a healthy GALT has been suggested based on the impaired development of the Peyer's patches and isolated lymphoid follicles with high levels of IgE^+ B cells, instead of the normally observed IgA^+ B cells (Durkin *et al*., 1981). Moreover, the induction of DCs to produce secretory IgA has been suggested to take place due to My-D88 signaling. My-D88, in turn, can be activated by the gut microbiota. Furthermore, IgA production can also occur due to the secretion of TGF-β, CXCL13, and B-cell activating protein (BAFF) by DCs that was stimulated by the gut microbiota (Suzuki *et al*., 2010). The gut microbiota has also been shown to be essential in the development and function of normal Foxp3+ T regulatory (Treg) cells essential in maintaining immune tolerance and homeostasis of the immune system. Accordingly, the involvement of gut-resident Treg cells is fundamental in suppressing effector T cell responses to the microbiota (Cosovanu & Neumann, 2020). Also, during post-natal development, both the abundance of a subpopulation of Tregs, RORγt+ pTreg cells, and uptake of luminal antigens, which is essential for the tolerance development of the immune system to gut bacteria, increase (Knoop *et al*., 2017). Furthermore, also the regulation of innate lymphoid cells and resident macrophages is likely regulated by gut microbes, either directly or indirectly (Jandhyala *et al.*, 2015).

1.1.7 Intestinal barrier function

A stable and healthy gut microbiota is not only necessary to ensure anti-microbial protection through the many microbial-mediated processes, but also to simply form a physical barrier against pathogens through competition. The gut commensals also promote pathogenic colonization resistance through the competition for resources, *i.e.* limited nutrient sources in the gut, as well as physical space (Pickard *et al.*, 2017). A so-called "nutrient niche" was already hypothesized in 1983, stating that "the populations of most indigenous intestinal bacteria are controlled by one or a few nutritional substrates which a given strain can utilize most efficiently" (Freter *et al.*, 1983). Subsequently, experiments have supported this hypothesis by illustrating the importance of nutritional substrates in the successful colonization of the gut for some bacteria. In *E. coli*, for example, the competitive balance between two almost identical strains changed due to the ability of one of the strains to utilize one sugar (Sweeney *et al.*, 1996). Other examples include intraspecies competition among Bacteroides due to a genetic locus likely related to host glycan utilization and the permanent rather than transient colonization of a probiotic strain of Bifidobacteria as a result of the presence of specific carbohydrate utilization genes (Lee *et al*., 2013 and Maldonado-Gómez *et al*., 2016). Gut commensals, especially the Bacteroides, carry a variety of genes able to digest complex carbohydrates (polysaccharides). This provides them with an important advantage since the host and other bacteria have no access to these polysaccharides (Pickard *et al*., 2017). Furthermore, sialic acid and fucose have been shown to be important sugars for the invasion of *Salmonella Typhimurium* and *Clostridioides difficile*. These sugars are provided by gut commensals such as Bacteroides species but were shown to only become available to pathogens after depletion of the bacteria that normally consume them by streptomycin (Ng *et al.*, 2013). That the availability of nutrients essentially decides the defense against pathogens is also demonstrated by the fact that in mice native Bacteroides species outcompete *Citrobacter rodentium* in the case of a diet low in polysaccharides but high in simple sugars. In contrary, it is native *E. coli* species and not Bacteroides species that successfully prevent the outgrowth of *C. rodentium* in a normal diet (Kamada *et al.*, 2012). In addition to nutrient-based niches, bacteria may also compete for physical space. Some species may prefer a habitat on the food matter in the lumen or in the outer mucus layer while others, although more uncommon, prefer the epithelial surface. Since close physical contact with the epithelium may be essential to certain pathogens (*e.g. C. rodentium*, some pathogenic *E. coli* and *S. Typhimurium*), physical competition for adhesion sites could prevent their infection or pathology. Another strategy of

gut commensals to prevent pathogenic adhesion is to change the presence of host adhesion sites, generally regarding glycan structures (Pickard *et al.*, 2017).

1.2 Dysbiosis

1.2.1 Dysbiosis in general

A functional microbiota is characterized by a stable microbiota. After a given disturbance or environmental stress, the healthy microbiota either (i) does not undergo a change in composition (resistance), (ii) restores the initial composition (resilience) or recovers the initial function despite compositional changes (functional redundancy) (Moya *et al.*, 2016). Functional redundancy is a very important phenomenon as it supports the theory that multiple species can be responsible for multiple functions, suggesting interchangeability of species in a functional microbiota. Here, the functionality of the gut depends on the metabolic profiles rather than microbial composition of the gut. Nevertheless, in certain situations, the effect of the disturbances on the gut microbiota can be so strong, leading to a dysbiotic state. Dysbiosis is referred to when the homeostasis of the microbiota is modified. Such a modification, or rather disruption, may lead to extensive consequences, affecting the collection of cells, genes and metabolites from the bacteria, eukaryotes and viruses inhabiting the host's body. A dysbiotic microbiome may not be capable to perform vital functions such as the ones described in the previous subchapter. Furthermore, dysbiosis of the microbiome has been associated with many health problems involving metabolic, immunological and developmental disorders, as well as susceptibility to infectious diseases. Although a wide variety of systems are involved in such diseases, research has suggested a significant impact of antibiotic use due to "collateral damage".

1.2.2 The impact of antibiotic use on the microbiota

Our control over microbial disease is diminishing due to the upcoming ineffectiveness of current antibiotics against (multi)drug-resistant pathogens, accountable for about 33,000 deaths and €1.5 billion in healthcare costs annually in Europe only (European commission). In addition, antibiotic use has been shown to significantly disrupt the ecology of the human

microbiome. Antibiotic-mediated dysbiosis takes place due to the antibiotic residues that reach the colon after each antibiotic administration. A great number of antibiotics have been shown to alter the microbiome of healthy individuals, short- and long-term. This alteration in microbial abundances usually occurs due to the depletion of one or several taxa (Table 1.2.2, Langdon *et al.*, 2016). It should be noted, however, that the effects of antibiotics on the microbial community are not easily predictable. The true impact of antibiotic use is most likely not translatable from *in vitro* studies on isolated strains alone, but rather depends on the phylogenic composition of the microbial community, including strains with different antibiotic susceptibility profiles. Moreover, other factors such as the varying antibiotic concentrations across the body, different microbial growth stages and protection due to endogenous production of resistance enzymes (discussed in Chapter 4.1), further complicates the prediction of antibiotic-mediated dysbiosis. Most of the observed shifts in microbiota composition last for some weeks or months and may depend on the body site (*i.e.* the restoration of microbial diversity in the throat and saliva occurs much quicker than that in the gut (Jakobsson *et al*., 2010 and Zaura *et al*., 2015). Moreover, even short-term use (seven days) of broad-spectrum antibiotics such as clindamycin was shown to last up to two years, associated with a persistent diversity of *Bacteroides* (Jernberg *et al*., 2007). Similarly, a triple therapy against *H. pylori* infection with clarithromycin resulted in a dramatic drop in *Actinobacteria* diversity and 1000-fold increase in the *ermB* resistance gene, which lasted for over four years in some patients while it recovered in others (Jakobsson *et al.*, 2010). Therefore, antibiotics not only alter phylogenetic composition of the microbiome, but may also stimulate the expression of antibiotic resistance, stress response and phage genes, and increase the overall level of mobile antibiotic resistance genes (Jernberg *et al*., 2007).

Table 1.2.2: Effect of common antibiotics on the host microbiome. The increase or decrease of microbial species is indicated by arrows. Adapted from Langdon et al., 2016.

Antibiotic	Class	Effect on microbiota
Amoxicillin	β-lactam	↓ enterobacteria
Ampicillin	β-lactam	↓ bacterial diversity, ↑ *Enterobacter spp*.
Cefotaxime	β-lactam (3rd generation cephalosporin)	↓ bacterial cell count, ↓ anaerobes, ↓ enterobacteria
Ciprofloxacin	Fluoroquinolone	↓ enterobacteria, ↓ bacterial diversity
Erythromycin	Macrolide	↓ Streptococci, enterococci and enterobacteria, ↑ staphylococci, alteration in abundance of anaerobes
Gentamicin	Aminoglycoside	↓ bacterial diversity, ↑ *Enterobacter spp*.
Streptomycin	Aminoglycoside	↓ bacterial diversity, ↑ Ruminococcaceae, ↑ Bacteroidaceae
Meropenem	Carbapenem	↓ enterobacteria, ↓ streptococci, ↓ *Bacteroides* spp., ↓ Gram-negative cocci
Tigecycline	Tetracycline	↓ enterococci, ↓ *E. coli*, ↓ lactobacilli, ↓ bifidobacteria, ↓ Bacteroidetes, ↑ other enterobacteria, ↑ yeasts, ↑ Proteobacteria
Vancomycin	Glycopeptide	↓ bacterial diversity

1.2.3. *Clostridioides difficile* infection

Many studies on antibiotic-mediated dysbiosis have focused on the susceptibility to *C. difficile* infection as it is a known side-effect that can occur from antibiotic administration. In the United states, a total of 223,900 estimated cases in hospitalized patients and 12,800 *C. difficile* deaths were reported in 2017 (CDC, 2019). *C. difficile* infections, which can lead to deadly diarrhea, most commonly occur in elder people (65 years and older) taking antibiotics and receiving medical care, people staying in hospitals and nursing homes for an extended time and people with a weakened immune system or people who were previously infected with the pathogen (CDC, 2019). Despite the high-dose and extended-duration treatment with multiple antibiotics, up to 65% of *C. difficile* infected patients relapse (Higa & Kelly, 2014). Moreover, a low-

diversity microbiota has been associated with the recurrence of *C. difficile*-associated diarrhea (Chang *et al.*, 2008). Specifically, clindamycin and tigecycline have been associated with decreased microbiome diversity and increased susceptibility to *C. difficile* infection (Buffie *et al*., 2012 and Bassis *et al*., 2014). It is also hypothesized that due to the disruption of interspecies interactions in a dysbiotic microbiota, the abundance of host-derived sialic acid is increased, allowing for the growth of pathogens such as *C. difficile* (Ng *et al*., 2013). High-throughput metabolomic studies showed that as a consequence of high concentrations of antibiotics, most products of bacterial metabolism are reduced or eliminated (*e.g.* SCFAs and secondary bile acids) and their precursors (*e.g.* oligosaccharides, sugar alcohols and primary bile acids) are increased (Theriot *et al*., 2014, Jump *et al*., 2014, Zhao *et al*., 2013, Yap *et al*., 2008 and Romick-Rosendale *et al*., 2009). Another metabolic route by which *C. difficile* can benefit from antibiotic use is through the depletion of the bile acid-hydroxylating activity of human gut microbiome *Clostridium scindens*, which is required for protection against *C. difficile* infection (Buffie *et al.*, 2015). A more obvious opportunity for *C. difficile* infection after antibiotic use is due to the failure of the microbiome to provide competitive exclusion, as a result of bacterial translocation out of the gut (Knoop *et al.*, 2015). Thus, the counterproductivity of broad-spectrum antibiotics should be considered when treating for antibiotic-resistant infections.

1.3 Prevention of antibiotic-induced dysbiosis and strategies currently in the drug development pipeline

1.3.1 Prevention of dysbiosis

It is clear by now that a dysbiotic microbiota can negatively impact an individual's health, either short-term or long-term and can even lead to deadly pathogenic outgrowth. Moreover, the disruption of the healthy microbiota may favor the expression of antibiotic resistant genes and the outgrowth of antibiotic-resistant organisms. Thus, the impact of dysbiosis prevention could be more significant and far-reaching than its possible treatment.

1.3.2 Microbial supplementation

An accepted custom during antibiotic treatment is the intake of fermented milk preparations. This has been especially recommended at the beginning of the antibiotic therapy in order to protect the microbiota (Andremont *et al.*, 2021). Furthermore, a specific supplementation was suggested to replace the bacteria that were eliminated during antibiotic therapy. This microbial supplementation is also known as 'probiotics', defined as "live microorganisms which when administered in adequate amounts confer a health benefit on the host" and includes yeasts or bacteria (Hill *et al*., 2014). With the latter, this especially includes lactic bacteria that are used as a probiotic (Wieërs *et al*., 2020). Another strategy rather focusses on promoting the growth of certain bacteria by supplementation with specific nutrients, also known as 'prebiotics' (Sanders *et al*., 2019). Many studies have discussed the clinical benefits of selected microorganisms, although limited scientific evidence was found to support these claims. Nevertheless, the supplementation of probiotics and pre-biotics remains significant to date (Suez *et al*., 2018 & Losurdo *et al*., 2015).

1.3.3. Protection of the microbiota against β-lactams: SYN-004 (ribaxamase) and DAV361

β-lactam antibiotics are an important class of antibiotics, representing 65% (from 2004-2014 in the United States) of all antibiotic prescriptions (Figure 1.3.3, Bush & Bradford, 2016). Hence, many rational based approaches for the prevention of dysbiosis have been focused on the protection of the intestinal microbiota from β-lactams. β-lactams all share a common chemical ring structure (β-lactam ring) that allows for their bactericidal action due to the interruption of the bacterial cell-wall formation. In turn, countless enzymes exist that are capable of hydrolyzing β-lactam rings and rendering these β-lactam antibiotics useless. Such enzymes, known as β-lactamases are produced by a variety of bacteria and are especially dangerous when secreted by pathogens such as *K. pneumoniae* and *E. coli*. Interestingly, Chachaty *et al*. (1992) found that patients with intestinal commensal β-lactamase-producing bacteria were less colonized by pathogenic bacteria such as *C. difficile* and presented no (measurable) antibiotics in their fecal material during treatment with cephalosporins.

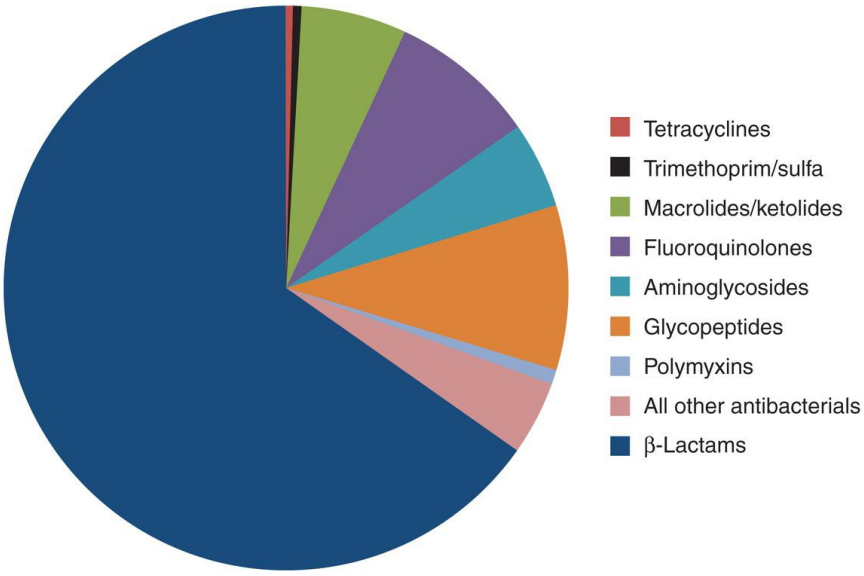

Figure 1.3.3: Diagram showing the proportion of injectable antibiotics in the United States by class for the years 2004-2014 with β-lactams, 65.24%; glycopeptides, 9%; fluoroquinolones, 8%; macrolides/ketolides, 6%; aminoglycosides, 5%; polymyxins, 1%; trimethoprim/sulfamethoxazole, 0.5%; tetracyclines (excluding tigecycline), 0.4%; all other antibiotics (including daptomycin, linezolid, and tigecycline), 4.21%. (Bush & Bradford, 2016).

The previously mentioned observation inspired a Finnish company, IPSAT, to use β-lactams as a strategy for the protection of the microbiota during antibiotic therapy. With a supplementation of an oral β-lactamase (P1A) during β-lactam treatment they aimed to inactivate the β-lactam residues in the colon before any microbiota alterations could take place. P1A is a recombinant β-lactamase produced by *Bacillus lichenformis* which hydrolyzes penicillins, including ampicillin and piperacillin. Moreover, to facilitate oral administration, the enzyme was synthesized by *Bacillus subtilis* and encapsulated in a gastro-resistant coating, allowing for the release of the protein in the intestine at a pH higher than 5.5. This approach has proven successful in Phase I and Phase II clinical studies by IPSAT with P1A and their successor Synthetic Biologics (U.S.) with P3A, a modified version of P1A (Tarkkanen *et al*., 2009, Pitout, 2009, Kokai-Kun *et al*., 2017 and Kokai-Kun *et al*., 2019). With P3A, also known as SYN-004 (or ribaxamase), Synthetic Biologics confirmed the possibility of dysbiosis prevention by preserving the microbiota and preventing the emergence of antibiotic resistance and *C. difficile* infections, all without affecting the therapeutic activity of intravenous penicillins and cephalosporins. The company is currently working on the development of a Phase III clinical trial and related products such as SYN-007, allowing for co-administration with oral β-lactams by delayed release formulation, and SYN-006, allowing for co-administration with carbapenems, are being developed.

Da Volterra, a French biotech company, has also been working on a β-lactamase enzyme for the prevention of dysbiosis during antibiotic treatment and especially the colonization with β-lactam resistant bacteria in intensive care unit patients. Their patented enzyme DAV361, however, was modified to achieve optimal stability and efficacy and provides protection against all (oral and IV) β-lactam antibiotics, including the last-resort carbapenem antibiotics (Da Volterra, 2022). DAV361 is currently in the research and development phase.

1.3.4 Protection of the microbiota against all types of antibiotics: DAV132

While the protection of the microbiota during β-lactam therapy is very promising, it may pose some limitations. For example, in real-life β-lactams are often co-administered with other types of antibiotics in order to achieve a synergistic effect or to prevent resistance-selection (Andremont *et al*., 2021). Thus, Da Volterra aimed for a broader approach that can inactivate all types of antibiotics during antibiotic treatment. Their specifically selected grade of adsorbent, DAV132, has been designed to protect the microbiota while leaving the effectiveness of the antibiotic therapy unaffected. More specifically, during antibiotic treatment a non-specific adsorbent gets released by DAV132 in the late ileum, cecum and colon which can irreversibly capture antibiotics before they can induce dysbiosis (Figure 1.3.4).

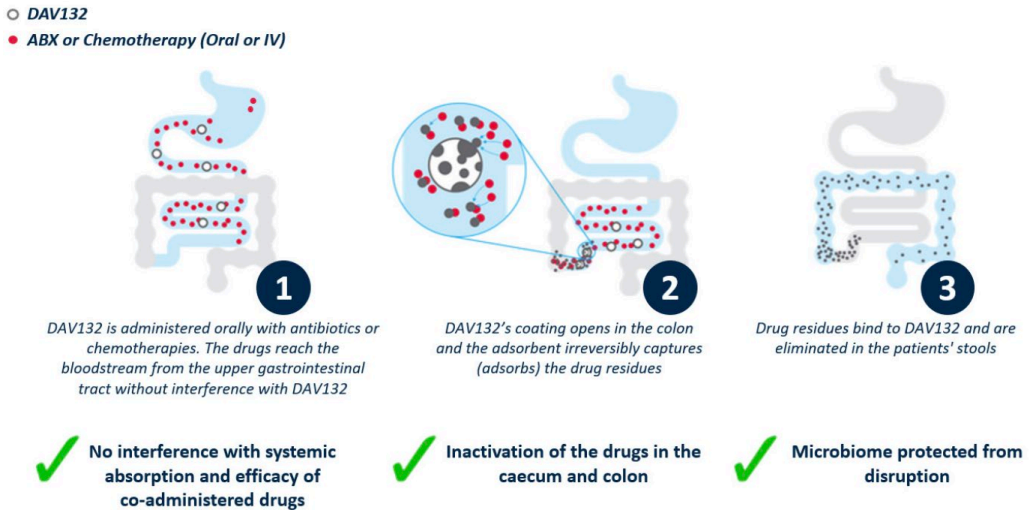

Figure 1.3.4: Description of the mode of action of the colon-targeted adsorbent, DAV132, in its prevention of antibiotic-induced disruption of the intestinal microbiome. ©2022 Da Volterra.

Mice studies have shown considerable reduction in *C. difficile*-associated mortality and gut colonization by resistant bacteria with DAV132 administration during antibiotic therapies (Burdet *et al.*, 2017, Burdet *et al*., 2018, Saint-Lu *et al*., 2019 and Grall *et al*., 2013). Furthermore, its safety has been confirmed in Phase I clinical studies, along with a 99% reduction in fecal antibiotic concentration and preservation of the intestinal microbiota diversity during oral moxifloxacin treatment (Pinquier *et al*., 2021 and De Gunzburg *et al.*, 2018). In addition, the positive results of DAV132 administration in hospitalized patients in Phase II trials emphasize its potential (Ducher *et al.*, 2020 and Vehreschild *et al*., 2022). Recently, DAV132 has also been suggested to increasing the life expectancy of cancer patients receiving immunotherapy by preventing the antibiotic-induced loss of responsiveness to PD-1 blockade cancer therapy (Da Volterra press release April 28, 2022). Currently, the multi-purpose use of DAV132 is further being investigated and Phase 3 studies are awaited.

2. AIM & OBJECTIVES

Modern medicine does not exist without antibiotics. After much delay, however, the negative collateral effects that are accompanied with antibiotic usage are finally being acknowledged. Not only may the disruption of the healthy microbiota impair its fundamental functions and further damage the host's health, it may also lead to antibiotic resistance selection. The usage of antibiotics therefore ought to be optimized in a way that it protects the patient during treatment and the effectiveness of antibiotics on the long run.

Two promising microbiota-protecting agents, SYN-004 and DAV132, are currently being developed for the purpose of preventing dysbiosis as a consequence of antibiotic therapy. While these products are heading towards Phase 3 clinical trials, they are still limited to a certain group of antibiotics (SYN-004) or non-specific inactivation of antibiotics (DAV132). Furthermore, these agents are currently accompanied by relatively high production costs due to high dosages and complicated manufacturing and formulation processes. We therefore aim for the development of a cost-effective delivery system for antibiotic-inactivation *in situ*.

By making use of the current advances in genetic engineering, we aim to develop a poly-functional and safe recombinant yeast probiotic, or life biotherapeutic product (LBP), with high levels of antibiotic-degrading capability to prevent antibiotic-associated dysbiosis. Probiotic yeasts, such as *S. cerevisiae* or *S. cerevisiae* var *boulardii*, are already considered as "GRAS" (generally recognized as safe) by the FDA and currently in use to treat acute diarrhea for example. In addition, we hypothesize that by artificially introducing (an) intron sequence(s) into the genes of antibiotic degrading enzymes, these enzymes can only be expressed by our LBP and not by bacteria in case of horizontal gene transfer to the gut commensals, thereby preventing the dissemination of functional resistance genes (containment). Antibiotic resistance enzymes (*e.g.* β-lactamases) are a potent group of naturally-occurring enzymes able to inactivate antibiotics. Their presence in pathogens have demonstrated their enzymatic potency when otherwise easy to treat infections can become life-threatening upon unresponsiveness to common or even late-generation antibiotics. Therefore, we suggest to fight nature with nature in order to protect the gut microbiota from dysbiosis during antibiotic treatment. To this end, we will:

I. Measure the endogenous β-lactamase production found in the healthy microbiota
II. Design a proof of concept (PoC) antibiotic-degrading system in yeast
III. Investigate the PoC system with different enzymes
IV. Investigate the activity of the engineered yeast probiotic in gut-like conditions

3. MATERIALS & METHODS

3.1 Growth media and reagents

The growth media used in this study were purchased from Oxoid (Basingstoke, Hampshire, UK), BD Bioscience (Becton, Dickinson and Company, Franklin Lakes, New Jersey, U.S.) or Difco (Detroit, Michigan, U.S.). Gelification of culture medium was obtained by the addition of agar to a final concentration of 1.7% (w/v) for bacterial growth media and 2% (w/v) for yeast growth media. Culture media was always autoclaved at 121 °C, pressure of 1 atm, for 20 minutes, unless otherwise specified. Furthermore, sterilized liquid medium or agar plates were supplemented by antibiotics from a 1000x stock of filter-sterilized ampicillin 100 mg/mL or kanamycin 50 mg/mL in water or chloramphenicol 80 mg/mL in 100% ethanol. Yeast YNB medium or plates, however, were supplemented with amino acids if necessary: 5 µL/mL of amino acid stocks containing 1% (w/v) of filter-sterilized leucine, histidine, lysine or tryptophan.

3.1.1 Luria-Bertani (LB) medium or Luria Broth

LB medium, originally named “Lysogeny Broth” by its inventor Giuseppe Bertani, is a rich medium commonly used to culture members of the *Enterobacteriaceae* (Bertani, 1951). It is extensively used in the field of molecular biology, allowing for the selection of cells containing a specific genetic element such as an antibiotic resistance cassette, when an antibiotic is added to the sterilized medium. LB is composed of tryptone 10 g/L, NaCl 10 g/L and yeast extract 5 g/L.

3.1.2 Müeller Hinton broth (II) and Müeller Hinton agar

Müeller Hinton broth (MHB) is recommended for antimicrobial susceptibility testing of common, rapidly growing aerobic and facultatively anaerobic bacteria by broth dilution procedures, as standardized by the Clinical and Laboratory Standard Institute (CLSI). In this study, MH agar plates and MHBII medium, cation-adjusted for calcium and magnesium ions, were used for *in vitro* susceptibility testing of *M. luteus* in the presence of erythromycin. MHA and MHBII were commercially obtained and have the following composition: beef infusion solids 2.0 g/L, casein hydrolysate, 17.5 g/L, starch 1.5 g/L and agar 17 g/L, pH 7.3 (MHA) and acid hydrolysate of casein 17.5 g/L, beef extract 3 g/L and starch 1.5 g/L, pH 7.3 (MHBII).

3.1.3 Super Optimal broth with Catabolite repression (SOC) medium

SOC medium is a nutrient-rich bacterial growth medium used in the final step of DNA transformation by electroporation. The medium is identical to SOB medium (tryptone 20 g/L, yeast extract 5 g/L and NaCl 0.5 g/L) with the addition of 1% (w/v) glucose and 20 mM $MgCl_2$.

3.1.4 BD DIFCO™ Antibiotic Medium 1

The DIFCO medium (BD) is a commercial medium suitable for the microbiological assay technique in order to determinate antibiotic potency. The medium was used in the meropenem diffusion assay and consists of: beef extract 1.5 g/L, yeast extract 3 g/L, pancreatic digest of casein 4 g/L, peptone 6 g/L, dextrose 1 g/L and agar 15 g/L.

3.1.5 P-0.5G

P-0.5G is a defined minimal medium used prior to auto-induction to grow high cell density cultures without (or little) induction of protein expression (Studier *et al*., 2015). The non-inducing medium is composed of 50 mM Na_2HPO_4, 50 mM KH_2PO4, 25 mM $(NH_4)_2SO_4$, 2 mM $MgSO_4$, 0.2x trace metals[1] and 0.5% (w/v) glucose. P-0.5G was used to prepare starter cultures that were stored at -80°C (1.5 mL + 0.15 mL 80% (v/v) glycerol), usable for a 1 L culture for protein expression.

3.1.6 ZYP-5052

ZYP-5052 is a rich medium for maximum auto-induced protein expression by the presence of α-lactose and is composed as follows: 1% (w/v) tryptone, 0.5% (w/v) yeast extract, 50 mM Na_2HPO_4, 50 mM KH_2PO4, 25 mM $(NH_4)_2SO_4$, 2 mM $MgSO_4$, 0.2x Trace metals and 0.5% (v/v) Glycerol, 0.05% (w/v) Glucose and 0.2% (w/v) Lactose (Studier *et al*., 2005).

[1] Trace metals are prepared as a 1000 x mix consisting of 50 mM $FeCl_3$, 20 mM $CaCl_2$, 10 mM each of $MnCl_2$ and $ZnSO_4$, and 2 mM each of $CoCl_2$, $CuCl_2$, $NiCl_2$, Na_2MoO4, Na_2SeO_3, and H_3BO_3 in 60 mM HCl.

3.1.7 Yeast Extract–Peptone–Dextrose (YPD)

YPD, or YEPD, is a complete liquid medium used to maintain yeast cell cultures. The medium is composed of yeast extract 10 g/L, bactopeptone 10 g/L, KH_2PO_4 3 g/L and 2% (w/v) D-glucose/dextrose (added after separate sterilization). Additionally, glucose can be replaced by 3% (v/v) glycerol for the selection of non-petite mutants *S. cerevisiae* cells and YPD can be buffered with 100 mM Tris-HCl.

3.1.8 Yeast nitrogen base (YNB)

YNB is a base medium for the preparation of minimal and synthetic defined medium containing nitrogen sources, vitamins, trace elements and salts. It lacks amino acids and therefore allows for selection of auxotrophic yeast strains. YNB was commercially purchased and is composed as follows: biotin 2 µg/L, calcium pantothenate 400 µg/L, folic acid 2 µg/L, inositol 2000 µg/L, niacin 400 µg/L, p-Aminobenzoic acid 200 µg/L, pyridoxine hydrochloride 400 µg/L, riboflavin 200 µg/L, thiamine hydrochloride 400 µg/L, boric acid 500 µg/L, copper sulfate 40 µg/L, potassium iodide 100 µg/L, ferric chloride 200 µg/L, manganese sulfate 400 µg/L, sodium molybdate 200 µg/L, zinc sulfate 400 µg/L, monopotassium phosphate 1 g/L, magnesium sulfate 0.5 g/L, sodium chloride 0.1 g/L and calcium chloride 0.1g/L.

3.1.9 *Ex vivo* medium from pig caecal extracts

Homogenized and pooled samples from the cecum of healthy pigs were provided by Da Volterra (MPS-AN-652) and stored at -80°C until further use. Aliquots were thawed on ice, transferred to a 50 mL Falcon tube by means of a spatula and for each gram of caecal material one mL of sterile milli-Q water was added. The 1:1 caecal mixture was then left to agitate horizontally for one hour at 30°C at 300 rpm. The medium was then clarified by two centrifugation steps: first 30 min at 30°C at 4000 × g, after which the supernatant was re-centrifuged for 40 min at 10°C at 77,000 × g. Finally, the caecal extract was filter-sterilized (0.2 µm) to obtain the clarified pig caecal extract that was stored at -80°C until further use.

3.2 Strains

Standard laboratory *Escherichia coli* strains were used for cloning purposes or DNA extraction (DH5α and XL-1 Blue) or protein expression (BL21(DE3)). *Micrococcus luteus* was used as an indicator strain for erythromycin susceptibility. Purified DNA was further propagated into yeast (*Saccharomyces cerevisiae* or *Saccharomyces cerevisiae* var b*oulardii*, abbreviated *S. boulardii*) to assess protein production.

3.2.1 *E. coli* DH5α

E. coli DH5α cells are the most frequently used *E. coli* strain for routine cloning applications. They have been engineered by biologist Douglas Hanahan (hence the 'DH' in DH5α) to maximize transformation efficiency and are defined by the three mutations recA1, endA1 and lacZΔM15.

3.2.2 *E. coli* XL-1 Blue

E. coli XL-1 Blue cells are also frequently used in cloning applications and allow for blue-white color screening of transformants. The strain is genotyped as follows: *recA1 endA1 gyrA96 thi-1 hsdR17 supE44 relA1 lac [F proAB lacIqZΔM15 Tn10 (Tetr)]*. These cells are commercially available from Agilent Technologies, Inc. (Santa Clara, California, U.S.)

3.2.3 *E. coli* BL21(DE3)

These *E. coli* cells are suitable for transformation and high-level protein expression with a T7 RNA polymerase-IPTG or auto-induction induction system. *E. coli* BL21(DE3) is genotyped as follows: *fhuA2 [lon] ompT gal (λ DE3) [dcm] ΔhsdS λ DE3 = λ sBamHIo ΔEcoRI-B int::(lacI::PlacUV5::T7 gene1) i21 Δnin5* and the cells are commercially available from Novagen Inc. (Madison, Wisconsin, U.S.)

3.2.4 *M. luteus* ATCC 9341

This environmental American Type Culture Collection (ATCC) strain, originally deposited as *Sarcina lutea* and currently reclassified as *Kocuria rhizophila*, has been designated as a quality-control strain in a number of *in vitro* susceptibility applications. The strain was used to assess

erythromycin activity by measuring the microbial growth inhibition zone on MHA plates and was kindly provided by Da Volterra.

3.2.5 *Bacillus subtilis* ATCC 6633

B. subtilis subsp. *Spizizenii* strain is often used for sterility testing and antibiotic assays.The strain was used to evaluate residual meropenem activity in the short-term colon (SHIME) study and was kindly provided by Da Volterra to ProDigest.

3.2.6 *S. cerevisiae* S150-2B

The S150-2B *S. cerevisiae* strain is a haploid yeast that has been well-described in literature for its use in recombinant protein expression (Mellor *et al*., 1985) and was assessed as potential probiotic yeast strain in our study. The strain is genotyped as follows: *MATa his3Δ-1 leu2-3/112 trp1-289 ura3-52 cir+ gal+*. The *S. cerevisiae* S150-2B strain was kindly provided by Dr. C. Galeotti.

3.2.7 *S. cerevisiae* INVSc1

S. cerevisiae INVSc1 is a fast-growing diploid yeast strain for protein expression. The strain is commercially available from Invitrogen Corportion (Waltham, Massachusetts, U.S.) and has the following genotype: *MATa his3D1 leu2 trp1-289 ura3-52 MAT his3D1 leu2 trp1-289 ura3-52*.

3.2.8 *S. boulardii* ura3^{-} M2

This ura3^{-} auxotrophic strain was created through UV radiation by the Anita Corbett lab from WT *S. boulardii* ATCC MYA-797 (Hudson *et al*., 2014). The Corbett lab kindly provided us the M2 strain described in Hudson *et al*. (2014).

3.3 Molecular methods

3.3.1 DNA extraction and estimation of DNA concentration

For standard cloning purposes, DNA was extracted from *E. coli* cells using the Wizard® Plus SV Minipreps DNA Purification System (Promega, Madison, Wisconsin, U.S.). When higher concentrations of DNA were required (*i.e.* for yeast transformation), we used the 'Preparation of Plasmid DNA by Alkaline Lysis with SDS: midi preparation' protocol from Sambrook and colleagues (Sambrook *et al*., 2006).

DNA extracts were qualified for purity and quantified for concentration using the RNA-DNA application of the Cary WinUV software with a Cary 100 UV-Vis spectrophotometer and quartz glass cuvettes (QS, Hellma, Jena, Germany).

3.3.2 Preparation and electroporation of competent *E. coli* cells

E. coli are naturally not competent and were made competent using the protocol described by Sambrook and colleagues (2006). A fresh culture of *E. coli* cells was grown until it reached the exponential phase (A_{600} = 0.5-0.7) after which the cells were left to rest on ice for 30 min. Cells were initially centrifugated at 4,000 × g for 10 min, after which the cell pellet was washed with an equal volume of 10% (v/v) glycerol. This wash step was repeated 3 times with half and one fifth of the original culture volume after centrifugation at 4,000 × g for 15 min at 4°C. The final pellet was resuspended in 1:500 of the original culture volume and 50 µL aliquots were stored at -80 °C until further usage.

An aliquot of electrocompetent cells was transformed with up to 5 µL of purified DNA (1-10 ng) or ligation mixture by transfering the *E. coli*-DNA mixture into a sterile electroporation cuvette (0.2 cm, Bio-Rad). Subsequently, an electric field of 2.5 keV was applied, through an electroporator (Gene Pulser Transfection Apparatus, Bio-Rad) for 20 seconds and cells were left to incubate with 800 - 1000 µL of SOC medium at 37 °C under agitation (200 rpm) for 1 hour. Finally, the cell pellet (6000 rpm for 4 min) was plated onto LB agar plates containing the necessary antibiotic for selection: kanamycin 50 µg/mL, ampicillin 100 µg/mL or chloramphenicol 80 µg/mL. Transformed clones were observed after overnight incubation at 37 °C.

3.3.3 Preparation and heat-shock of (frozen) competent yeast cells

Two transformation methods, heat-shock with lithium chloride (LiCl) or lithium acetate (LiAc), were used for the transformation of yeast. For chromosomal integration we used the LiCl method from freshly prepared competent cells and for episomal transformation we used either the LiCl method or the LiAc method on frozen competent cells.

Transformation with LiCl

We used the transformation method described by Ito *et al*. (1983). One colony of yeast cells was inoculated into 100 mL of YPD medium and incubated at 30°C at 180 rpm for at least 16 hours until an A_{640} = 0.5 was reached. In the case of overgrowth, the overnight culture was diluted to an A_{640} = 0.5 and left to incubate for an additional 30 min. The cell pellet (obtained by centrifugation at 1,100 × g for 7 min) was washed with 10 mL of ice-cold TE (Tris-EDTA; 10 mM Tris-HCl and 1 mM EDTA, pH = 8.0) and finally resuspended in 1.5 mL of 0.1 M LiCl in TE. The lithium-ions containing cells were then incubated on ice for 3-8 hours after which 200 µL of competent cells was used for each transformation. Cells were transformed with 5 (episomal replication) or 10 µg (linearized DNA for chromosomal integration) DNA. The cells-DNA mixture was left to incubate for 30 min at RT, after which 1.5 ml of 40% (w/v) PEG 4000 in 0.1 M LiCl was added to the cells and the cells were left to incbuate for another hour at RT. Heat shock was performed at 42°C for 20 min. Cells were then washed by first removing the PEG after brief centrifugation and subsequent washing with 2 ml of sterile Milli-Q water. Washed cells were then plated onto two selective medium agar plates per transformation and left to incubate for at least four days at 30°C.

Transformation with LiAc

Frozen competent cells for LiAc transformation were prepared by a combination of the protocol described by the Gottschling lab (Fred Hutchinson Cancer Research Center, available online), adapted from Gietz *et al*., (2007), and the protocol decribed by Hudson *et al*. (2016). 25 mL of YPD medium were inoculated with 1 yeast colony and left to incubate overnight at 30°C at 180 rpm. A new culture was inoculated in 250 ml of YPD to contain 5×10^6 cells/mL and incubated once more until a titer of $>2\times10^7$ cells/mL was reached (~4 hours). Cells were then harvested by centrifugation at 2,000 × g for 5 min and resuspended in 5 ml of frozen competent cell solution consisting of 5% (v/v) glycerol and 10% (v/v) good-quality Dimethyl

sulfoxide (DMSO). 50 µL aliquots were slowly frozen to -80°C using a layer of (styrofoom) packaging.

For the transformation, cells were briefly thawed on ice and washed (by brief centrifugation at 2000 rpm for 3 min) in 1 mL of sterile Milli-Q water and, subsequently, 1 ml of LiOAc 0.1 M in TE, twice. Cells were resuspended in 360 µL transformation mix prepared freshly (260 µL 50% PEG 4450 in 0.1M LiAc, 36 µL LiAc 1.0 M, 50 µL salmon sperm DNA 2 mg/mL and 14 µL DNA and water) and incubated at 30°C for 30 min. After incubation, 35 µL of DMSO were added and cells were heat-shocked at 42°C for ~25 min. Cells were then briefly centrifuged and left to incubate in 1 ml YPD medium at 30°C for 2-3 hours at 180 rpm. After incubation, cells were briefly centrifuged and plated onto two selective medium plates per transformation and left to incubate for at least four days at 30°C.

3.3.4 Agarose gel electrophoresis

The nucleic acid electrophoresis for the analysis of DNA products was visualized by running DNA with sample loading buffer (1:6 ratio, containing one part of 15% (w/v) Ficoll-400, 0.25% (w/v) bromophenol blue and 0.25% (w/v) Xylene cyanol) onto a 0.8-1% (w/v) agarose gel in TAE buffer (40 mM TRIS-acetate, 1 mM EDTA; pH 8,0) at a voltage of 95 V, followed by gelstaining with GelRed® Nucleic Acid Gel Stain (Biotium Corporate, Fremont, California, U.S.) according to the manufacturer's recommendations. A 1 Kb or 100 bp DNA ladder marker (Promega) was used as a standard for molecular weight.

3.3.5 Polyacrylamide gel electrophoresis and gel staining

Protein samples were run on NuPAGE™ 10% Bis-Tris Precast Gels (Invitrogen). Prior to gel loading, protein samples were denatured in NuPAGE™ LDS Sample Buffer (Invitrogen) at a 1:6 ratio by heating the mixture at 98 °C for 5 minutes. Gel electrophoresis was performed in NuPAGE® MES SDS Running Buffer (Invitrogen) at a constant voltage of 150 V for 45 minutes. Protein bands were visualized by means of Coomassie blue dye, according to the manufacturer's protocol (Biorad, Hercules, California, U.S.). A Broad-Range SDS-PAGE Standards protein ladder (Biorad) was used as a standard for molecular weight.

3.3.6 Colony PCR on transformed cells

Polymerase chain reaction (PCR) on the colonies of transformed bacterial cells was performed to verify correct DNA insertion and was performed by transferring some colony material (about half of a 1 mm sized colony), by means of a sterile wooden toothpick or sterile 10 µL pipette tip, to a PCR tube already containing the PCR mixture. PCR mixture (25 µL) and program with the Dreamtaq DNA polymerase (Thermo fisher scientific, Waltham, Massachusetts, U.S.) are reported in Table 3.3.6.1. Colony PCR on transformed yeast cells was performed using the same PCR program and reaction but with 0.4 µL of 'quick yeast extract' (and 10.9 µL water). The quick yeast extract was obtained by transferring about half the material of a 1-2 mm yeast colony to a PCR tube containing 20 µL 0.25% (w/v) SDS, vortexing for 10 sec and heating for 5 min at 90°C. The yeast extract was then centrifuged for 30 seconds and 0.4 µL of the supernatant was used for a 25 µL PCR reaction. Table 3.3.6.2 contains a list of the primers used for the screening of transformed colonies.

Table 3.3.6.1 PCR reaction and program used for colony PCR with the Dreamtay DNA polymerase.

PCR reaction (1x)	PCR program	
11.3 µL Milli-Q water	94 °C – 5 min	
5 µL dNTP (1.25 mM)	94 °C – 30 sec	30 x
3 µL primer 1 (10 µM)	*T_{ann} – 30 sec	
3 µL primer 2 (10 µM)	72 °C – 1 min 30 sec	
2.5 µL Dreamtaq buffer	72 °C – 5 min	
0.2 µL Dreamtaq	20 °C – ∞	
Total 25 µL		

* Calculated using the online Thermo fisher Tm calculator

Table 3.3.6.2 List of primers used for the screening of transformed clones by means of PCR or sequencing of extracted DNA.

Primer name	Primer sequence 5' – 3'	Primer purpose
T7 promoter	TAATACGACTCACTATAGGG	Primers outside of promoter and terminator region to screen for the presence of insert
TEF1-Pr-seq	CTTCTTGCTCATTAGAAAG	
tADH1_Rv	CCTACAGGAAAGAGTTACTC	
NdeI_K1_Fw	AGTAGCATATGAATATATTTTACATATTTTTGTTTTTGC	
T3	ATTAACCCTCACTAAAGG	
T3 new	ATTAACCCTCACTAAAGG	
URA3_YI_Rv	CGTTCCTTATATGTAGCTTTCGAC	
T3_YI_Rv	GTGAGGGTTAATTTCGAGCTTGGCG	
URA3_ext_Fw	ACGGTTCATCATCTCATGGATCTG	External primers of URA3 gene on the chromosome of *S. cerevisiae*
URA3_ext_Rv	AGCTTTGATGTTGTGAAGTCATTGAC	
HIS3_ext_Fw	CCTGATTCTTGATCTCCTTTAGC	External primers of HIS3 gene on the chromosome of *S. cerevisiae*
HIS3_ext_Rv	GTAACCACCACGACGGTTG	

3.3.7 Cloning of PCR fragments and restriction free (RF) cloning

PCR reactions for cloning purposes were performed using the Q5® High-Fidelity DNA Polymerase (New England Biolabs (NEB), Ipswich, Massachusetts, U.S., Table 3.3.7.1). If necessary, *Dpn*I enzyme was added directly to the PCR mixture after PCR. For all other digestions, the PCR product was purified using The Wizard® SV Gel and PCR Clean-Up kit (Promega). Table 3.3.7.2 contains a list of the different primers designed for cloning purposes.

Table 3.3.7.1: PCR reaction and program used for cloning purposes with the Q5® High-Fidelity DNA Polymerase.

PCR reaction (1x)	PCR program	
16.5 µL Milli-Q water		
8 µL dNTP (1.25 mM)	98 °C – 1 min	
5 µL primer 1 (10 µM)	98 °C – 8 sec	30 x
5 µL primer 2 (10 µM)	*T_{ann} – 20 sec	
10 µL Q5 buffer 5x	72 °C – 2-4 min	
0.5 µL Q5 DNA polymerase	72 °C – 2-10 min	
5 µL DNA (0.1-1 ng)	20 °C – ∞	
Total 50 µL		

* Calculated using the online NEB Tm calculator

Table 3.3.7.2 Overview of the primers designed in this study and their purpose. Color shading indicates relatedness to expressed protein with in grey non-specific primers, in green P3A, blue I8M, yellow BcII, purple EreB and orange OXA10L48.

Primer name	Primer sequence 5' – 3'	Primer purpose
BL1_into_YEpsec1_Fw	GTTCAAGGTACCCGGGGATCCAAGGACGACT TCGCTAAGTTG	RF-cloning to get yP3A-I gene into YEpsec1 plasmid
BL1_into_YEpsec1_Fw	TGCTATCATTTCCTTTGATATTGGATCATAAGCT TTTACTTACCGTTCATGTTCAAAGC	
K1-BL1_into_ pRG226PrTr_Fw	TAGCAATCTAATCTAAGTTTTAATTACAAGAATT CATGAATATATTTTACATATTTTTGTTTTTGCTG	RF-cloning to get BL1 with K1 signal peptide from YEpsec1 plasmid into pSRD-I plasmid
K1-BL1_into_ pRG226PrTr_Rv	ATAAAAATCATAAATCATAAGAAATTCGCAAG CTTTTACTTACCGTTCATGTTCAAAGC	
BL1_NdeI-BamHI_Fw	GGGAATTCCATATGAAGGACGACTTCGCTAAG	Addition of *Nde*I (5') and *Bam*HI (3') restriction sites to yP3A-I gene to allow for cloning into pET9 plasmid
BL1_NdeI-BamHI_Rv	CCAGGATCCTTACTTACCGTTCATGTTCAAAGC	
α-factor-BL1_Fw	GAAAGCATAGCAATCTAATCTAAGTTTTAATTA CAAGAATTC	RF-cloning to replace K1 signal peptide with α-factor
α-factor-BL1_Rv	TCTTCCAACTTAGCGAAGTCGTCCTTCAGAG CTTCAGCCTCTCTTT	
BL2 alone_Fw	ATCGAATTCATGAAGGATGATTTTGCTAAGTTGG	RF-cloning to remove α-factor from αf-yP3A-II synthetic gene into pSRD-I
BL2 alone_Rv	CATGAATTCTTGTAATTAAAACTTAGATTAG	
No2uOri_Fw	AAAGCTAGCACTCTGGCGCGCCACTAC	Replacement of 2 micron with *Nhe*I sites for recirculation of plasmid without 2 micron ori; YIp constructs
No2uOri_Rv	TTTGCTAGCCAGGTGGCACTTTTCGGG	
BamHI-BL2_Fw	ATAGGATCCAAGGATGATTTTGCTAAGTTG	Replacement of yP3A-I with yP3A-II after K1 signal peptide
P3A_EcoRI-HindIII_Fw	TTCTAGAATTCATGAAAGATGATTTTGCAAAACTTG	Addition of *Eco*RI (5') and *Hind*III (3') restriction sites to bP3A gene for cloning from pET9 into pRG226 plasmid
P3A_EcoRI-HindIII_Rv	CCCAAGCTTATTTGCCGTTCATGTTTAAGG	

BL1 (84-103)_Fw	TGTTGCTTACAGACCAGACG	Primers outside of PRE3 intron, inside of yP3A-I gene, for RF-subcloning of PRE3 intron into K1-yP3A-I
BL1 (372-391)_Rv	GGTTAGTAACTTCGTCACCG	
NdeI_I8M_Fw	AGTAGCATATGGACTCTTCTGGTGAATACCCAAC	Addition of *Nde*I (5') and *Bam*HI (3') restriction sites to yI8M-I gene to allow for cloning into pET9 plasmid
BamHI_I8M_Rv	TAGGGATCCTTAGTTAGTGTGAGCCTTAACAACG	
NdeI_BcII_Fw	CGTAGCATATGAGCCAAAAGGTTGAGAAAACTG	" " yBcII
BamHI_BcII_Rv	CACGGATCCTCATTTCAATAAATCCAAAGTATGC	
NdeI_EreB-I_Fw	AGTAGCATATGAGATTCGAAGAATGGGTTAAGG	" " yEreB-I
NdeI_EreB-I_Rv	GTGGGATCCTTATTCGTAAACAACTTCAGAAACAG	
NdeI_OXA10L48_Fw	AGTAGCATATGGGTTCTATCACTGAAAACACTTC	" " yOXA10L48
BamHI_OXA10L48_Rv	TAGGGATCCTCAACCACCGATGATACCTTC	

3.4 Culture preparation, extraction methods and activity determination

3.4.1 Preparation of bacterial cultures for activity assessment

Protein production in *E. coli was* evaluated using the auto-induction method as described by Studier *et al.* (2005). Briefly, cell growth (37°C, 200 rpm) was saturated without production in a so-called starter medium after inoculating a colony from plate into 10 mL of P-0.5G medium. After 24 hours of growth, 1.5 mL of starter culture was used to inoculate one liter of rich induction medium, ZYP5052. Kanamycin (50 µg/mL) was always included in all cultures to allow for growth selection. Production was measured after 18-24 of growth in the lysed cells or culture supernatant.

3.4.2 Preparation of yeast cultures for activity assessment

For reproducibility of our data, yeast cultures were inoculated at a precise cell density, based on the optical density of a concentrated pre-culture or cell suspension, measured at 640 nm.

During initial studies with *S. cerevisiae* and the PoC enzyme, the cultures were inoculated from a pre-culture in which a single colony was grown to high cell density at 30°C in selective medium and stored at RT. The pre-culture was then diluted accordingly in fresh culture medium to $A_{640} = 0.01$ (selective medium) or 0.001 (rich medium). In further studies with other enzymes and with *S. boulardii*, a cell suspension was prepared from freshly grown colonies on plate (selective medium) and diluted accordingly for inoculation. Unless indicated otherwise, yeast cultures were always grown at 25-37°C, in a medium-to-flask ratio of 1:5 -1:10, and with an agitation speed of 180 or 200 rpm. Protein production was measured after 16–48 hours of growth.

3.4.3 Lysis of bacterial cells

Transformed *E. coli* BL21(DE3) cells were lysed to assess cytoplasmic protein production with the pET9a vector. Cell disruption was either performed by physical lysis (for EreB constructs) or chemical lysis (for the β-lactamase constructs). Physical lysis was performed by sonication (4 cycles, 30 s each, U50 Control ultrasonicator, IKA Labortechnik) of the pellet of a 1 mL culture, resuspended in 250 µL of HZn buffer (50 mM (2-hydroxyethyl)-1-piperazineethanesulfonic acid (HEPES) buffer, pH 7.5, supplemented with 50 µM $ZnSO_4$). Chemical lysis was performed using FastBreak™ Cell Lysis Reagent (Promega), according to the manufacturer's protocol in HZn buffer.

3.4.4 Lysis of yeast cells

To assess cytoplasmic protein production, yeast cells were lysed either physically by means of glass beads or chemically with CelLytic™ Y Cell Lysis Reagent (Sigma-Aldrich, St. Louis, Missouri, U.S.). Cell extract preparation by means of glassbeads was performed as follows: 2-5 mL of yeast culture was centrifuged at 3000 rpm for 5 min. The pellet was frozen at -20°C for at least one hour to facilitate lysis. After thawing, the pellet was washed with 1 mL of Milli-Q water and centrifuged at 15,000 × g for 30 sec. To each pellet, we then added 200 µL (measured with a 1.5 mL Eppendorf) glass beads (425-600 µm dia.), 200 µL lysis solution (150 mM KCl, 20 mM Tris-HCl pH 8, 1 mM EDTA, 1 mM DTT added freshly from an aliquot stored at -20°C, 0.2% (w/v) Triton X-100 and 0.2% (w/w) SDS) and 2 µL protease inhibitor (cOmplete™ Protease Inhibitor Cocktail, Roche, Basel, Switzerland). Cells were then subjected to four cycles of 30 sec vortexing and 30 sec on ice, after which the supernatant

(6000 rpm for 1 min) was transferred to a new Eppendorf tube. Glassbeads were then washed with another 200 µL of lysis solution by brief vortexing and subsequent centrifugation. The supernatant of the washed glassbeads was united with the previous supernatant and centrifuged once more at 6000 rpm for 1 min at 4°C and the final supernatant was transferred to a fresh Eppendorf tube and kept on ice for analysis.

Chemical lysis with CelLytic™ Y Cell Lysis Reagent was performed according the manufacturer's protocol with 5 mM DTT and 5 mL CelLytic™ Y Cell Lysis Reagent per gram of yeast cell pellet.

3.4.5 Extraction of frozen stool samples for β-lactamase determination

Frozen feces samples (stored at - 80°C) were thawed on ice for 20 min, where after 100 - 300 mg of feces material was collected in a 2-mL Eppendorf tube. Ice-cold HZn buffer was then added to the feces material at a concentration of 5 mL/g feces. Samples were briefly mixed by means of vortexing and incubated horizontally for 1 hour under agitation (400 rpm). Samples were clarified by two centrifugation steps of 15 minutes and 30 minutes at 4 °C, respectively, in which the supernatant was transferred to a new 1.5-mL Eppendorf tube. Each sample was measured (3-20 µL) in triplicate and in certain cases was also extracted up to three times (DAV-132-CL-1006). All assays always included at least a buffer control to assess substrate stability and, additionally, a positive control (TEM-1 β-lactamase purified and produced in our laboratory; qualified batch no. SIP-T1-310717/1).

3.4.6 Determination of kinetic parameters

Enzymes were previously purified in our laboratory and stored at -20°C. Kinetic parameters were determined by following substrate hydrolysis at different concentrations by the enzymes at 30°C using a Cary 100 UV-Vis spectrophotometer (Varian Instruments, Walnut Creek, CA, U.S.), in a in a total reaction volume of 500 µL, as described by Docquier and colleagues (Docquier *et al*., 2003). Assays were performed in HEPES buffer pH 7.5 (buffer H, serine β-lactamases) or buffer HZn (metallo- β-lactamase enzymes) and enzymes were prepared in the reaction buffer supplemented with 20 µg/mL bovine serum albumin (BSA, Pierce™ Bovine Serum Albumin, Thermo Scientific). The final enzyme concentration was 85 nM for P3A and ranged from 31 to 66 nM for MBL I8M and 2.4 to 4.8 nM for MBL BcII. Steady-state kinetic

parameters (K_m and k_{cat}) were determined under initial-rate conditions using the Hanes–Woolf plot.

3.4.7 Spectrophotometric determination of β-lactamase activity

Assays were performed in buffer H or buffer HZn using 5-20 µL of freshly clarified feces sample. Reactions were carried out in a final volume of 200 µL (96-well plate) or 500 µL (1-cm cuvette) with 100 µM nitrocefin (NCF), 1 mM ampicillin (AMP) or 150 µM imipenem (IMP) at a wavelength of 482 nm, 235 nm or 300 nm, respectively. Substrate concentration was calculated with the Beer-Lambert law. Activity was either expressed in nmol substrate hydrolyzed per minute per gram of feces (nmol/min·g) in the endogenous β-lactamase production studies or mg of enzyme per liter of culture (mg/L), per A_{640} = 1 (mg/A_{640}) or per billion yeast cells (mg/10^9) in the LBP activity assays, calculated from first order kinetic data using the Henri-Michaelis-Menten equation described below and known parameters (Tables 3.4.7.1 and 3.4.7.2).

Beer-Lambert law

$$c = \frac{A}{\varepsilon \cdot l}$$

c is the concentration in
A is the absorbance
ε is the molar absorptivity in
l is the optical path length in cm

Henri-Michaellis-Menten equation

$$[E_0] = \frac{V_0 \cdot (k_M + [S])}{k_{cat} \cdot [S]}$$

E_0 is initial enzyme concentration
V_0 is initial velocity of reaction
$[S]$ is the substrate concentration in
k_{cat} is the first-order rate constant

Table 3.4.7.1: Spectral properties of β-lactams used in this study.

Substrate	λ (nm)	ε_M ($M^{-1}\cdot cm^{-1}$)	$\Delta\varepsilon_M$ ($M^{-1}\cdot cm^{-1}$)
NCF	$386^{Substrate}$ $482^{Product}$	17500	+15000
AMP	235	1860	-820
IMP	300	9000	-9000

Table 3.4.7.2: Steady-state kinetic parameters of β-lactams used in this study.

Enzyme	Mw (g/mol)	K_M (μM)	k_{cat} (s^{-1})
P3A	29143	48^{NCF} 176^{AMP}	159^{NCF} 1345^{AMP}
I8M	24972	15^{NCF} 12^{IMP}	344^{NCF} 198^{IMP}
BcII	24960	27^{NCF} 217^{IMP}	16^{NCF} 116^{IMP}

3.4.8 Determination of total protein concentration

Total protein concentration in yeast cultures was estimated using the Bradford assay (Bradford, 1976). Samples were diluted in deionized water to a volume of 800 μL and resuspended with 200 μL Bradford reagent (Bio-rad, Hercules, California, U.S.). Absorbance between 0.06 and 0.6 was recorded at 595 nm.

3.4.9 Erythromycin diffusion assay for evaluation of EreB activity

The antibiotic diffusion assay was performed to assess the erythromycin-inactivating activity produced by transformed yeast cells. Erythromycin (0.3 mg/mL) was incubated 1:5 with yeast sample (culture supernatant or lysed cells) at 37°C. Residual presence of active erythromycin after incubation was determined by spotting the incubation mixtures onto a 60 mL MHA plate containing the erythromycin-sensitive *M. luteus* ATCC 9341 as an indicator strain. Inhibition diameters were measured after 18-20 hours growth at 37°C.

3.4.10 Meropenem diffusion assay for β-lactamase estimation in reactor

The meropenem diffusion assay was performed to assess the degradation of meropenem in the reactor due to protein production by transformed yeast strains. Reactor samples were spotted (20 μL) onto a DIFCO agar plate containing *B. subtilis* ATCC 6633 (approximately 2×10^8 CFU/mL). On the same plate, four known meropenem concentrations (0.625, 1.25, 5 and 10 μg/mL) were included in the assay in order to estimate the residual meropenem concentration. Each sample was spotted in triplicate and *B. subtilis* growth at 37°C was evaluated after 18-20 hours.

4. RESULTS & DISCUSSION

4.1 Endogenous fecal β-lactamase activity

4.1.1 Background

Antibiotic-mediated dysbiosis is a complex process that involves many factors. One of the factors that make dysbiosis difficult to predict is the production of β-lactamases by naturally occurring bacteria in the gut (or resident anaerobes), such as members of the genus *Bacteroides*, sometimes also referred to as 'the gut resistome' (Léonard *et al*., 1989, Stiefel *et al*., 2015 and Van Schaik, 2015).

The presence of β-lactam hydrolyzing activity in the healthy population is something that was also observed first-hand in our laboratory. Previous involvement in two independent clinical studies, CEREMI (ClinicalTrials.gov Identifier: NCT02659033) and DAV-132-CL-1006, regarding the microbiota and antibiotic treatment provided our laboratory access to homogenized human fecal samples (collected between 2016-2020, and stored at -80 °C) from healthy[2] subjects, originating from France. These samples were subjected to an extraction procedure (see Materials & Methods section) and analyzed for hydrolyzing activity with relevant substrates. The chromogenic cephalosporin nitrocefin was used as a first substrate for its broad-spectrum, sensitive and rapid detection and dosing of β-lactamases (O'Callaghan *et al.*, 1972). Avibactam and ethylenediaminetetraacetic acid (EDTA) were used as inhibitors of serine β-lactamases and metallo-β-lactamases, respectively (Ehmann *et al.*, 2013 and Hernandez Valladares *et al.*, 1997). For a more specific identification of the β-lactamase activity present in the samples, imipenem (carbapenem) and cefotaxime (third-generation cephalosporin) were, additionally, used as substrates (CEREMI only). Specific β-lactamase activity was calculated based on the hydrolysis rate of the substrate in the presence of fecal extract.

4.1.2 Work

Both studies included homogenized fecal samples of healthy subjects one day prior to antibiotic exposure. CEREMI included 22 fecal samples and DAV-132-CL-1006 132. In both studies,

[2] Including clinically examined adults with no disease or current treatment and that did not receive antibiotics in the last six months and were not hospitalized in the last 12 months.

samples were extracted using the same protocol. The activity data from CEREMI was measured in duplicate and inhibition was measured after 20 min incubation with EDTA, avibactam or buffer (baseline value). The activity data from DAV-132-CL-1006, however, is expressed as a mean value of two independent extractions, measured in triplicate. Specific activity was expressed in nmol substrate hydrolyzed per min per gram of feces and the cut-off minimal values for hydrolysis activity, based on substrate stability in buffer, were set as follows: 4.8 nmol/min·g for nitrocefin (NCF), 11.7 nmol/min·g for imipenem (IMP) and 3.4 nmol/min·g for cefotaxime (CTX) in CEREMI and 3.4 nmol/min·g nitrocefin (NCF) for DAV-132-CL-1006. It should be noted that the lower detection limit for nitrocefin hydrolysis in DAV-132-CL-1006 compared to CERMI is due to the higher number of replicates. Furthermore, inhibition values below 10% were considered not significant. The activity data of CEREMI are represented in Table 4.1.2 and those of DAV-132-CL-1006 in Figure 4.1.2.

Table 4.1.2: Overview of substrate hydrolyzing activity in fecal extracts of samples collected one day prior to antibiotic exposure in CEREMI with nitrocefin (NCF), imipenem (IMP) and cefotaxime (CTX).

Subject ID	NCF spec act (nmol/min·g)	% inh. Avibactam	% inh. EDTA	IMP spec act (nmol/min·g)	CTX spec act (nmol/min·g)
1	24.5	100.0	No inhibition	N.S.[a]	4.7
2	49.6	99.7	No inhibition	N.S.	3.9
3	N.S.	N.A.[b]	N.A.	N.S.	N.S.
6	12.0	100.0	No inhibition	N.S.	N.S.
8	59.8	100.0	No inhibition	N.S.	4.3
9	7.1	67.9	No inhibition	N.S.	N.S.
11	16.3	78.4	No inhibition	N.S.	4.1
12	4.8	100.0	No inhibition	N.S.	N.S.
13	7.2	100.0	No inhibition	N.S.	N.S.
14	40.5	100.0	2.2	N.S.	4.8
16	N.S.	N.A.	N.A.	N.S.	N.S.
17	9.9	86.9	2.3	N.S.	N.S.
18	19.7	93.2	9.0	N.S.	4.0
20	106.7	100.0	No inhibition	N.S.	5.6
22	N.S.	N.A.	N.A.	N.S.	N.S.
23	442.8	100.0	No inhibition	N.S.	5.9
24	44.4	96.7	3.5	N.S.	5.4
25	17.3	90.4	1.1	N.S.	3.7
27	13.1	93.3	No inhibition	N.S.	N.S.
28	N.S.	N.A.	N.A.	N.S.	N.S.
29	12.5	98.8	No inhibition	N.S.	N.S.
34	33.1	100.0	No inhibition	N.S.	N.S.

[a] Not significant, < 4.8 nmol/min·g
[b] Not applicable

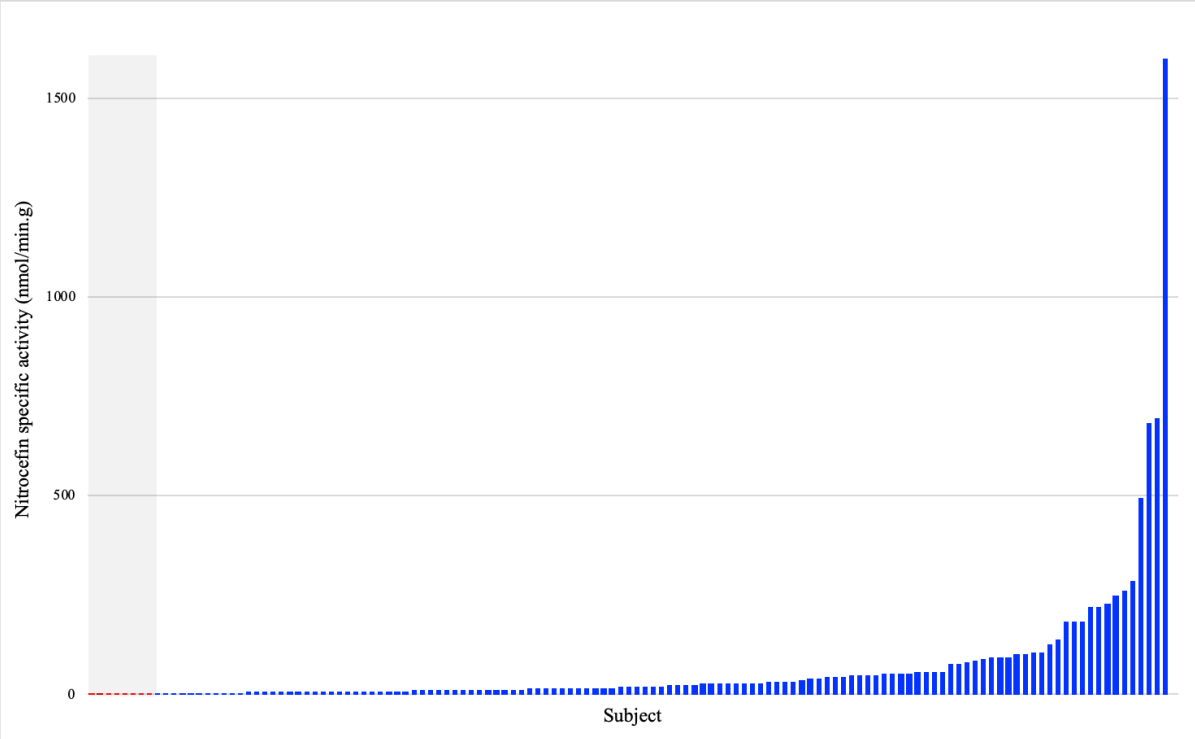

Figure 4.1.2: Graphical representation of the distribution and variability of nitrocefin-hydrolyzing activity in the baseline samples, prior to antibiotic exposure, of 132 subjects (lowest to highest). The grey zone and red bars represent the eight samples with activity below the detection limit threshold (set at 3.4 nmol/min·g).

In CEREMI, significant β-lactamase activity was detected in 18 out of 22 healthy subjects, ranging from 4.8 to 443 nmol NCF/min·g feces (Table 4.1.2). In DAV-132-CL-1006, significant β-lactamase activity was detected in 123 out of 132 healthy subjects, ranging from 3.9 to 1599 nmol NCF/min·g feces (Figure 4.1.2). When combining both studies, we detected measurable β-lactamase activity in the fecal material from 141 out of 154 (92%) healthy subjects, prior to antibiotic exposure. Furthermore, in CEREMI the majority of samples were represented by enzymes that were fully inhibited by avibactam (>90% inhibition) but not by EDTA (<10% inhibition): 83% of all nitrocefin-active samples above the detection limit. In three out of 18 samples (subjects 9, 11 and 17) we also identified samples that were only partially (68-87%) inhibited by avibactam. Furthermore, none of the samples showed imipenem-hydrolyzing activity and 10 out of 18 samples showed ceftriaxone-hydrolyzing activity, although very limited.

4.1.3 Conclusion

In this study we determined the presence of significant levels of β-lactamase activity in 92% of all healthy subjects tested. Although the samples were collected in different years and in

different studies, the findings in both groups confirm the convincing presence of β-lactamase enzymes in fecal material of healthy individuals. Furthermore, the total β-lactamase activity showed high variability between samples with up to a 100-fold difference in CEREMI and a 400-fold difference between samples in DAV-132-CL-1006. Since nitrocefin is sensitive to hydrolysis by all β-lactamases, it should be taken in consideration that these values provide no further information on the types of enzymes present in the fecal material nor their individual contribution. However, it can be assumed that the samples consisted of serine-β-lactamase(s) since all samples were inhibited by avibactam (CEREMI), a non-β-lactamase inhibitor capable of inhibiting most serine β-lactamases including β-lactamase enzymes of Ambler's classification classes A, C and D (Ehmann *et al.*, 2013). Three samples showed only partial inhibition by avibactam, which could indicate the presence of another type of β-lactamase. None of the samples were significantly inhibited EDTA, which excludes the presence of any metallo-β-lactamases as a consequence of the zinc scavenging effect of the EDTA (Hernandez Valladares *et al.*, 1997). Furthermore, the presence of cephalosporin-hydrolyzing enzymes is also likely although their contribution was rather limited.

Overall, these data suggest the presence of (a combination of) β-lactamase producing commensals in the majority of the healthy population. Although the results in CEREMI presented an indication of the nature of the β-lactamases potentially present in these samples, we cannot rule out the simultaneous presence of several β-lactamases in individual samples. Indeed, the metagenomic data created by d'Humières and colleagues suggested high intra-individual variability in bacterial microbiome richness before antibiotic treatment administration (d'Humières *et al*., manuscript in preparation). In their analyses, they identified a great number of β-lactamase encoding genes among the different subjects of which β-lactamases of class B (MBLs), class A and class D were identified in decreasing order.

The work from CEREMI was included in a publication in mBIO (American Society for Microbiology) with the title "A clinical study provides the first direct evidence that inter-individual variations in fecal β-lactamase activity affect the gut mycobiota dynamics in response to β-lactam antibiotics" (Appendix 8.5). These data are also included in an additional manuscript in preparation for submision to Microbiome (BMC Journal) titled "Perturbation and resilience of the gut microbiome three months after β-lactams exposure in healthy volunteers suggest an important role of endogenous β-lactamases".

4.2 Design of probiotic expression vectors

4.2.1 Background

The selection of the right expression vector is the first and one of the most important factors to influence the success of recombinant protein production. An expression vector is usually a plasmid that is designed for gene expression in cells. To allow for efficient cloning, our expression vector should contain an origin of replication (*ori*) site for *E. coli* that allows for the replication of DNA and ensures high plasmid copy number, marker genes for selection and unique restriction sites. To allow for gene expression in yeast, however, our expression vector should additionally contain a yeast *ori* and a selection cassette, making it a suitable shuttle vector, and a strong yeast promoter and terminator to control gene transcription. In the case of chromosomal integration, the yeast vector should also contain homologous sequences found in the yeast genome.

The shuttle vector pRG226, belonging to a family of pRG vectors, was designed and developed by Robert Gnügge and colleagues (Gnügge *et al.*, 2016, Figure 4.2.1) to allow for cloning in *E. coli* and yeast expression through both episomal replication and chromosomal integration through a double crossover recombination mechanism. This *E. coli*-*S. cerevisiae* shuttle vector contains all the necessary components previously described and was therefore purchased from Addgene (plasmid #64529) as initial expression vector.

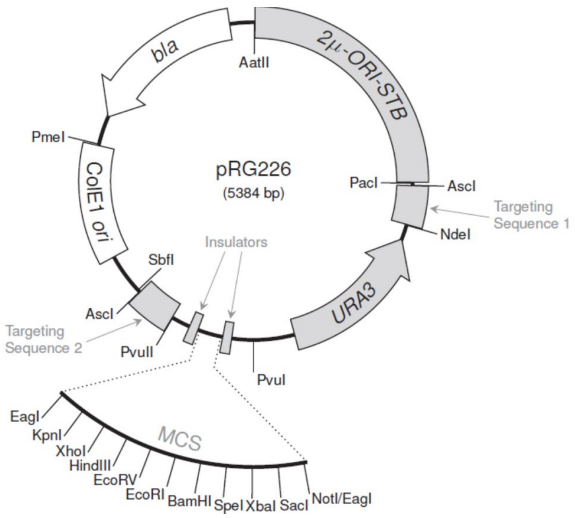

Figure 4.2.1: Schematic representation of pRG226 vector map with bacterial ori and bla gene, yeast 2 μ ori, a set of target sequences that are homologous to a yeast genomic integration site, wild-type URA3 gene and multiple cloning sites (MCS).

4.2.2 Work

Promoter and terminator

The promoter and terminator regions, especially the former, play a crucial role in the efficiency of recombinant protein expression. The promoter of the translation elongation factor 1 gene of *S. cerevisiae*, pTEF1, has been described as a strong and stable constitutive promoter of *S. cerevisiae* and has been well described in literature for its use in both *S. cerevisiae* and *S. boulardii* expression strains (Gatignol *et al*., 1990 and Durmusoglu *et al*., 2020). Likewise, the terminator region of the Alcohol dehydrogenase 1 (tADH1) gene of *S. cerevisiae* was selected. Figure 4.2.2.1 represents the promoter-terminator region that was ordered as synthetic gene (Invitrogen) and cloned into pRG226, creating pSRD-I, through *Sac*I and *Kpn*I restriction sites. The promoter and terminator sequences were separated by *Eco*RI and *Hin*dII restriction sites to allow for the insertion of the gene of interest.

Figure 4.2.2.1: Promoter-terminator region that was ordered as synthetic gene with external (SacI and KpnI) and internal (EcoRI and HindIII) restriction sites.

Secretion signal peptide

In our final system, the secretion of the recombinant enzyme *in situ* will be required. Hence, we designed two systems for secretion using either the widely used *S. cerevisiae* α-mating factor prepro peptide, abbreviated α-factor, or the leader peptide sequence of the *Kluyveromyces lactis* killer toxin gene, abbreviated K1. The α-factor signal peptide consists of 86 amino acids: the 19-amino acid pre-sequence and the 67-residue pro-sequence. Furthermore, its secretion takes place in three steps by which the pre- and pro-cleavage sites are processed in the endoplasmic reticulum (ER) and Golgi apparatus (Brake *et al*., 1984). The α-factor signal peptide has been efficiently used for the secreted production of proteins for over 30 years and the nucleotide sequence was therefore ordered as synthetic gene. In 1984, Baldari and colleagues demonstrated the functionality of a putative leader sequence from the *K. lactis*

killer toxin with presumptive cleavage site Val-Gln-Gly (Baldari *et al*., 1987). In their work they fused the 16 amino acid sequence to the human interleukin 1, β (IL-1 β) through a poly-linker sequence, comprising three amino acids (Thr-Arg-Gly), and *Bam*HI site (additional Ser from IL-1 β) in a so-called YEpscec1 plasmid and confirmed secretion into the culture medium. To assess the secretion potential of K1 in our system, we cloned our proof of concept (PoC) gene into YEpsec1, containing a galactose inducible promoter, by means of restriction-free (RF) cloning and subcloned the K1-polylinker-*Bam*HI site + PoC gene into the pRG226 plasmid (Figure 4.2.2.2).

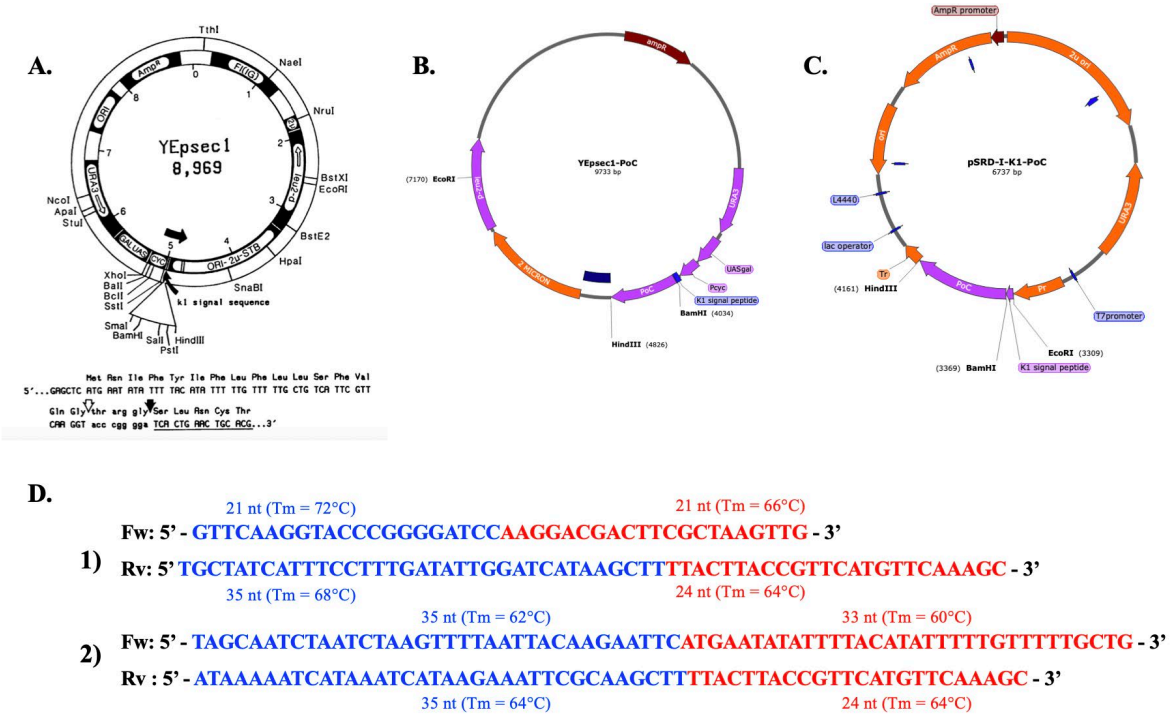

Figure 4.2.2.2: Cloning procedures for the creation of pSRD-I-K1. A. YEpsec1 vector with the partial sequence of K1 (including hypothetical cleavage site with empty arrow) and the polylinker sequence (Thr-Arg-Gly, including experimentally determined cleavage site indicated with filled arrow) in the lower panel (Baldari et al., 1989). B. YEpsec1 vector with PoC gene downstream the K1 signal peptide. C. pSRD-I-K1 vector with PoC gene cloned from YEpsec1-PoC by RF-cloning. D. Primers designed for the RF-cloning of PoC gene into YEpsec1 (step 1) and K1-PoC from YEpsec1-PoC into pSRD-I (step 2) with in blue the sequence corresponding to the plasmid and in red the sequence corresponding to the insert, creating the so-called 'megaprimer'. Tm values (calculated using the NEB Tm calculator tool) and primer size are indicated in the corresponding color. Plasmid images were created using the SnapGene® software.

Chromosomal integration

In order for the integration of a sequence to be successful, the presence of homologous sequences, corresponding to a location on the yeast chromosome, is necessary. Although our pRG226 originating plasmids included such sequences, the presence of the 2 micron yeast *ori* could disturb yeast transformation since episomal replication is more efficient than replication through chromosomal integration. For this reason, we designed a set of universal primers ('No2uOri', see Table 3.3.7.2 in the Materials & Methods section) that would re-amplify the plasmid by excluding the 2 micron *ori* through the addition of a *Nde*I restriction site on both ends, allowing for the recirculation of the plasmid without 2 micron *ori*. All plasmids created for this purpose were prefixed with 'YIp_' for yeast integrating plasmid.

HIS3 auxotrophic marker

The pRG226 plasmid contains the necessary elements to select for URA3 auxotrophy. However, HIS3 was also described to show high activity through episomal replication with the 2 micron *ori* (Durmusoglu *et al*., 2020). Furthermore, both the URA3 and HIS3 genes of *S. cerevisiae* are identical in *S. bouladrii* (Liu *et al*., 2016). In order to assess any differences in production with either markers and to allow for a potential double integration, we created a new plasmid, pSRD-II, in which the URA3 gene, including promoter and terminator region, and homologous regions were replaced with that of HIS3. Furthermore, in order to circumvent the extra cloning step to obtain the 'YIp' plasmid, only the integration part of pSRD-II was cloned into pLBII, a plasmid previously created in our laboratory (Borgianni *et al*., 2010). Table 4.2.2.1. shows an overview of the plasmids designed in this study and table 4.2.2.2 shows a full overview of all plasmids and yeast constructs created in this study, on which we will further elaborate in the following subchapters.

Table 4.2.2.1: Overview of plasmids created in this study.

Plasmid name	Plasmid content
pSRD-I	pRG226 plasmid + pTEF1 + tADH1
YIp_SRD-I	" without 2 micron *ori*
pSRD-I-K1	pRG226 plasmid + pTEF1 + tADH1 + K1 signal peptide/polylinker/*Bam*HI
YIp_SRD	" without 2 micron *ori*
pSRD-I-αf	pRG226 plasmid + pTEF1 + tADH1 + α-factor signal peptide
YIp_SRD-I-αf	" without 2 micron *ori*
pSRD-II-K1	pRG226 + HIS3 + pTEF1 + tADH1
pLB-SD	Only the HIS3 encoding elements were inserted into pLBII by means of *Xba*I and *Bam*HI

Table 4.2.2.2: Overview of the yeast expression constructs created in this study. Color shading indicates expressed protein with in grey the empty vectors only, green P3A, blue I8M, yellow BcII, purple EreB and orange OXA10L48.

Strain	Replication system	DNA construct
S. cerevisiae S150-2B *S. cerevisiae* INVSc1	episomal	YEpsec1 (empty vector)
S. cerevisiae S150-2B *S. cerevisiae* INVSc1	episomal	pRG226 (empty vector)
S. boulardii ura3^{-} M2	episomal	pSRD-I (empty vector)
S. boulardii ura3^{-} M2	chromosomal (URA3)	YIp_SRD-I (empty vector)
S. cerevisiae S150-2B	episomal	YEpsec1-yP3A-I
S. cerevisiae S150-2B *S. boulardii ura3*$^{-}$ M2	episomal	pSRD-yP3A-I
S. cerevisiae S150-2B *S. cerevisiae* INVSc1 *S. boulardii ura3*$^{-}$ M2	chromosomal (URA3)	YIp_SRD-yP3A-I
S. cerevisiae INVSc1 *S. cerevisiae* S150-2B	episomal	pSRD-I-αf-yP3A-I
S. cerevisiae S150-2B *S. cerevisiae* INVSc1 *S. boulardii ura3*$^{-}$ M2	episomal	pSRD-I-K1-yP3A-I
S. cerevisiae S150-2B	episomal	[b]pSRD-I-K1-yP3A-I*
S. cerevisiae S150-2B *S. cerevisiae* INVSc1 *S. boulardii ura3*$^{-}$ M2	chromosomal (URA3)	YIp_SRD-I-K1-yP3A-I
S. cerevisiae S150-2B *S. cerevisiae* INVSc1	episomal	pSRD-yP3A-I-PRE3
S. boulardii ura3^{-} M2	chromosomal (URA3)	YI_ pSRD-yP3A-I-PRE3
S. cerevisiae S150-2B *S. boulardii ura3*$^{-}$ M2	chromosomal (URA3)	[c]YIp_SRD-yP3A-I-iPRE3*
S. cerevisiae INVSc1 *S. cerevisiae* S150-2B *S. boulardii ura3*$^{-}$ M2	episomal	pSRD-I-K1-yP3A-iPRE3
S. boulardii ura3^{-} M2	chromosomal (URA3)	YIp_SRD-I-K1-yP3A-iPRE3
S. cerevisiae S150-2B	episomal	pSRD-yP3A-II

Table 4.2.2.2 continued.

Strain	Replication system	DNA construct
S. boulardii ura3^{-} M2	episomal	pSRD- k1-yP3A-II
S. cerevisiae INVSc1 *S. cerevisiae* S150-2B	episomal	pSRD- αf-yP3A-II
S. boulardii ura3^{-} M2	episomal	pSRD-I-K1-yI8M
S. cerevisiae INVSc1 *S. cerevisiae* S150-2B *S. boulardii ura3*$^{-}$ M2	episomal	pSRD-I-K1-yI8M-iPRE3-I
S. boulardii ura3^{-} M2	chromosomal (URA3)	YIp_SRD-I-K1-yI8M-iPRE3-I
S. boulardii ura3^{-} M2	episomal	pSRD-I-K1-yI8M-iPRE3-II
S. boulardii ura3^{-} M2	episomal	pSRD-I-K1-yI8M-iEFB1-I
S. boulardii ura3^{-} M2	episomal	pSRD-I-K1-yI8M-iEFB1-II
ongoing	chromosomal (HIS3)	pLBSD-K1-yI8M-iPRE3-II
ongoing	chromosomal (HIS3)	pLBSD-K1-yI8M-iEFB1-I
S. boulardii ura3^{-} M2	episomal	pSRD-I-K1-yBcII
S. cerevisiae INVSc1 *S. cerevisiae* S150-2B *S. boulardii ura3*$^{-}$ M2	episomal	pSRD-I-K1-yBcII-iPRE3-I
S. boulardii ura3^{-} M2	episomal	pSRD-I-K1-yEreB-I
S. boulardii ura3^{-} M2	episomal	pSRD-I-K1-yEreB-I-iPRE3-I
S. boulardii ura3^{-} M2	episomal	pSRD-I-K1-yEreB-II-iEFB1-II
S. boulardii ura3^{-} M2	episomal	pSRD-I-K1-yOXA10L48-iPRE3

[b] Point-mutation in yP3A-I gene (amino acid mutation R231K)
[c] Point-mutation in PRE3 intron (C64A)

4.2.3 Conclusion

Here, we designed a set of plasmids that theoretically can be utilized for protein expression in probiotic yeasts *S. cerevisiae* and *S. boulardii.* The plasmids were designed in way to allow for flexibility in the assessment of different components. Furthermore, we anticipated the different yeast constructs created in this study. In the next subchapters we will discuss the actual activity that can be obtained with the different plasmids and different antibacterial enzymes.

4.3 Gene design: codon optimization, intron choice and intron insertion position

4.3.1 Background

In this subchapter we focus on the design of the genes that eventually will be cloned into our pSRD plasmids. We will discuss the design of our PoC gene (further discussed in the next subchapter) although these methods were also applied to all other genes that were expressed in yeast in this study. We describe our codon optimization approach and the artificial insertion of an intron.

Codon optimization

The nucleotide sequence of a bacterial enzyme should be suitable for expression in probiotic yeast cells and may require some host-specific modification, also defined as codon optimization. Codon optimization has been described to significantly increase protein expression and aims to change the codons according to the preferential usage of particular codons for a certain organism, based on their genomic tRNA pool. Codon usage bias of a species can be measured using the Codon Adaptation Index (CAI, Sharp *et al.*, 1987). By means of a reference set of highly expressed genes from a species, a score between 0 and 1 is calculated for the codon use in a gene. The CAIs of different optimization methods were compared to the CAIs of six highly expressed genes in *S. cerevisiae* as a reference. The CAIs of the optimized gene and the prediction model based on the reference genes were visualized with the gene design software Visual Gene developer 1.7 (Jung & McDonald, 2011).

Introns

Introns can be found in the genome of all eukaryotes where they are part of a gene structure and are eventually removed by a complex molecular machinery called the spliceosome (Chorev & Carmel, 2012). While introns are present in DNA transcription, they do not participate in protein-coding sequences. Although the presence of introns seems to be unnecessary energy consuming, studies have demonstrated an increase in protein abundance of intron-containing genes in several eukaryotic organisms, including yeast (Juneau *et al.*, 2006). The lack of a

spliceosome in bacteria and the potential protein expression advantage of an intron-containing gene inspired us to design intron-containing genes for the production of bacterial enzymes in yeast in the gut.

4.3.2 Work

Codon optimization

The sequence of our PoC gene underwent *S. cerevisiae*-specific modification in order to favor protein expression in our non-bacterial host. In this study me made use of several online gene optimization tools (method A) of which we compared their CAI profiles with that of the average of six highly expressed genes in *S. cerevisiae*, serving as a prediction model. With a different approach, method B, we attempted to adapt the codon usage of our gene manually, accordingly the CAI profile of the highly expressed TDH2 gene in yeast.

In method A we made use of three online codon optimization tools: JCat (Java Codon Adaptation Tool; Grote *et al.*, 2005), COOL (Codon Optimization On-line; Chin *et al.*, 2015) and IDT (Integrated DNA Technologies, available at: https://eu.idtdna.com/CodonOpt). The six reference genes, representing the highest expressed genes in *S. cerevisiae* were as follows: Glyceraldehyde-3-phosphate dehydrogenase 2 and 3 (TDH2, TDH3), Translational elongation factor eEF-1 alpha (TEF1, TEF2), 2-Phosphoglycerate dehydratase (ENO2) and Acidic ribosomal protein L10 (RPL10E) (Velculescu *et al*., 1997). In Figure 4.3.2A the CAI profiles of all sequences for *S. cerevisiae* were visualized by means of Visual Gene developer 1.7. With Method B we aimed to follow the CAI profile of the highly expressed TDH2 gene in *S. cerevisiae* by manually changing the codons in a way that was not only favorable for *S. cerevisiae* but that also resembles the CAI score pattern observed for TDH2 (Figure 3.3.2B). From Method A, the sequence obtained with the JCat optimization was selected as the most promising sequence to test *in vitro* (yPoC-I) due to the strongest resemblance of its CAI profile to that of the reference genes. Although the CAI profiles of the manually optimized gene, yPoC-II, and yPoC-I showed a similar CAI profile, the actual variations in gene sequence were still aberrant with 127 nucleotide differences (Table 4.3.2).

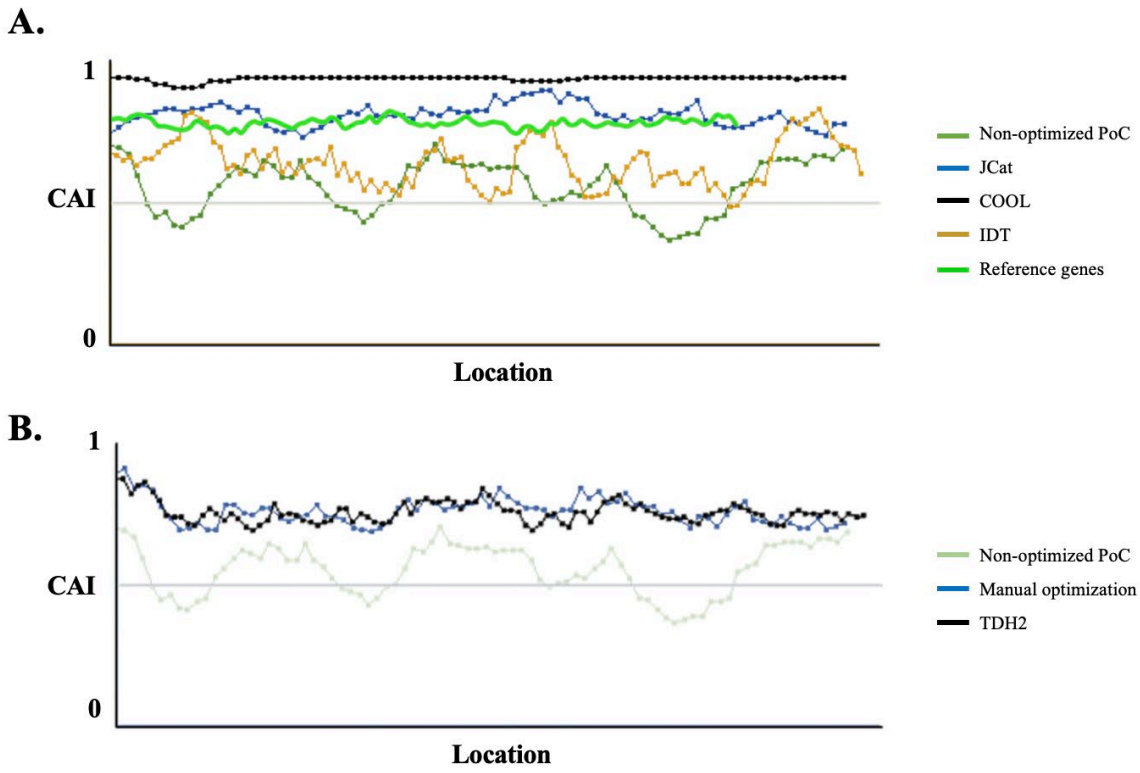

Figure 4.3.2.1: CAI profiles of optimized genes for S. cerevisiae with in A. the comparison of CAI profiles obtained with different online optimization tools (method A) and B. the comparison of the CAI profile obtained with a manual optimization method to resemble the CAI profile of TDH2, the highest expressed gene in S. cerevisiae (method B). The y-axis reports the CAI score 0-1 and the x-axis the location of the sequence, with each point representing an average of 3 CAI values.

Table 4.3.2: Comparison of codon optimization methods in terms of nucleotide differences.

Sequence comparison	# nucleotide differences
yPoC-I *vs.* bPoC	244
yPoC-II *vs.* bPoC	198
yPoC-I *vs.* yPoC-II	127

Intron choice

The genome of *S. cerevisiae* consists of 5749 open reading frames (ORFs) of which 285 (5%) contain introns (usually one intron per gene, Juneau *et al.*, 2006). Upon further analysis of naturally-occurring intron-containing genes in *S. cerevisiae*, a couple of characteristics are

evident: most introns are closely present to the 5' splice site of the sequence (a mean of 39 nt distance), the 5' splice site is often GUAUGU, the 3' splice site is often YAG, in 55% of cases an A precedes the YAG, the branchpoint sequence is either UACUAAC or UUUACUAACAA and in 66% of cases an A follows the branchpoint sequence (Spignola *et al*., 1999). Computational analysis by Juneau and colleagues also showed that the closer an intron to the transcriptional start of a gene, the better its expression and that genes with longer introns seem to be more successful in gene expression as well (Juneau *et al*., 2006). Furthermore, Yofe and colleagues created a synthetic gene expression library testing the effect of 240 native *S. cerevisiae* introns in the yellow fluorescent protein (YFP) gene (Yofe *et al*., 2014). Although the majority of introns tested showed reduced reporter gene expression compared to WT and intron-less YFP, the intron from the elongation factor 1 subunit beta (EFB1 or YAL003W) gene showed a slightly beneficial splicing efficiency and was therefore selected for assessment in our study (Table S1 in Yofe *et al*., 2014). Moreover, for a limited number of introns (n = 10) also the intron insertion position was assessed based on the secondary structure and GC content at the intron-exon junctions. Here, they tested four insertion positions within the YFP gene with minimal folding energy of the intron-exon junctions ranging from weak to very strong. From the 10 introns tested, YJL001W and YGL103W showed the most flexibility in terms of intron position as the expression levels were similar to the WT situation for all four positions, whereas other introns showed dramatic increased in expression levels with certain insertion positions (Figure 4.3.2.2). Furthermore, intron YJL001W had been ranked number 8 from all 240 tested introns and YGL103W number 24. Thus, we decided to also include the intron from the YGL103W gene, also referred to as PRE3, in our study. Finally, we also analyzed whether the main characteristics of natural yeast introns and the enhancer motifs, motifs associated with enhanced slicing efficiency, could be found in our selected introns (Spignola *et al*., 1999 & Yofe *et al*., 2014). Figure 4.3.2.2B shows the intron analysis of the PRE3 intron.

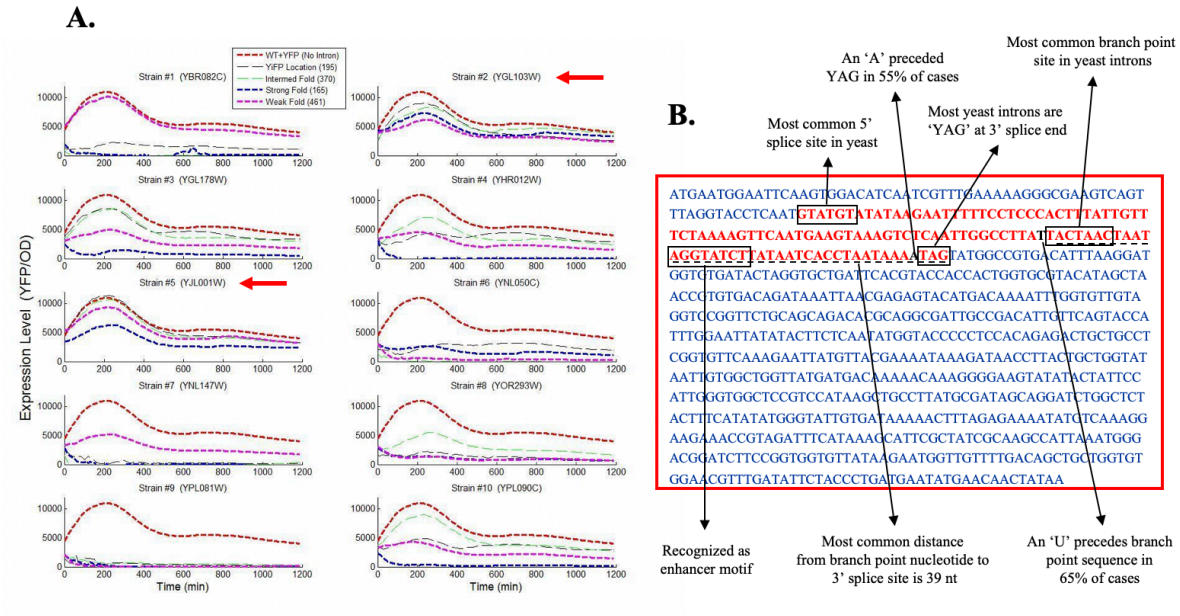

Figure 4.3.2.2: Selection and analysis of PRE3 (YGL103W) intron with in A. the expression level analysis of 10 yeast introns at 4 different insertion positions showing flexibility of 2 introns for all four positions (Yofe et al., 2014) and B. analysis of PRE3 intron (indicated in red) naturally present in its PRE3 gene (chromosome X: 435163-435926).

Intron insertion position

Literature shows that in nature, the introns of the majority of intron-containing genes are close to the 5' splice site and within the first 5% of gene length (Spignola *et* al., 1999 and Sakurai *et* al., 2002). In our study, however, the artificial insertion of an intron has two main goals: 1. the loss of functionality of the gene in a bacterial host and 2. the improvement of gene expression compared to the intron-less gene. To this end, we aim to insert the intron in a position where it disrupts the active site, completely rendering the gene useless in case of partial gene transfer to bacteria, and a position favorable for gene expression. Our PoC enzyme belongs to the class-A, or Serine, β-lactamases (further discussed in the next subchapter) that are characterized by three conserved motifs: the active Serine-site or SxxK motif (part of the active site), the [SYF]xN motif and the [KR][TS]G motif responsible for catalytic activity of substrate binding (Ambler *et al*., 1991 and Brandt *et al*., 2017). In our case, we aimed for disruption between the catalytic Serine in the 'STIK' motif and the next conserved SDN motif. Furthermore, studies have shown that pre-mRNA local folding strength may significantly affect splicing efficiency (Zafrir & Tuller, 2015). Likewise, in their experimental intron study Yofe and colleagues found the secondary structure at intron-exon junctions to significantly impact splicing efficiency and

therefore also gene expression (Yofe *et al*., 2014). For example, strong artificial junction folding negatively regulated gene expression for all ten introns tested (Figure 4.3.2.2A). Although a weak folding did not show increased expression levels compared to the intron-less gene, weaker pre-mRNA folding at the intron-exon junction does seem to be preferred, corresponding to the general consensus for fungi in nature (Zafrir & Tuller, 2015). Zafrir and Tuller (2015) hypothesized that the preferred weaker local pre-mRNA folding at intron-exon boundaries in fungi may have evolved to improve splicing efficiency. Therefore, we hypothesized the ideal intron insertion position between the two conserved motifs described above by analyzing the folding energy of potential intron-exon junctions. More specifically, we calculated the minimal folding energy (MFE) with a 40 nt window downstream of the intron. The MFE was calculated using *rnafold* (Vienna) as was done by Yofe *et al*. (2014) and Zafrir & Tuller (2015) by using the online server available at http://rna.tbi.univie.ac.at/cgi-bin/RNAWebSuite/RNAfold.cgi (Gruber *et al*., 2008). *rnafold* predicts the MFE secondary structure of single sequences by means of algorithms described by Zuker & Stiegler (1981).

Figure 4.3.2.3 shows the MFE at the intron-exon junction, based on the hypothetical intron insertion positions for our yeast optimized PoC gene, y-PoC-I. As a reference baselines, we included the MFE value for the PRE3 intron naturally present in *S. cerevisiae*, along with the MFE values obtained with the two artificial insertion sites of the PRE3 intron in the YFP gene showing highest expression levels. In our study the insertion positions are +3 nt compared to that described by Yofe *et al*. as we also counted the start codon, with position 2 being directly after the A in ATG. Furthermore, we highlighted the potential insertion positions: yellow and blue for insertion positions between the two conserved motives (amino acid sequence indicated in red) and with MFE values between -4.9 and 5.2 kcal/mol (native PRE3 and PRE3 at position 195 in YFP) and -3.5 and -4.9 (PRE3 at positions 373 and 195 in YFP and in green) and blue for insertion positions in the middle of the second conserved motif with MFE values between -4.9 and 5.2 kcal/mol (native PRE3 and PRE3 at position 195 in YFP). Finally, we determined insertion position 157 as the best hypothetical intron insertion position for the following main reasons: 1. Interruption of the STIK catalytic Serine and SDN conserved motif, 2. intron-exon junction MFE of -5.1 kcal/mol, 3. Intron insertion position relatively close to 5' site, after catalytic Serine, and 4. within a plateau region of the intron-exon junction MFE, potentially allowing for more insertion flexibility compared to other sites where a 1 nt shift resulted in a dramatic change in MFE.

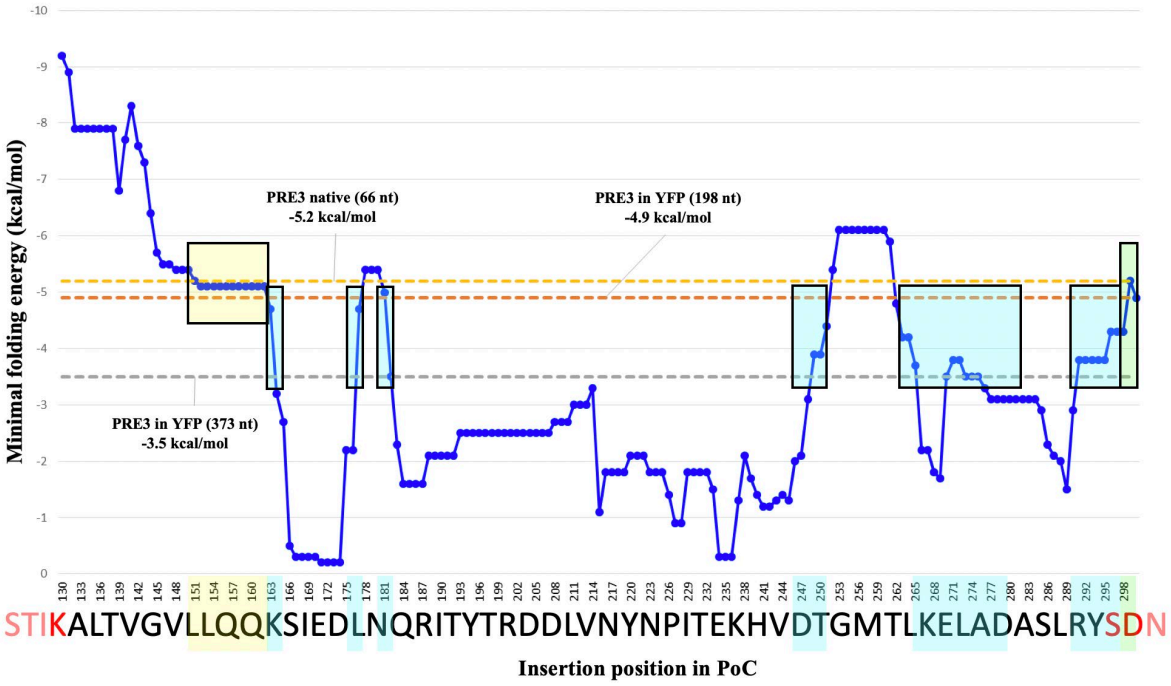

Figure 4.3.2.3: MFE analysis of secondary structure of potential intron-exon junctions in the yPoC-I gene with a 40 nt window with on the x-axis the nucleotide insertion position, and the corresponding amino acid sequence, and on the y-axis the inverted display of the calculated MFE values. Baseline MFE values are depicted as reference for the MFE of the PRE3 intron in the PRE3 gene of S. cerevisiae or artificially in the YFP gene on positions 198 or 373, as described in Yofe et al., 2014.

4.3.3 Conclusion

In this subchapter we evaluated two approaches for the yeast optimization of bacterial genes. In both approaches we determined the hypothetical best optimization method based on the CAIs of the highest expressed gene(s) in *S. cerevisiae*. Using method A (online codon optimization tools), we determined that the CAI obtained with the JCat optimization of our PoC resembled most that of our reference CAI, varying in 244 nucleotides with respect to the CAI of the bacterial (non-optimezed) sequence in *S. cerevisiae*. Furthermore, other genes used in this study were additionally tested with the following online optimization tools: vectorbuilder (https://en.vectorbuilder.com/tool/codon-optimization.htmL), ExpOptimizer from NovoPro (https://www.novoprolabs.com/tools/codon-optimization) and GenSmart™ Codon Optimization from Genscript (Version Beta 1.0., https://www.genscript.com/tools /gensmart% 2dcodon%2doptimization). Appendix 8.1 contains the CAI profiles of all other genes optimized in this study. Here, we can observe that the CAI profiles are different for each gene. Although each optimization method makes use of a different algorithm, we can conclude that some optimization tools, such as the one from Vectorbuilder, generally optimized the gene

too strong as the CAI profiles for all genes were always the highest and overall closest to the value 1. Furthermore, it should be noted that the CAI profile of the reference genes is generally longer than that of the genes in this study, except for EreB. However, the average CAI of the six highly expressed genes serves merely as a reference rather than an exact guideline. The determination of the correct optimization is essential for the second part of the gene design, being the insertion position. In our study we based the intron insertion position on the MFE at the intron-exon junction which depends on the (optimized) nucleotide sequence of the gene. Our MFE analysis on the PoC gene and all other genes in Appendix 8.2 show that a single nucleotide shift may significantly affect the secondary structure, *i.e.* MFE value, of the intron-exon junction and possible splicing efficiency. With the combination of our plasmids and gene design approach we aimed for an efficient expression system that ensures containment of antibiotic resistance enzymes in the gut and allows for accurate and efficient processing of artificially inserted introns. In order to assess the hypotheses of our molecular biology designs, however, we require actual laboratory *in vitro* studies in living yeast.

4.4 Enzyme production in *S. cerevisiae* with PoC enzyme

4.4.1 Background

To demonstrate the feasibility of an antibiotic degrading yeast probiotic, ribaxamase was selected as a first enzyme candidate to be expressed. Ribaxamase, also known as P3A, is a broadly acting cephalosporinase (class A β-lactamase) that was engineered from the naturally-occurring P1A (D276N variant) from *B. licheniformis* by Ipsat Therapeutics and is currently being developed as a therapeutic agent by Synthetic Biologics, Inc. (SYN-004). As many enzymes originating from Bacillus spp., P3A is especially interesting for its stability in a wide range of temperatures and pH. P3A is currently in a Phase 1b/2a clinical trial and heading towards a Phase 3 clinical program and was therefore selected as the ideal model or PoC enzyme in this study.

4.4.2 Work

The P3A gene sequence was codon optimized as previously described, creating yP3A-I (JCat optimization) and yP3A-II (manual optimization). The natural *S. cerevisiae* intron of the PRE3 gene was selected as (initial) intron choice and inserted into position 157, after the catalytic Serine and before the SDN β-lactamase conserved motif. yP3A was cloned into the pSRD plasmids and transformed, episomal or chromosomal, into *S. cerevisiae* through heat-shock transformation using LiCl or LiAC (see Materials & Methods section). P3A production was assessed in the cytoplasm or culture supernatant with a K1 or α-factor signal peptide in the absence and presence of the artificially inserted PRE3 intron. P3A production was quantified in milligrams per liter of culture using spectrophotometric assays and the Henri-Michaelis-Menten equation (See Materials & Methods section). In order to calculate the enzyme concentration, the equation requires the steady-state kinetic parameters k_{cat} and k_M. We determined these parameters for purified P3A[3] with nitrocefin after direct fit of the initial rate-conditions using the Hanes-Woolf plot (Segel, 1975). Figure 4.4.2.1 illustrates these fits for P3A with nitrocefin, resulting in a K_M value of 48 ± 4 μM and k_{cat} of 159 ± 20 s^{-1}. All other graphical representations of enzyme kinetics determined in this study (unless previously determined) can be found in Appendix 8.3.

[3] Internal purified P3A, qualified batch no. SIP-P3A-27102016/1.

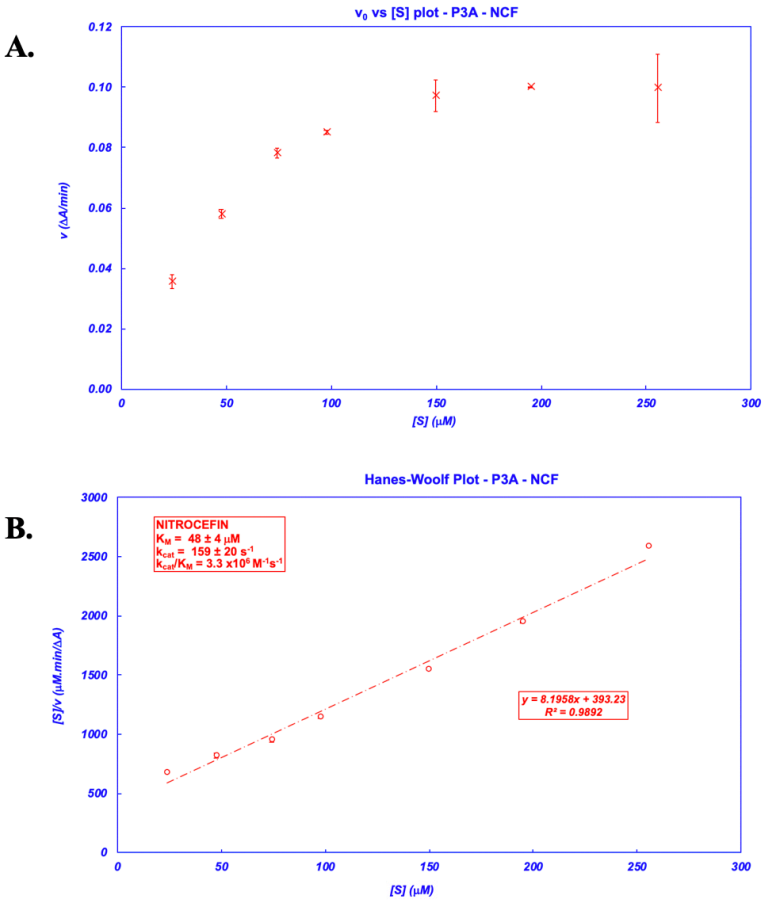

Figure 4.4.2.1: Determination of the kinetic parameters of P3A for nitrocefin hydrolysis. (A) reaction rate vs substrate concentration (Henri-Michaelis-Menten) plot and (B) the Hanes-Woolf plot.

Initial expression experiments were performed with the transformed *S. cerevisiae* INVSc1 strain. Yeast cells containing the empty vector (pRG226) or P3A gene (pSRD-I-yP3A-I) were inoculated from a pre-culture in selective medium (yeast nitrogen base; YNB) supplemented with glucose and necessary amino acids at a cell density of A_{640} = 0.01 or 0.0001 in selective medium or rich medium (Yeast Extract–Peptone–Dextrose; YPD), respectively (see Materials & Methods section). Cultures were grown at 30 °C, under agitation (180 rpm) and with a medium-to-flask ratio of 1:10 and cell growth was monitored at a wavelength of 640 nm and activity of lysed cells was spectrophotometrically determined using ampicillin[4] as substrate. In Figure 4.4.2.2 the diauxic growth of *S. cerevisiae* in glucose-rich medium, characterized by an exponential and post-diauxic phase, can be observed (Busti *et al.*, 2010). Furthermore, yeast growth does not seem to be affected by the expression of P3A since after 30 hours both the

[4] Steady-state kinetic parameters for P3A with ampicillin were previously determined in our laboratory (K_M = 176 μM and k_{cat} = 1345 s^{-1}).

P3A producing and empty vector strains reached the same cell density. The lysed cells of the strain carrying the empty vector showed no hydrolysis of ampicillin, whereas the P3A producing cells showed significant ampicillin hydrolysis, corresponding to ~ 5 mg/L in the exponential phase in both media (A_{640} = 0.4 in YNB and 1.3 in YPD) and ~ 5 mg/L and 15 mg/L in the post-diauxic phase in selective medium (A_{640} = 1.0) and rich medium (A_{640} = 8.4), respectively. Noteworthy, protein production is more efficient in selective medium since the total protein in the lysed cells is represented a 5-fold more by P3A in the selective medium cultures compared to the rich medium cultures (Figure 4.4.2.2).

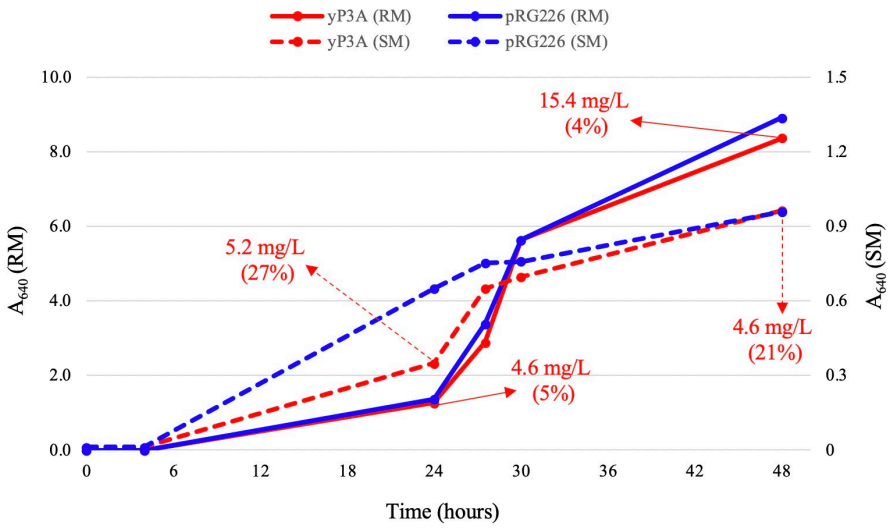

Figure 4.4.2.2: Yeast growth and P3A production with ampicillin hydrolysis in S. cerevisiae INVSc1 cells carrying the empty vector (pRG226) or P3A (pSRD-I-yP3A-I) grown in YPD (rich) medium or YNB (selective) medium supplemented with glucose and necessary amino acids.

We also evaluated cytoplasmic protein production in yeast carrying the non-optimized P3A gene, bP3A, compared to the yeast optimized P3A gene, y-P3A-I, and observed a 10-fold lower production yield in rich medium under similar conditions (data not shown). Furthermore, we evaluated periplasmic production over time in the culture supernatants of the yeast constructs with K1 or α-factor signal peptide. While the α-factor signal peptide resulted in very limited or no detectable activity, the K1 signal peptide resulted in significant activity in both the YEpsec1 plasmid with (galactose) inducible promoter and our pSRD-I plasmid with constitutive TEF1 promoter (Table 4.4.2.2). Figure 4.4.2.3 shows the production of an overnight culture in rich medium with the pSRD-I-K1-yP3A-I construct. Production was corrected for cell density to better understand the production dynamics over time. Clarified culture supernatants (or lysed cell pellets) were collected and stored on ice until analysis in a 96-well plate with 100 µM

nitrocefin as substrate. Up to 25 µL of sample were measured in a total volume of 200 µL and each timepoint activity represents and average of three measurements. Although periplasmic activity was minimal, it still represented over 80% of total activity produced by the yeast, as observed by the cytoplasmic activity data from timepoints 20, 23 and 25 hours. Furthermore, periplasmic production seems more efficient early in growth, reaching a production saturation at $A_{640} \approx 2.5$. To evaluate culture conditions over time better, we monitored the change in pH in yeast cultures with both *S. cerevisiae* laboratory strains S150-2B and INVSc1 (Figure 4.4.2.4). Growth was normalized per colony forming units (CFU) to directly compare both strains.

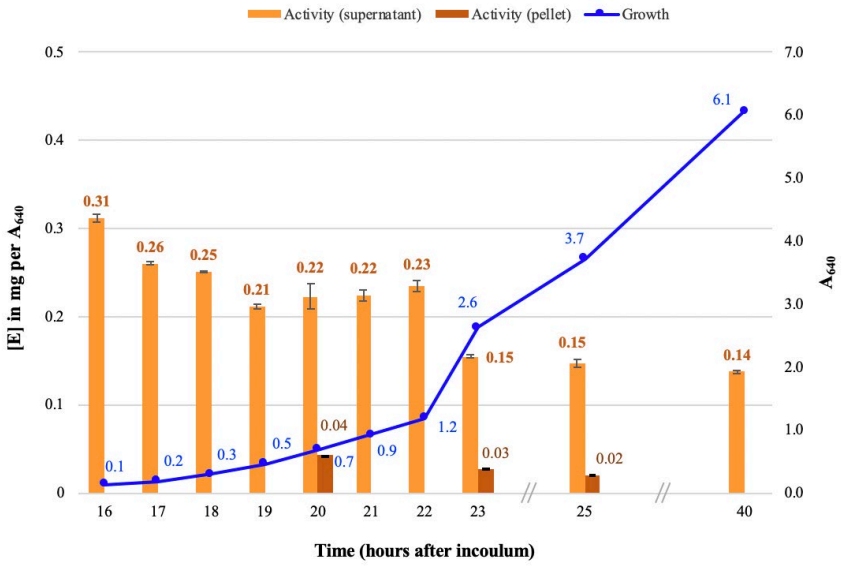

Figure 4.4.2.3: Yeast growth (right y-axis and blue line) and P3A production with nitrocefin hydrolysis (left y-axis, periplasmic production in orange and cytoplasmic production in brown) in S. cerevisiae INVSc1 cells carrying pSRD-I-K1-yP3A-I, grown in YPD medium at 30°C. Activity values are reported above columns with error bars representing the standard deviation.

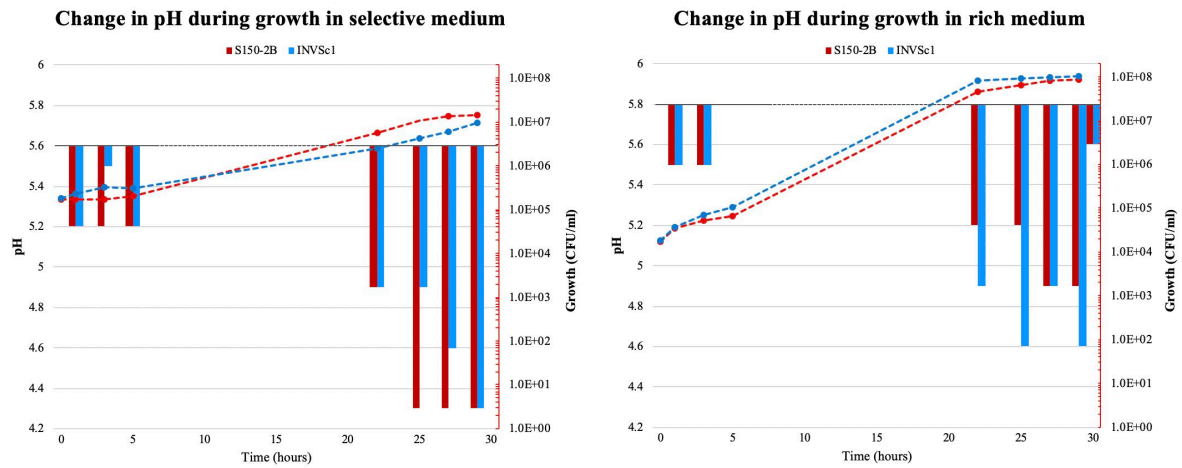

Figure 4.4.2.4: pH (left y-axis) in yeast cultures, with S. cerevisiae laboratory strains S150-2B and INVSc1, and during growth (right y-axis) in selective medium (left graph) and rich medium (right graph).

Overall, we observed about one pH of acidification during the exponential growth. There was no clear difference between both strains and rather a correlation between culture density and acidification. To understand whether the changed conditions in the medium, such as pH or secreted proteases, were negatively impacting enzyme stability, we incubated (20 min at RT, 1:10 enzyme dilution in buffer or medium) purified P3A in either HZn buffer (positive control), YPD medium, the clarified supernatant of an overnight YPD culture with *S. boulardii* with pH 5.2 or the heat-inactivated (25 min at 95°C) version of this clarified culture supernatant (negative control). The activity data of the non-incubated sample was used as baseline activity (100%). Residual activity (average of triplicate measurement) and standard error are reported as percentage (Table 4.4.2.1). Since we observed no significant difference (<20%) between the activity data after incubation with HZn buffer, YPD medium (pH = 5.8) and a clarified yeast culture in YPD medium (pH = 5.2), we can conclude that acidification of the medium does not negatively impact P3A activity. Furthermore, we observed no difference between incubation with the culture supernatant and the heat-inactivated culture supernatant, excluding the negative impact of soluble components secreted by the yeast such as proteases.

Table 4.4.2.1: Stability of purified P3A in different buffers and media, reported as % residual activity from baseline.

pH	Incubation medium	% residual activity	% error
7.5	No incubation (baseline)	100	3
7.5	Inc. with HZn	96	6
5.8	Inc. with YPD medium	105	2
5.2	Inc. with YPD culture supernatant	106	2
5.2	Inc. with heat-inactivated YPD culture supernatant	100	2

Table 4.4.2.2 contains an overview of the activity data observed with the different P3A constructs in the *S. cerevisiae* strains grown rich medium. The cultures were grown with a medium-to-flask of at least 1:8 under agitation (180 rpm) and at the optimal temperature of the *S. cerevisiae* strains: 25°C for S150-2B and 30°C for INVSc1. We found that the conventional optimization method, *i.e.* using an existing optimization tool, worked significantly (at least 6-fold) better than the manual codon optimization method. Furthermore, the introduction of a yeast intron in the P3A optimized gene does not seem to hinder its production and rather suggests to have a beneficial impact. Also, yeast integration resulted in successful expression of the P3A protein, although to a lower extent. Noteworthy, the haploid *S. cerevisiae* strain, S150-2B, was overall more efficient in P3A production.

Table 4.4.2.2: P3A activity from P3A producing yeast cells early in their growth in YPD medium (A_{640}<2.0), normalized for cell density in mg P3A per A_{640} or mg P3A per 10^9 yeast cells.

	Plasmid	Signal peptide	Gene	Intron	Replication	Strain	Activity (mg/A_{640})	Activity (mg/10^9 cells)
Cytoplasmic activity	pSRD-I	-	yP3A-I	-	episomal	*S. cerevisiae* (S150-2B)	9.47	0.56
	pSRD-I	-	yP3A-I	-	episomal	*S. cerevisiae* (INVsc1)	3.56	0.2
	pSRD-I	-	yP3A-II	-	episomal	*S. cerevisiae* (S150-2B)	1.5[a]	0.09[a]
	pSRD-I	-	yP3A-II	-	episomal	*S. cerevisiae* (INVsc1)	0.33	0.02
	pSRD-I	-	yP3A-I	iPRE3	episomal	*S. cerevisiae* (S150-2B)	12.6	0.75
	pSRD-I	-	yP3A-I	iPRE3	episomal	S. cerevisiae(INVsc1)	11.7	0.65
integration	YIp_pSRD-I	-	yP3A-I	-	chromosomal (URA3)	*S. cerevisiae* (S150-2B)	1.1	0.07
	YIp_pSRD-I	-	yP3A-I	-	chromosomal (URA3)	*S. cerevisiae* (INVsc1)	1.5	0.08
Periplasmic activity	pSRD-I	α-factor	yP3A-I	-	episomal	*S. cerevisiae* (S150-2B)	0.02	<0.01
	pSRD-I	α-factor	yP3A-I	-	episomal	*S. cerevisiae* (INVsc1)	bdl	bdl
	pSRD-I	α-factor	yP3A-II	-	episomal	*S. cerevisiae* (S150-2B)	0.43	0.03
	pSRD-I	α-factor	yP3A-II	-	episomal	*S. cerevisiae* (INVsc1)	0.28	0.02
	pSRD-I	K1	yP3A-I	-	episomal	*S. cerevisiae* (S150-2B)	0.82	0.05
	pSRD-I	K1	yP3A-I	-	episomal	*S. cerevisiae* (INVsc1)	0.31	0.02
	YEpsec1[b]	K1	yP3A-I	-	episomal	*S. cerevisiae* (S150-2B)	11.9	0.7

4.4.3 Conclusion

In this subchapter we successfully demonstrated the feasibility of a yeast with antibiotic degrading capability *in vitro*. By means of the hydrolysis of a real-life antibiotic or chromogenic substrate we were able to determine significant levels of enzyme production in yeast cells. Yeast optimization with an online optimization tool successfully improved the production of our enzyme in yeast and worked significantly better than a manual optimization approach. Furthermore, we demonstrated the correct processing of an artificially inserted yeast intron into the yeast optimized gene, that showed to have little, or even a beneficial impact on protein production. Protein secretion was successfully achieved with the K1 signal peptide and to limited extent with the α-factor signal peptide.

Although we were able to observe higher levels of enzyme production in rich medium cultures where higher cell densities where obtained, we found the production yield to be more efficient in selective medium cultures. This is likely explained by the selection pressure in selective medium and the potential loss of plasmid in rich medium cultures. Moreover, P3A secretion was observed to be less efficient at higher cell densities in rich medium compared to the production early in growth. We confirmed that medium acidification and secreted soluble components in the medium do not negatively influence P3A stability, as was expected from this robust enzyme. Therefore, we hypothesize that protein efficiency might have decreased due to the loss of plasmid and/or the increasing presence of non-viable cells. Nevertheless, we demonstrated the efficient production of different P3A constructs, including the artificial intron-containing P3A and chromosomal integrated P3A. These results are very promising and suggest further exploration of other, more relevant antibiotic degrading enzymes. In addition, the haploid *S. cerevisiae* strain S150-2B is presumably a better LBP candidate than the diploid INVSc1 since it was more efficient in P3A production, regardless the DNA construct. Reason for this remains unclear and will be further investigated in the next subchapter.

4.5 Yeast probiotic *Saccharomyces boulardii*

4.5.1 Background

The data in the previous subchapter suggests the *S. cerevisiae* S150-2B strain as a better LBP host candidate. However, these data might have been biased by the growth temperature at 25°C, compared to that of the INVSc1 strain (30°C), which might be more favorable for the enzyme. Either way, 25°C is not a relevant temperature for production since it is 12 degrees below that of the human body. We therefore compared both *S. cerevisiae* laboratory strains to the probiotic strain *S. cerevisiae* var *boulardii* (abbreviated *S. boulardii*). *S. boulardii* CNCM I-745 is the first yeast that was described for its use as a probiotic in human medicine. The strain was discovered in 1920 by French microbiologist Henri Boulard who observed that people who drank an extract prepared from the outer skin of the lychee and mangosteen fruits did not develop diarrhea (Czerucka & Rampal, 2019).

Currently, *S. boulardii* is being prescribed for the prevention and treatment of diarrhea, including antibiotic mediated diarrhea associated with *C. difficile*, in adults and children. Furthermore, many other studies have described the (potential) beneficial impact of *S. boulardii* administration during disease (prevention). The yeast is considered a safe microorganism with non-toxic and non-pathogenic effects and can be administered in large quantities in the gastrointestinal tract, or gut, while maintaining a constant level of viability due to its resistance to low gastric pH and bile acids. Despite the close genomic relatedness (>99% as determined by average nucleotide identity) of *S. cerevisiae* and *S. boulardii*, studies have described the superior survival of *S. boulardii* in gut-like conditions regarding temperature, pH and bile salts concentration (Khatri *et al*., 2017 and Fietto *et al*., 2004). Here, we compared *S. boulardii* to *S. cerevisiae* in our *in vitro* laboratory setting to evaluate the best candidate in terms of antibiotic degrading LBP potential in relevant growth conditions.

4.5.2 Work

First, we performed a yeast cell count to determine the correlation of optical cell density determined at 640 nm to actual cell density in CFU/mL. To this end, we prepared two dilutions in duplicate from a fresh yeast culture in exponential phase in rich medium and plated these

(100 µL) onto medium-sized petri dishes containing YPDA medium. After 48 hours of growth at 30°C, the number of colonies were counted and the conversion factor for A_{640} = 1 per strain was determined as follows:

S. cerevisiae S150-2B: 1.7×10^7 CFU/mL
S. cerevisiae INVSc1: 1.8×10^7 CFU/mL
S. boulardii: 3.3×10^7 CFU/mL

To further understand the differences in yeast cell densities measured at a 640 nm wavelength, we performed a standard Gram stain on fixed yeast cells that were grown on rich medium agar plates. We immediately observed a difference in morphology and cell size between the three strains and namely between *S. cerevisiae* and *S. boulardii* cells: *S. boulardii* is smaller in cell size and also has a more elongated cell shape whereas *S. cerevisiae* has a rounder cell shape (Figure 4.5.2.2). The differences in cell size and morphology is likely to contribute to the different conversion factor due to different light scattering at 640 nm. Furthermore, *S. boulardii* was also documented to have an enhanced ability for pseudo-hyphal switching as compared to *S. cerevisiae* (Edwards-Ingram *et al*., 2007). Although all yeast strains were grown under the same conditions and prepared on the same microscopic slide, we observed pseudo-hyphae only for *S. boulardii*.

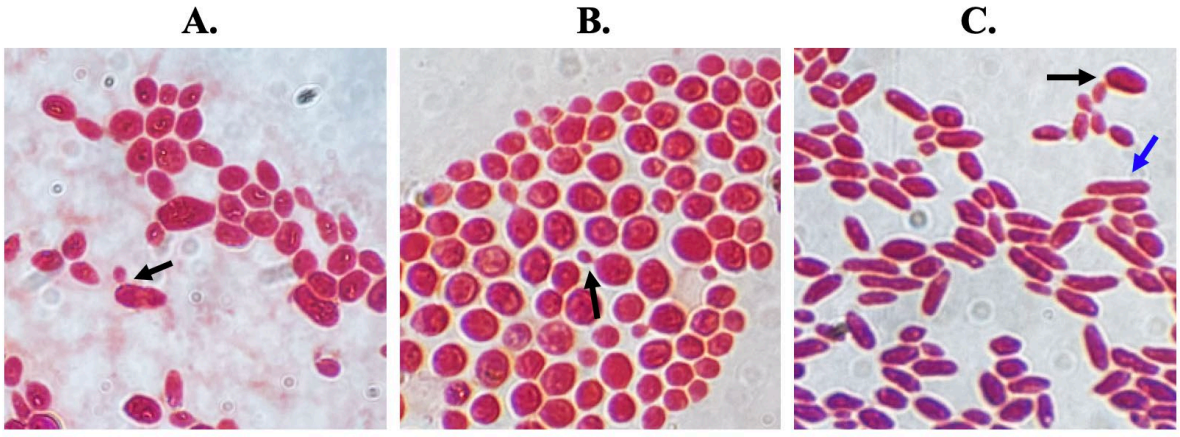

Figure 4.5.2.2: Microscopic images of S. cerevisiae S150-2B (A.), S. cerevisiae INVSc1 (B.) and S. boulardii (C.) after Gram-stain with a 100X oil objective. Examples of budding cells are indicated with a black arrow and pseudo-hyphae with a blue arrow.

Next, we determined the growth and survival of the strains at 37°C. Yeast cells were grown in rich YPD medium under agitation (200 rpm) with a medium-to-flask ratio of 1:8 for 24 hours (Figure 4.5.2.1). All three strains followed a similar growth curve although the *S. cerevisiae* laboratory strains reached earlier saturation around 6×10^7 CFU/mL ($A_{640} \approx 3.5$), whereas *S.*

boulardii was still in its exponential growth phase. Although we had observed high cell densities ($A_{640} > 8$) with the *S. cerevisiae* strains in the same medium at 30°C (data not shown), their reproductive capabilities seem to saturate earlier at a higher temperature.

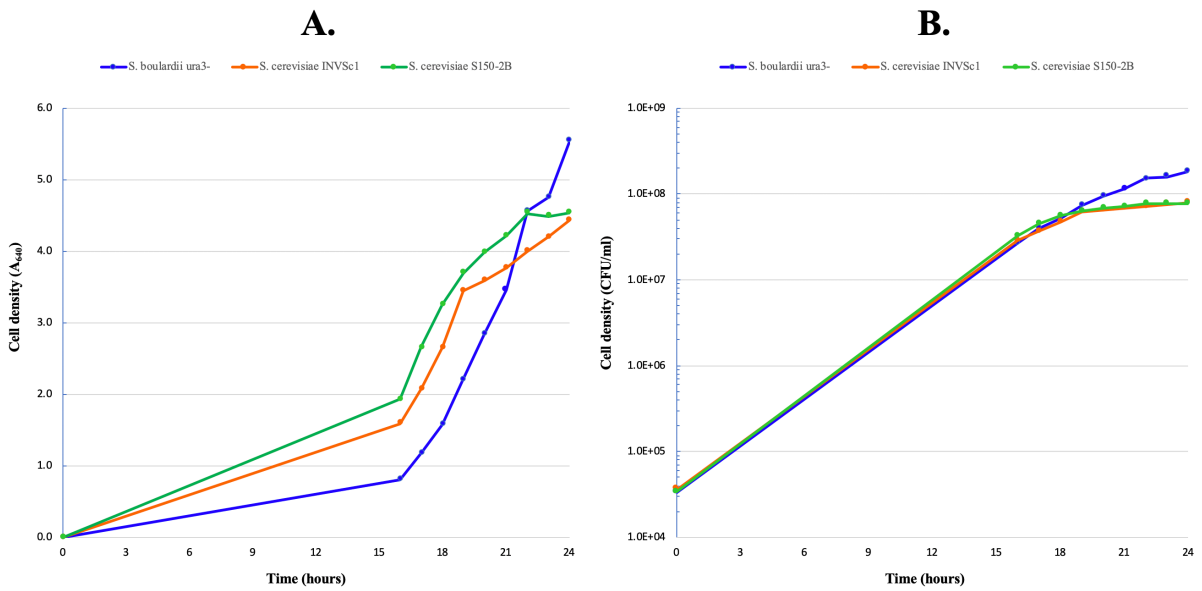

Figure 4.5.2.1: Growth curves of S. boulardii (blue), S. cerevisiae INVSc1 (orange) and S. cerevisiae S150-2B (green) in YPD medium at 37 °C with cell densities reported as A_{640} (A.) or CFU/mL (B.)

Although the two go hand in hand, rather than growth, we are seeking efficient protein expression at 37°C. Therefore, we evaluated the secretion of two metallo-β-lactamase (MBL) enzymes (further discussed in the next subchapter) in all three strains at 37°C (Figure 4.5.2). Since we are aware that enzyme efficiency can greatly change depending on the yeast's growth phase, we solely included activity data from cultures in the exponential phase with a cell density between 10^7 and 4×10^7 CFU/mL. We confirmed that *S. boulardii* was able to grow faster than the *S. cerevisiae* strains and reach higher cell densities (data not shown). Out of the two *S. cerevisiae* strains, we also confirmed that the S150-2B strain was the most efficient producer at 37°C for both enzymes tested. Surprisingly, I8M production with the S150-2B strain was more efficient when grown with limited oxygen distribution (no agitation and a higher medium-to-flask ratio), whereas it seemed to have a slightly limiting effect with the INVSc1 strain. Furthermore, I8M production was found similar between *S. cerevisiae* S150-2B and *S. boulardii*, with a 15 and 22% superior production by S150-2B for I8M and BcII, respectively.

Table 4.5.2: Secreted activity data for two MBL enzymes with three yeast strains in their exponential phase at 37°C, normalized for mg per 10 billion yeast cells. Each data point represents an average of 2 biological replicates, measured in triplicate.

Enzyme	Growth conditions	Activity	
		Yeast strain	(mg/10^{10} cells)
I8M	37°C, agitation (180 rpm), 1:5 (medium:flask)	*S. boulardii*	0.09 ± 0.01
		S. cerevisiae (S150-2B)	[a]0.08 ± 0.01
		S. cerevisiae (INVsc1)	[a]0.08 ± 0.01
	37°C, no agitation, 3:5 (medium:flask)	*S. boulardii*	0.11 ± 0.01
		S. cerevisiae (S150-2B)	0.13 ± 0.02
		S. cerevisiae (INVsc1)	0.06 ± 0.01
BcII	37°C, no agitation, 3:5 (medium:flask)	*S. boulardii*	0.28 ± 0.02
		S. cerevisiae (S150-2B)	0.36 ± 0.06
		S. cerevisiae (INVsc1)	0.16 ± 0.05

[a] Data from one experiment only

4.5.3 Conclusion

Here, we showed that each yeast strain has a different conversion factor from optical density (A_{640}) to CFU/mL. This is also supported by the fact that the cell size and morphology of *S. boulardii* differs from that of the *S. cerevisiae* strains. However, we must note that since we observed mainly pseudo-hyphal *S. boulardii* cells and not budding ones in the Gram-stain, the difference in cell morphology between *S. cerevisiae* and *S. boulardii* might be biased. Pseudo-hyphal switching has been described as a survival mechanism that can take place during nutrient deprivation or challenging conditions. The fact that only the *S. boulardii* cells showed pseudo-hyphal growth, despite having been prepared under the same conditions as the *S. cerevisae* cells, confirms the finding of Edwards-Ingram and colleagues (2007) that *S. boulardii* has enhanced ability for pseudo-hyphal switching, a phenomenon that might contribute to its success as probiotic. Furthermore, *S. boulardii* was clearly better adapted to growth at 37°C compared to the *S. cerevisiae* strains that reached growth saturation much earlier than they usually do at 30 °C. With regards to protein activity at 37°C, we observed similar production with *S. boulardii* and *S. cerevisiae* S150-2B in our *in vitro* laboratory setting, with even slightly better production with the latter. Nevertheless, we continued with *S. boulardii* as expression host since it is presumably the best and most studied yeast for *in vivo* application.

4.6 Production of clinically relevant β-lactamases with probiotic yeast

4.6.1 Background

As already anticipated by the results in the previous subchapter, we further exploited the antibiotic degrading capability of our probiotic with other β-lactamases. Although P3A, a class A β-lactamase, is a strong enzyme candidate regarding stability, it is only active against cephalosporins. Carbapenems on the other hand, are considered the most reliable last-resort drugs since they are highly effective against many Gram-positive and Gram-negative, β-lactam-resistant, bacteria. MBLs, or class B β-lactamases, are bacterial enzymes able to hydrolyze almost all β-lactam antibiotics, including carbapenems by means of zinc ions. Unlike other β-lactamases, MBLs are insensitive to all current β-lactamase-inhibitors (Bush, 2013). We therefore believe that an MBL producing probiotic could be of superior clinical importance and propose the exploration of three different MBLs. The first, named I8M, is an MBL variant previously optimized in our laboratory for biotech companies Da Volterra and Bioaster and described in three different patent families by De Gunzburg & Docquier (US10982205B2, US10988749B2 and US11365403B2). The second is the BcII enzyme from *Bacillus cereus*, the first MBL for which a crystal structure was solved and the most extensively studied MBL (Carfi *et al*., 1995). The last β-lactamase enzyme is an OXA-10 variant in which the β5–β6 loop was replaced by that of OXA-48, abbreviated OXA10L48 from now on, conferring carbapenemase activity to the narrow-spectrum OXA-10 class D β-lactamase (De Luca *et al*., 2011).

4.6.2 Work

The DNA sequences of all three enzymes were codon optimized and interrupted by an artificially inserted intron as was done for the PoC enzyme (Appendices 8.1 and 8.2). These sequences were cloned into pSRD-I-K1 and transformed either episomally or integrated into the chromosome. Secreted β-lactamase activity was assessed in the clarified culture supernatants as previously described with imipenem or nitrocefin as substrate.

I8M

The nucleotide sequence of I8M was yeast optimized using the JCat optimization tool (yI8M) and interrupted by yeast introns PRE3 or EFB1 (iPRE3 and iEFB1). The introns were inserted into the theoretically 'best' or 'worst' position, positions I and II respectively, based on their secondary structure (MFE) at the intron-exon junction. The introns were inserted at positions 283 (position I, MFE = -5.1 kcal/mol) or 322 (position II, MFE = -8.8 kcal/mol), downstream of the HxHxD zinc-binding motif. Like all MBLs, I8M is a zinc-dependent enzyme and we therefore tested the supplementation of different zinc concentrations in YPD medium at 37°C (Table 4.6.2.1). The culture containing 1 mM $ZnSO_4$ did not grow at all, indicating a toxicity for yeast at this concentration. Supplementation of 50 µM $ZnSO_4$ seemed to have the most beneficial impact on yeast growth, although the highest level of I8M production was observed with 250 µM $ZnSO_4$. Noteworthy, we observed a sudden decrease in activity in the cultures with 50 and 250 µM $ZnSO_4$ one time point after the highest level of activity was observed, with complete loss of all activity within three hours of the latter. Furthermore, we did not observe any I8M activity in the culture without zinc despite considerable growth at time point 40.

Table 4.6.2.1: I8M activity in mg/L in the culture supernatants of S. boulardii [pSRD-I-K1-yI8M-iPRE3-I] in YPD medium (37°C) supplemented with different zinc concentrations, calculated with imipenem as substrate (average of three measurement). Growth (A_{640}) is reported between brackets.

Time point (hours)	No $ZnSO_4$	50 µM $ZnSO_4$	250 µM $ZnSO_4$	1 mM $ZnSO_4$
19	bdl[a] (0.1)	0.06 (0.1)	bdl (0.1)	bdl (<0.1)
21	bdl (0.1)	0.09 (0.2)	0.03 (0.1)	bdl (<0.1)
23	nd[b] (0.1)	0.13 (0.2)	0.05 (0.1)	bdl (<0.1)
40	bdl (1.8)	bdl (3.4)	0.72 (2.6)	nd
43	nd	nd	bdl (4.1)	nd

[a] Below detection limit, < 0.01 mg/L
[b] Not determined

To assess whether the sudden decrease in activity could be related to the change in physiological conditions in the cultures over time, we performed stability assays with purified

I8M as was described in chapter 4.4.2 with the addition of a freezing step of the culture supernatant prior to incubation. These results demonstrate a sensibility of the I8M enzyme to acidification of the culture medium and soluble components secreted in the culture medium (Table 4.6.2.2). Heat-inactivation of the culture supernatant, as well as a freezing treatment, prior to enzyme incubation increased residual activity with 30% but did not recover all activity which might indicate the hindrance of a low pH. Therefore, we further investigated the potential beneficial impact of growth in buffered medium.

Table 4.6.2.2: Stability of purified I8M in different buffers and media, reported as % residual activity from baseline (average of three measurements).

pH	Incubation medium	% residual activity	% error
7.5	No incubation (baseline)	100.0	3
7.5	Inc. with HZn	108	3
5.8	Inc. with YPD medium	113	26
5.2	Inc. with YPD culture supernatant	52	7
5.2	Inc. with heat-inactivated YPD culture supernatant	84	1
5.2	Inc. with frozen-treated YPD culture supernatant	83	2

We prepared buffered YP medium with 100 mM Tris-HCl at pH 6.5, 7.0 and 7.5, and measured medium acidification of overnight *S. boulardii* cultures. YPD pH 6.5 acidified to pH = 5.2 (A_{640} = 4.3), YPD pH 7.0 acidified to pH = 6.5 (A_{640} = 3.8) and YPD 7.5 acidified to pH = 6.8 (A_{640} = 3.0). We then assessed protein stability in these media and clarified culture supernatants in these media after 30, 60 and 90 minutes of enzyme incubation (Table 4.6.2.3). I8M was 100% stable in these buffered media for up to 90 min (data not shown). However, in the culture supernatant of YPD pH 6.5, at a pH of 5.2, protein activity decreased immediately after 30 min of incubation and continued to decrease over time. In the culture supernatants of YPD pH 7.0 and 7.5, I8M was stable for up to 90 min. Since *S. cerevisiae* is an acidophilic organism, we chose YPD pH 7.0, from now one abbreviated 'YPD7', over YPD pH 7.5 for future experiments. We then re-evaluated the effect of zinc with up to 250 µM $ZnSO_4$ on *S. boulardii* [pSRD-I-K1-yI8M-iPRE3-I] growth and I8M secretion under optimal yeast growth conditions (medium-to-flask ratio 1:8 at 30°C and under agitation (Figure 4.6.2.1A) to get a better understanding of the impacting factor of zinc on our yeast and under more relevant conditions (medium-to-flask ratio 3:5 at 37°C without agitation, Figure 4.6.2.1B).

Table 4.6.2.3: Stability of purified I8M in culture supernatants of buffered YPD medium, reported as % residual activity from baseline after incubation.

pH	Incubation medium	% residual activity after incubation		
		30 min	60 min	90 min
7.5	Inc. with HZn buffer	87	93	87
5.2	Inc. with culture sup YPD pH 6.5	42	32	23
6.5	Inc. with culture sup YPD pH 7.0	85	111	111
6.8	Inc. with culture sup YPD pH 7.5	86	99	95

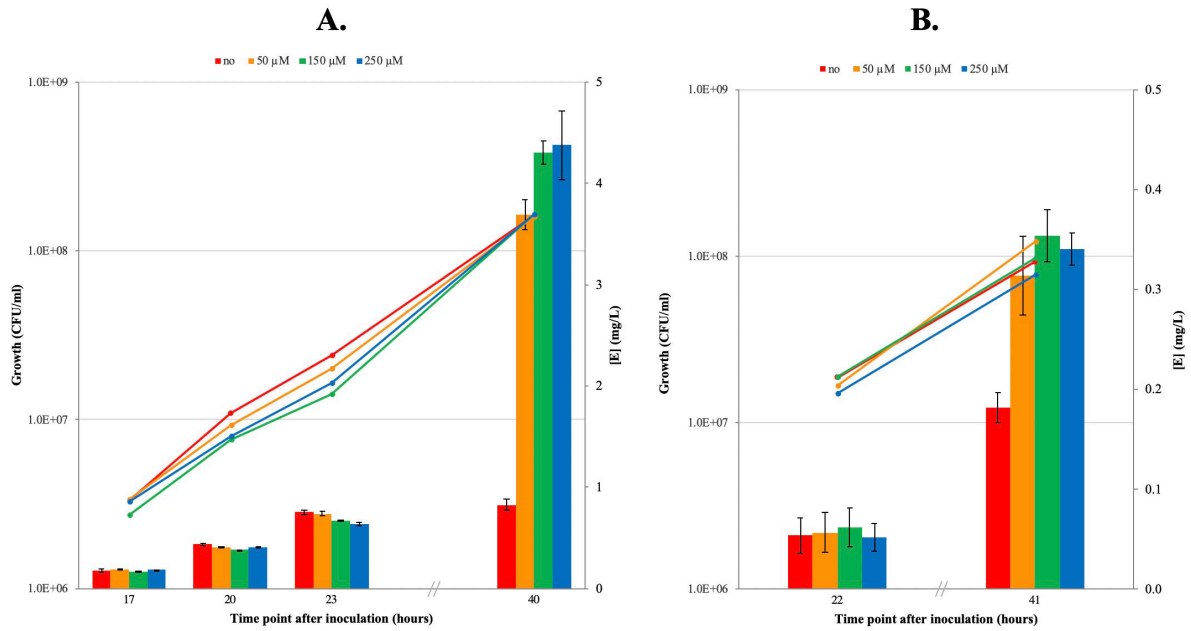

Figure 4.6.2.1: The effect of zinc (0 - 250 µM $ZnSO_4$) on the growth (left y-axis) of S. boulardii [pSRD-I-K1-yI8M-iPRE3-I] and secreted I8M production (right y-axis) in YPD7 medium at A. 30°C with agitation and B. 37°C without agitation, calculated with imipenem as substrate. The activity data of graph A represents an average of three measurements and that of graph B an average of two independent experiments measured in triplicate.

Overall, yeast growth was similar among both experiments although I8M activity was found ~5-fold lower at 37°C with limited oxygen distribution. Furthermore, the necessity of zinc is again confirmed by both experiments and especially at high cell density. While at 30°C I8M production was similar in all cultures for up to 23 hours, at time point 40 the absence of zinc significantly affected I8M activity: the culture without zinc remained at a yield of < 1 mg/L whereas all other cultures reached ~4 mg/L. Moreover, the addition of 250 µM $ZnSO_4$ might slightly delay yeast growth. Overall, we found the impact of zinc to be most beneficial with

regards to growth and production with 50 µM $ZnSO_4$ and therefore used this concentration in further experiments. YPD pH 7.0 medium with the addition of 50 µM $ZnSO_4$ will be referred to as 'YPD7+' medium from now on.

In order to assess the effects of integration, different introns and different intron positions on enzyme secretion, we grew different *S. boulardii* I8M constructs in YPD7+ medium at 37°C with limited oxygen distribution, *i.e.* medium-to-flask ratio 3:4 without agitation, and assessed secreted enzyme production early in growth (Table 4.6.2.4). Surprisingly, all constructs showed similar production yields under these conditions. The biggest difference was observed between the intron-less construct, 0.2 mg/A_{640} and the yeast integrated intron-containing construct, 0.13 mg/A_{640}. Both that can be explained by the fact that the presence of an intron is more energy-consuming and that a chromosomal integrated gene contains only one copy rather than the reported 55 copies of the pRG226 plasmid (Gnügge *et al*., 2016). Furthermore, despite the PRE3 intron showing slightly better activity, its activity was found very similar to that of the EFB1 intron-containing I8M gene. Regarding chromosomal integration, the less than 25% decreased activity compared to the episomal construct, is very encouraging since integration might be preferred in the final LBP to ensure construct stability. Particularly since we observed a >70% loss of plasmid in non-selective culture medium when an overnight culture was spotted onto rich medium and selective medium plates (data not shown).

Table 4.6.2.4: Activity data for different S. boulardii I8M constructs grown to similar cell densities (A_{640} ≈ 0.4) in YPD7+ medium at 37°C (no agitation), calculated with imipenem as substrate. Activity (mg) is normalized per liter of culture or per A_{640} = 1 and data represents an average of two independent experiments measured in triplicate.

Plasmid	Signal peptide	Gene	Intron	Replication	Activity (mg/L)	Activity (mg/A_{640})
pSRD-I	K1	yI8M	-	episomal	0.07 ± 0.01	0.20 ± 0.03
pSRD-I	K1	yI8M	iPRE3-I	episomal	0.07 ± 0.01	0.17 ± 0.02
YIp_SRD-I	K1	yI8M	iPRE3-I	chromosomal (URA3)	0.06 ± 0.01	0.13 ± 0.01
pSRD-I	K1	yI8M	iPRE3-II	episomal	0.07 ± 0.01	0.18 ± 0.02
pSRD-I	K1	yI8M	iEFB1-I	episomal	0.06 ± 0.01	0.16 ± 0.03
pSRD-I	K1	yI8M	iEFB1-II	episomal	0.06 ± 0.01	0.15 ± 0.02

BcII

The nucleotide sequence of BcII was optimized using the Vectorbuilder optimization tool, creating yBcII, and PRE3 intron (iPRE3) was inserted at position 274, downstream of the HxHxD zinc-binding motif. Since BcII is an MBL like I8M, its stability was directly assessed in buffered YPD medium. BcII was completely stable in buffered YPD medium, pH 6.5, 7.0 and 7.5, up to 90 min (data not shown). In the culture supernatants of these buffered media, however, BcII was not stable in cultures grown in YPD pH 6.5 and stability decreased over time as was previously observed with I8M (Table 4.6.2.5). Therefore, zinc supplementation was assessed in YPD7 medium (Figure 4.6.2.2).

Table 4.6.2.5: Stability of purified I8M and BcII in culture supernatants of buffered YPD medium, reported as % residual activity from baseline after incubation.

pH	**Incubation medium**	**% residual activity after incubation**					
		30 min		60 min		90 min	
		I8M	BcII	I8M	BcII	I8M	BcII
7.5	Inc. with HZn buffer	87	88	93	95	87	-
5.2	Inc. with culture sup YPD pH 6.5	42	48	32	42	23	29
6.5	Inc. with culture sup YPD pH 7.0	85	109	111	119	111	127
6.8	Inc. with culture sup YPD pH 7.5	86	118	99	116	95	114

The effect of zinc on BcII secretion at 37°C was similar to that observed with I8M, although production levels were significantly higher (~5-fold). While we observed a slightly negative effect of 250 µM $ZnSO_4$ supplementation on yeast growth with the I8M-producing yeast, this did not seem to be the case with the BcII construct and even resulted in highest BcII activity. Nevertheless, highest activity early in growth was observed with 50 µM $ZnSO_4$ supplementation and, thus, we continued with YPD7+ medium when evaluating the impact of the intron-containing BcII construct and its chromosomal integration. Cultures were grown with limited oxygen distribution at 37°C in YPD7+ medium (Table 4.6.2.6). As observed with I8M, the impact of an artificially inserted intron is trivial (<15%). Surprisingly, however, the impact of chromosomal replication *versus* episomal replication was much more abundant in the BcII constructs. Whereas activity decreased with 35% with chromosomal replication for I8M, it decreased over 80% with BcII.

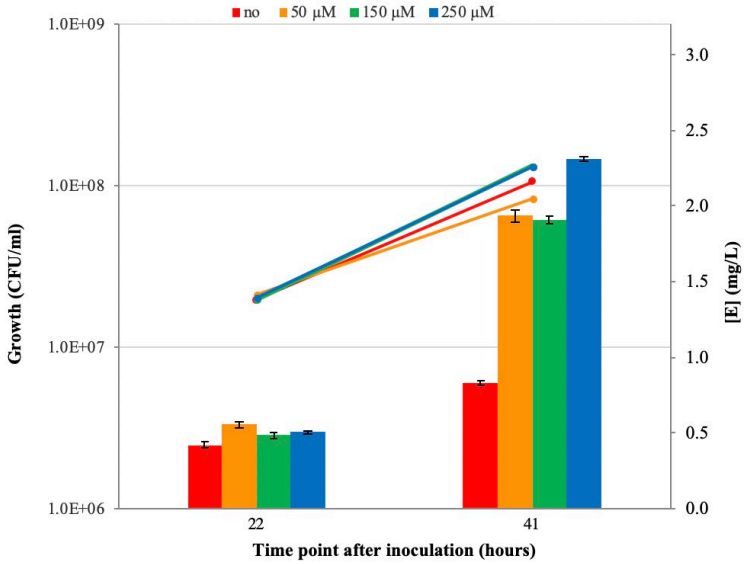

Figure 4.6.2.2: The effect of zinc (0 - 250 µM $ZnSO_4$) on the growth (left y-axis) of S. boulardii [pSRD-I-K1-yBcII-iPRE3-I] and secreted BcII production (right y-axis) in YPD7 medium at 37°C without agitation, calculated with imipenem as substrate. The activity data represents an average of two independent experiments measured in triplicate.

Table 4.6.2.6: Activity data for different S. boulardii BcII constructs grown to similar cell densities (A_{640} ≈ 0.4 or 2.0) in YPD7+ medium at 37°C (no agitation), calculated with imipenem as substrate. Activity (mg) is normalized per liter of culture or per A_{640} = 1.

Plasmid	Signal peptide	Gene	Intron	Replication	Activity (mg/L)	Activity (mg/A_{640})
			A_{640} ≈ 0.4			
pSRD-I	K1	yBcII	-	episomal	[a]0.66 ± 0.05	[a]1.66 ± 0.25
pSRD-I	K1	yBcII	iPRE3-I	episomal	[a]0.66 ± 0.05	[a]1.44 ± 0.03
			A_{640} ≈ 2.0			
pSRD-I	K1	yBcII	iPRE3-I	episomal	[b]1.23 ± 0.01	[b]0.018 ± 0.001
YIp_SRD-I	K1	yBcII	iPRE3-I	chromosomal (URA3)	[b]0.21 ± 0.01	[b]0.003 ± 0.01

[a] Average values of two independent experiments measured in triplicate
[b] Average values of one experiment measured in triplicate

OXA10L48

The nucleotide sequence of the OXA10 variant, OXA10L48, was optimized using the JCat optimization tool, creating yOXA10L48, and PRE3 intron (iPRE3) was inserted at position 205. *S. boulardii* [pSRD-I-K1-yOXA10L48-iPRE3-I] was grown in YPD7+ medium and enzyme activity was assessed in the clarified culture supernatant. Although no significant activity could be detected with imipenem, we did observe significant nitrocefin hydrolysis of 48 ± 5 nmol nitrocefin/min·g.

4.6.3 Conclusion

β-lactams are the most frequently prescribed antibiotics worldwide and, therefore, β-lactamases represent a clinically relevant group of enzymes to be produced by a probiotic yeast. Within the β-lactamases, MBLs are an important class of enzymes as they can degrade carbapenems, a potent group of β-lactams with broad antibacterial activity and are resistant to all current β-lactamase inhibitors.

Here, we demonstrated that our yeast probiotic *S. boulardii* can successfully secrete three different β-lactamases; two MBLs (β-lactamase class B) and one serine β-lactamase (β-lactamase class D). Both MBLs showed significant secreted production in challenging conditions, *i.e.* growth at 37°C with limited oxygen distribution. Compared to I8M, BcII showed superior secretion levels in the culture supernatant: ~ 2 mg/L *versus* ~ 0.4 mg/L. Both enzymes were similarly sensitive to the acidification of the culture medium during growth and showed enzyme stability (up to 90 min) in (acidified) culture supernatants of YPD medium buffered at pH 7.0 or 7.5. Furthermore, the necessity of zinc was not evident in early growth cultures for both enzymes, whereas activity significantly improved a 2-4-fold (depending on the growth conditions) with zinc supplementation at high cell densities. Noteworthy, we demonstrated that our artificial intron insertion design is very flexible. We found similar levels of I8M production with either the PRE3 or EFB1 intron and at position I, hypothetically the best position regarding the secondary structure at the intron-exon junction or position II, hypothetically the 'worst' insertion position regarding the secondary structure at the intron-exon junction. Furthermore, we demonstrated that the presence of an intron does not hinder I8M and BcII production since activity with the intron-less construct was only slightly (~ 15%) more efficient compared to the intron-containing gene, which is very promising for future

construct designs. Interestingly, we observed the loss in activity with chromosomal integration to differ significantly between the two MBLs: <25% for I8M and >80% for BcII. Reason for this is still unclear and needs to be investigated further since chromosomal integration might be preferred in a final LBP. Finally, we demonstrated the successful secretion of an intron-containing OXA10 variant with carbapenems activity. Although we did not detect imipenemase activity in initial experiments, we did measure significant nitrocefin hydrolysis in the culture supernatants which will need to be investigated in further detail.

4.7 Production of a non-β-lactamase antibiotic degrading enzyme with probiotic yeast

4.7.1 Background

After β-lactams, macrolides, together with fluoroquinolones, are the most prescribed drugs in the United States (Bush & Bradford, 2016). For over 70 years, macrolide antibiotics have been used to treat infections in humans and animals. In 1952, erythromycin was introduced as the first macrolide in human medicine and works by inhibiting protein synthesis of susceptible microorganisms through the binding to the 50S subunit of 70S ribosomes (Washington & Wilson, 1985). Ten years after its discovery, chemists have worked on improving the natural drug for enhanced pharmacodynamic properties and, to date, four generations of macrolides have been introduced into clinical use for the treatment of especially respiratory diseases such as (community-acquired) pneumonia (Morar *et al*., 2012). Enzyme-catalyzed inactivation, or more precisely hydrolysis of the macrolactone ring, is one of the major mechanisms of macrolide resistance by macrolide esterases. Currently, five erythromycin esterases exist: EreA, EreA2, EreB, EreC and EreD, the only chromosomally encoded member of the family.

EreA and EreB are most frequently detected in the clinical setting or in environmental isolates, respectively, and share only 25% protein sequence identity. In an extensive study, Morar and colleagues described the enzymatic mechanisms of both enzymes and found superior activity of EreB against the most prescribed macrolides azithromycin, clarithromycin, and erythromycin. Therefore, we optimized the sequence of EreB and investigated its heterologous activity in yeast in the presence of an intron.

4.7.2 Work

In order to understand the flexibility of our system in a macrolide esterase, two construct versions of EreB were created with different optimization methods, different introns and different intron insertion positions. The nucleotide sequence of the EreB gene (accession number X03988) was optimized using the JCat and Vectorbuilder optimization tools, creating yEreB-I and yEreB-II, respectively. Yeast introns PRE3 (iPRE3) and EFB1 (iEFB1) were inserted at positions 142 and 130, respectively, interrupting after the third or first residue of the

active site pocket, respectively, as described by Morar and collogues (2012) (Figure 4.7.2.1 and Appendix 8.2).

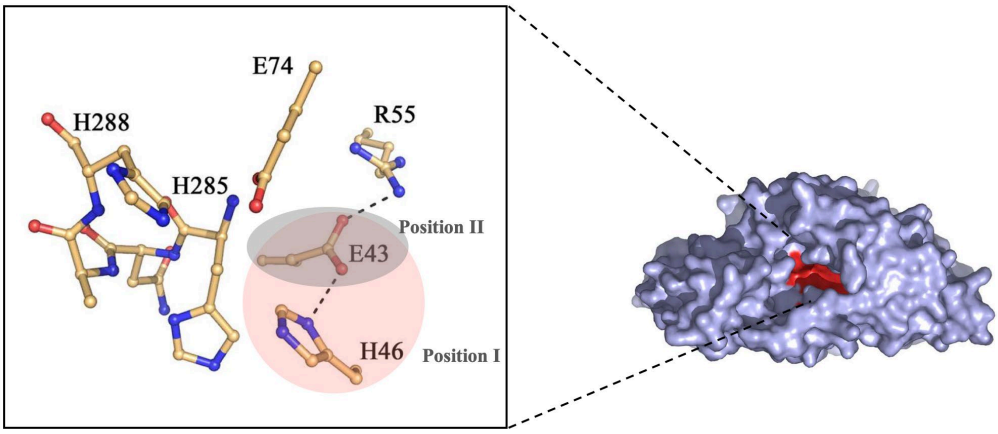

Figure 4.7.2.1: Detailed representation of the described EreB model with strictly conserved residues E43, H46, E74, H285 and H288 in the active site pocket. Theoretical interruption of active site pocket by intron insertion is depicted with a red (position I; 142 nt) and grey (position II; 130 nt) background. Images were adapted from Morar et al., 2012.

EreB production in transformed yeast cells was assessed through an antibiotic diffusion assay with commonly used macrolide erythromycin, and susceptible indicator strain *M. luteus* ATCC 9341. Prior to the assay, we tested the susceptibility of our strain with a range of erythromycin quantities to determine the best dosage for analysis. We measured the growth inhibition of *M. luteus* (layered on an MHA plate with $A_{640} = 0.015$) for erythromycin (40 ng to 5 µg) on plate and after 18-20 hours of growth at 37°C we observed that erythromycin-inhibited growth is not dose-dependent (data not shown). Nevertheless, we detected the highest dose-dependent sensitivity around 0.2 µg of erythromycin. Therefore, and for technical practices, erythromycin inactivation by EreB in yeast was assessed in 0.06 mg/mL erythromycin, of which 4 µL (containing 0.24 µg erythromycin) was spotted on an *M. luteus* containing plate.

Yeast cultures of *S. boulardii* [pSRD-I] (negative control), [pSRD-I-K1-yEreB-I], [pSRD-I-K1-yEreB-I-iPRE3-I] and [pSRD-I-K1-yEreB-II-iEFB1-II] were inoculated at $A_{640} = 0.01$ and grown in YPD medium at 30°C at 180 rpm for 18 hours with an medium-to-flask ratio of 1:6. Culture supernatant was collected after centrifugation at 15,000 × g for 5 min and cell extracts from a 5 mL pellet were prepared by chemical lysis as described in the Materials & Methods section. Subsequently, 10 µL of 0.3 mg/mL erythromycin was incubated with 40 µL of sample

at 37°C, after which 4 µL of the reaction mixture was spotted on an MHA plate layered with *M. luteus*, immediately (< 5 min), after 30 min and after 5 hours. Two independent experiments were performed and confirmed erythromycin inactivation in the cellular extracts of the yEreB constructs within minutes (Table 4.7.2). Although no quantitative conclusions can be drawn from these results, we did demonstrate an erythromycin-inactivating activity of >0.8 nmol/min in the cellular extracts, or >1.6 nmol/min·g cells.

Despite the presence of a K1 leader sequence upstream of our EreB genes, we did not detect erythromycin inhibition with the culture supernatants, suggesting insufficient periplasmic production. Noteworthy, we observed a precipitation in the incubation mixtures with cellular extracts that increased over time (data not shown). This precipitation, however, was only observed in the incubation mixture with the yeast extracts from *S. boulardii* cells carrying the EreB gene and not in the extracts from the empty vector. Therefore, the precipitation may be an indication of instability of our protein in the CelLytic™ Y Cell Lysis Reagent (see Material and Methods). Furthermore, this precipitation could also explain the limited (~ 5 mm) and droplet-sized growth inhibition observed where the EreB cell lysates were spotted, indicating the toxicity of these precipitates. Furthermore, at 5 hours of incubation, the 'spot'-sized growth inhibition was better observed in these samples than at the beginning of incubation (see Table 7.4.2 and Figure 7.4.2).

Table 4.7.2: M. luteus growth inhibition by erythromycin previously incubated with samples from S. boulardii transformants carrying the empty vector or (intron-containing) EreB gene. Growth inhibition was measured 18-20 hours after spotting.

Construct	**Sample**	**A_{640}**	**Inhibition zone (mm)**		
			5 min	**30 min**	**5 hours**
Vector only	supernatant	4.7	30	28	22
	pellet		30	30	26
K1-yEreB-I	supernatant	4.5	30	28	22
	pellet		0	0	5*
K1-yEreB-I-iPRE3-I	supernatant	4.6	30	28	22
	pellet		0	0	5*
K1-yEreB-II-iEFB1-II	supernatant	4.4	30	28	22
	pellet		0	0	5*

[a] Limited inhibition observed

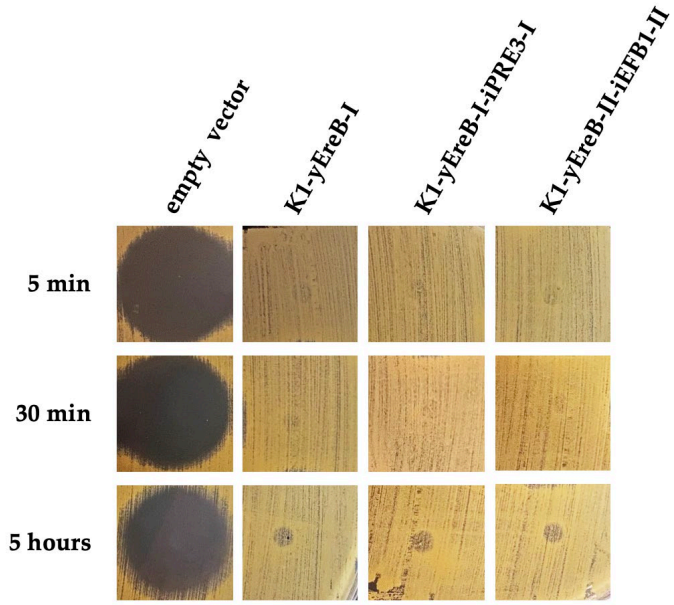

Figure 4.7.2: M. luteus growth inhibition by erythromycin previously incubated with cellular extracts from S. boulardii transformants carrying the empty vector or (intron-containing) EreB gene. Images were taken 48 hours after growth inhibition measurement for optimal visualization.

After overnight storage of the cellular extracts at -20°C, erythromycin incubation was repeated with diluted sample extracts (1:5, in Milli-Q water). Interestingly, the minimal growth inhibition zones of *M. luteus* were less intense in the reaction mixtures containing diluted yeast extract, compared to non-diluted yeast constructs (data not shown). This suggests sensitivity of our protein to components of the commercial lysis reagent and requires further investigation. Furthermore, erythromycin was found to be more stable in the presence of cellular extract compared to culture supernatant since the inhibition zone with the latter (empty vector construct) decreased a 2-fold more after 5 hours of incubation (Table 4.7.2).

4.7.3 Conclusion

With these data, we confirmed the functionality of a macrolide degrading enzyme of bacterial origin in yeast. We also demonstrated that the artificial insertion of two different yeast introns does not obstruct the production of the functional enzyme. To which extent the presence of the introns might influence protein production is unclear. Furthermore, although erythromycin-inactivating activity in the yeast extracts was found to be efficient, no activity was detected in the culture supernatants, which might be due to the low sensitivity of our microbiological assay. Spectrophotometric assays with chromogenic esterase substrate p-nitrophenyl butyrate, for example, could provide more detailed information on secreted protein production levels (Morar

et al., 2012). Nevertheless, with the current findings we added a new enzyme to the repertoire of antibiotic resistance enzyme candidates for our LBP(s) in the prevention of antibiotic-mediated dysbiosis.

4.8 Containment strategy with intron-containing genes

4.8.1 Background

Horizontal gene transfer (HGT), the process of transferring genetic materials between species, takes place in all three domains of life. Especially in bacteria, evolution is mainly driven by HGT, allowing for genome diversification for survival for example. Thanks to the multiple natural genetic tools, such as mobile genetic elements, bacteria can exchange genetic material between strains, species genera, and even higher taxa (intraspecies) (Lerner *et al*., 2017). The wide dissemination of antibiotic resistance genes in bacteria is a well-documented HGT event, providing the bacteria with protection against the pressure of antibiotic selection. In addition, the human intestinal tract provides conditions that are favorable to HGT: *e.g.* the continuous flow of food, high density of the microbiota and an optimal and stable temperature. Intraspecies, or trans-kingdom HGT, however, is very rare and although the transfer of genetic information from bacteria to yeast has been described, the chances of HGT from yeast to bacteria are very small (Moriguchi *et al*., 2013 and Jaramillo *et al*., 2015). Nevertheless, our antibiotic resistance carrying LBPs are designed in a way that they limit the HGT of the resistance genes from the LBP to commensal bacteria and completely prevent the functionality of such resistance enzymes in bacteria in case HGT does occur.

First, the integration of genetic material in the chromosome of yeast prevents easy, if any, access of the genetic information to bacteria. Secondly, by interrupting the resistance genes with a yeast intron, prokaryotic organisms cannot process this information. Since bacteria do not possess the splicing machinery (spliceosome) necessary to remove introns from pre-mRNA and generate the fully mature mRNA, an intron-containing gene disrupting the catalytic site in bacteria can theoretically never result in a functional protein. In the previous subchapters we have already demonstrated that the highly regulated process of RNA splicing can successfully take place in our yeasts with antibiotic resistance genes containing artificially inserted introns. Here, we provide further evidence for the non-functionality of the same intron-containing genes in bacteria.

4.8.2 Work

In order to assess the functionality of the yeast optimized genes with artificial intron in case of potential HGT, we cloned the entire gene into an *E. coli* expression vector by means of restriction enzyme cloning. More specifically, *Nde*I and *Bam*HI sites were added on the external ends of our genes (5' and 3' respectively) by means of PCR (See Table 3.3.7.2 in the Materials & Methods section for primer sequences used) and cloned into the MCS of the pET9a expression vector with the same restriction sites. The pET9a vector is a T7 expression system allowing for high-level expression of recombinant proteins thanks to the strong bacteriophage T7 promoter (Novagen). The *E. coli* BL21(DE3) strain carries an inducible T7 RNA polymerase and therefore allows for controllable protein production levels in an efficient manner. Table 4.8.2.1 contains an overview of all the bacterial expression vectors used in this study. After transformation of the pET9a construct into BL21(DE3), cells were grown to high cell density in P-0.5G medium and inoculated into ZYP5052 to allow for auto-induction of protein production overnight (see Materials & Methods section).

Our PoC enzyme, P3A, was assessed for cytoplasmic production in *E. coli* with the bacterial gene (positive control) and the yeast optimized gene, with and without PRE3 intron (Table 4.8.2.2). The empty vector was included as negative control. Cell lysates were obtained using using the FastBreak™ Cell Lysis Reagent in HZn buffer (Promega, See Materials & Methods section). Enzyme activity was calculated using ampicillin as substrate or nitrocefin for more sensitive hydrolysis measurements. Here, we observed that in the *E. coli* cells containing the intron-containing gene, no P3A activity could be detected, suggesting improper processing of the genetic information. Surprisingly, however, we found higher activity levels with the intron-less yeast-optimized P3A gene in bacteria compared to the original bacteria-originating gene (positive control).

Table 4.8.2.1: Overview of the bacterial expression constructs created in this study. Color shading indicates expressed protein with in grey the empty vector only, green P3A, blue I8M, yellow BcII and purple EreB.

Strain	Replication system	DNA construct
E. coli BL21(DE3)	episomal	[a]pET9 (empty vector)
E. coli BL21(DE3)	episomal	[a]pET9-bP3A
E. coli BL21(DE3)	episomal	pET9-yP3A-I
E. coli BL21(DE3)	episomal	pET9-yP3A-I-iPRE3
E. coli BL21(DE3)	episomal	pET9-yI8M
E. coli BL21(DE3)	episomal	pET9-yI8M-iPRE3-I
E. coli BL21(DE3)	episomal	pET9-yI8M-iPRE3-II
E. coli BL21(DE3)	episomal	pET9-yI8M-iEFB1-I
E. coli BL21(DE3)	episomal	pET9-yI8M-iEFB1-II
E. coli BL21(DE3)	episomal	[a]pET9-bBcII
E. coli BL21(DE3)	episomal	pET9-yBcII
E. coli BL21(DE3)	episomal	pET9-yBcII-iPRE3
E. coli BL21(DE3)	episomal	pET9-yEreB-I
E. coli BL21(DE3)	episomal	pET9-yEreB-I-iPRE3-I

[a] Previously available in our laboratory

Table 4.8.2.2: Cytoplasmic activity data (average of triplicate measurement) of (yeast optimized) P3A gene, with or without intron, expressed in E. coli BL21(DE3) in rich autoinduction medium (ZYP5052) after 24 hours of growth, with ampicillin or nitrocefin as substrate.

Plasmid	Signal peptide	Gene	Intron	Activity (mg/L)
pET9a	-	-	-	[ab]bdl
pET9a	-	bP3A	-	543 ± 34
pET9a	-	yP3A-I	-	860 ± 228
pET9a	-	yP3A-I	iPRE3-I	[b]bdl

[a] Below detection limit, < 0.01 mg/L
[b] Activity measured with nitrocefin as substrate

As with P3A, we also confirmed the non-functionality of an intron-containing gene in MBLs I8M and BcII (Tables 4.8.2.3 and 4.8.2.4). With I8M, we found evidence suggesting that the intron choice and intron position are insignificant in the prevention of enzyme functionality in bacteria since no activity was observed with neither intron PRE3 nor EFB1, and regardless the insertion position. Although significant production levels were obtained with both the original and yeast-optimized I8M gene, we found a yield of 3.5-fold lower in the yeast-optimized gene. For BcII, we confirmed the absence of activity in the yeast optimized intron-containing gene *versus* the yeast optimized intron-less gene.

Table 4.8.2.3: Cytoplasmic activity data (average of triplicate measurement) of (yeast optimized) I8M gene, with or without intron, expressed in E. coli BL21(DE3) in rich autoinduction medium (ZYP5052) after 24 hours of growth, with imipenem as substrate.

Plasmid	Signal peptide	Gene	Intron	Activity (mg/L)
pET9a	-	-	-	bdl[a]
pET9a	-	bI8M	-	145 ± 2 [b]
pET9a	-	yI8M	-	41 ± 3
pET9a	-	yI8M	iPRE3-I	bdl
pET9a	-	yI8M	iPRE3-II	bdl
pET9a	-	yI8M	iEFB1-I	bdl
pET9a	-	yI8M	iEFB1-II	bdl

[a] Below detection limit, < 0.01 mg/L
[b] Sample collected after 18 hours of growth

Table 4.8.2.4: Cytoplasmic activity data (average of triplicate measurement) of yeast optimized BcII gene, with or without intron, expressed in E. coli BL21(DE3) in rich autoinduction medium (ZYP5052) after 22 hours of growth, with imipenem as substrate.

Plasmid	Signal peptide	Gene	Intron	Activity (mg/L)
pET9a	-	-	-	bdl[a]
pET9a	-	yBcII	-	138 ± 3
pET9a	-	yBcII	iPRE3-I	bdl

[a] Below detection limit, < 0.05 mg/L

In the case of the EreB macrolide esterase, we made use of the antibiotic diffusion assay previously described to assess cytoplasmic protein production in *E. coli*. Cellular lysates were prepared by means of sonication in HZn buffer (see Materials & Methods section) and the empty vector was included as negative control. In the case of EreB we also did not detect any

inactivating activity when an intron was included in the gene (same growth inhibition as observed with empty vector). However, antibiotic degrading activity in *E. coli* was of substantial proportion with the yeast optimized gene without intron since immediate (< 5 min incubation) inactivation of erythromycin was observed, even when the sample was diluted a 100-fold, corresponding to a specific activity of >400 nmol/min·g cells.

Table 4.8.2.4: Erythromycin inactivation of yeast optimized EreB gene, with or without intron, expressed in E. coli BL21(DE3) in rich autoinduction medium (ZYP5052) after 24 hours of growth and 5 min or 4 hours of incubation with erythromycin.

Plasmid	Signal peptide	Gene	Intron	Inhibition zone (mm)	
				5 min	4 hours
pET9a	-	-	-	27	25
pET9a	-	yEreB-I	-	0*	0*
pET9a	-	yEreB-I	PRE3-I	27	25

*The same observation was made when the sample was diluted up to 1:100 prior to incubation with erythromycin

4.8.3 Conclusion

These findings confirm our hypothesis that while the artificial insertion of a yeast intron may lead to efficient (or improved) protein production levels in yeast, it prevents any protein activity in bacteria. Our results also show that yeast codon optimization of a gene does not necessarily limit its efficiency in bacteria, as was observed with P3A, but rather depends on the enzyme. P3A is a Bacillus-originating enzyme, a genus known for its production of robust enzymes that can withstand many physiological conditions. I8M, on the other hand, is a variant of an enzyme discovered in the clinical setting. The origin of both enzymes might therefore explain their different flexibilities in different hosts. BcII also originates from the Bacillus genus and, therefore, its production in *E. coli* could be compared with the yeast optimized BcII gene to confirm this hypothesis. Finally, we also demonstrated the containment property of the artificially inserted intron with EreB. These experiments validate the most unique aspect of our LBP design: the safety in using the heterologous production of antibiotic resistance enzymes for the purpose of eliminating antibiotic traces in the gut.

4.9 Enzyme production with probiotic yeast in SHIME®

4.9.1 Background

In order to further assess the functionality of our yeast probiotics, beyond our *in vitro* laboratory setting, we made use of a commercial gut simulation model, SHIME® (Simulator of Human Intestinal Microbial Ecosystem, Van de Wiele *et al*., 2015). The SHIME® model is provided by a pre-clinical CRO (contract research organizations) ProDigest (Gent, Belgium) and has been developed after more than 15 years of research. The SHIME® technology artificially simulates the physiological, chemical and microbiological properties of the gastrointestinal tract and has been considered as a 'clinical trial *in vitro*'. Furthermore, in addition to mimicking *in vivo* parameters such as temperature, intestinal volumes, enzyme concentrations, feeding cycles and pH, the SHIME® model also simulates microbial diversity across the gut compartments using human fecal material. Since the SHIME® model was previously described with yeasts *S. cerevisiae* and *S. boulardii* in gastrointestinal studies, it was presumed to be a suitable model for our research as well (Roussel *et al*., 2021 and Duysburgh *et al*., 2021).

For initial studies, we made use of a simplified version of the SHIME system, the "short-term colon" that could allow for easy scalable *in vitro* data. This model differs from the SHIME in that it includes the colon compartment only, rather than the entire system from stomach to colon. In this model, samples can be monitored in 50 mL reactors for up to 48 hours providing insights into the kinetics of our LBP with the colonic simulation over time.

4.9.2 Work

The first LBP candidates that were selected for analysis were *S. boulardii* [pSRD-I-K1-I8M-PRE3], [pSRD-I-K1-BcII-PRE3] and [YIp_SRD-I-K1-I8M-PRE3-I]. Initially, we had designed three different LBP dosages of 10^9, 10^8 and 10^7 CFU/mL to be tested, considering the current dosage of the *S. boulardii* probiotic (5-20×10^9 CFU daily, Codex®) and the size of the small intestine. However, in the current laboratory set-up it was not possible to reach such high levels of growth in selective medium (data not shown). Therefore, we went for the alternative dosages of 10^6 and 10^7 CFU/mL prepared from concentrated frozen stocks (-80°C, 15% (v/v) glycerol) that were washed with phosphate-buffered saline (PBS) prior to inoculation and an

additional dosage of 10^7 CFU/mL prepared freshly from cells grown on selective agar plates. Actual inoculum sizes were determined using the PMA-qPCR method prior to freezing or spiking of the reactor (fresh inoculum). To maximize production levels, 50 µM $ZnSO_4$ was added to the 50 mL reactors. Furthermore, we selected the fecal microbiome of a single donor (donor A) that was previously screened for endogenous imipenem hydrolyzing activity. The fecal microbiome was added to the reactors at a concentration of 7 g/L from a 10% cryostock (corresponding with an initial concentration of approximately 10^8 - 10^9 cells/mL). The positive controls (PC) contained the purified enzymes (final concentration 10 mg/L) for stability assessment and the negative controls (NC) contained no LBP or purified enzyme in the reactors. A total of fourteen conditions were tested and reactors were incubated under anaerobic conditions for 48 hours at 37°C, under limited agitation (90 rpm). Samples were collected (flash-frozen with liquid nitrogen and stored at -80°C) upon inoculation and 1, 2, 4, 6, 24 and 48 hours after incubation.

Quantification of viable yeast cells was measured by means of the propidium monoazide (PMA) qPCR method described by Moens *et al*. (2019). Quantification of β-lactamase production was performed by spectrophotometric assays using imipenem as substrate. A further protein quantification method was applied with the integrated I8M construct. In this reactor meropenem was added (final concentration 0.3 mg/mL) after 24 hours of incubation. The potential inactivation of meropenem was assessed through an antibiotic degradation assay, in which the residual meropenem concentration in the reactor was estimated based on the growth inhibition of *B. subtilis* and the growth inhibition with known meropenem concentrations (see Materials & Methods, time points 24 and 48 hours only). An overview of the experimental design and actual inoculation sizes (colony count from stocks) can be found in Table 4.9.2.1. All experiments and analyses were performed by ProDigest in Belgium after transfer of yeast material and β-lactamase quantification methods. A set of samples were, additionally, analyzed in our laboratory for verification after shipment of the flash-frozen samples from Gent to Siena.

Table 4.9.2.1: Overview of the 14 conditions tested by ProDigest with the short-term colon simulation model.

Condition/ reactor	*S.b.* I8M (CFU/mL) [a]	*S.b.* BcII (CFU/mL) [a]	*S.b.* YI_I8M (CFU/mL) [a]	MEM (mg/mL)	I8M (mg/mL)	BcII (mg/mL)
1 (NC)[b]						
2	9.5×10^5 (I)					
3	9.5×10^6 (II)					
4	2.7×10^7 (III)					
5		1.0×10^6 (I)				
6		1.0×10^7 (II)				
7		2.0×10^7 (III)				
8			1.3×10^6 (I)			
9			1.3×10^7 (II)			
10			1.5×10^7 (III)			
11			1.3×10^6 (II)	0.3		
12 (NC)				0.3		
13 (PC)					0.01	
14 (PC)						0.01

[a] Desired yeast concentration were: 10^6 (I) and 10^7 (II) CFU/mL from cryostock and 10^7 (III) CFU/mL prepared freshly from plate

[b] NC is negative control and PC is positive control

Prior to the short-time colon study, the PMA-qPCR method was validated for our yeast. Each *S. boulardii* strain was inoculated at a certain concentration in the presence of colon medium with microbiota. Table 4.9.2.2 shows that the primers used, targeting the 26S rRNA gene of *S. cerevisiae,* were specific enough for our yeast and that no other *S. cerevisiae* were detected in the colon medium with microbiota (Moens *et al*., 2015 and Chang *et al*., 2007). Furthermore, but not surprisingly, we observed discrepancies between the number of countable cells and the estimated number of cells with the PMA-qPCR method. In this set-up, the concentration obtained with the PMA-qPCR is systematically ~ 1 log higher. Reason for this may be due to the presence of multiple 26S gene copy numbers or viable but non-culturable (VBNC) cells, that are also detected with PMA-qPCR. The latter is a known limitation of PMA-qPCR when comparing it to the colony-counting technique (Navarro *et al*., 2020). Nevertheless, it was confirmed that the growth of our yeast can be evaluated in various media using this method.

Table 4.9.2.2: Preliminary evaluation of PMA-qPCR with our yeast strains in the physiological conditions of the short-term colon model.

Inoculation of colon medium with microbiota	**CFU count (CFU/mL)**	**PMA-qPCR (copies/mL)**
none	-	< LoQ[a]
S. b. I8M	1.4×10^6	5.1×10^7
S. b. BcII	2.1×10^6	5.0×10^7
S. b. YI_I8M	2.7×10^6	3.8×10^7

[a] Limit of quantification

Yeast growth in short-term colon model

We observed limited growth of the yeast in the short-term colon model. Overall, we observed similar patterns for all three strains and with all three inoculum sizes: a short period of growth between 2-6 hours after incubation, followed by a decrease in cell number back to the initial level after 48 hours (Figure 4.9.2.1). The addition of meropenem did not alter yeast growth as a similar curve was observed to that of the reactor containing no meropenem (data not shown). Furthermore, the most significant increase in cell number, ~1 log, was observed with the lowest inoculum sizes of 10^6 CFU/mL. With 10^7 CFU/mL, the yeast cells only increased ~ 0.5 log in the first six hours. We should mention, however, that between 6 and 24 hours no time samples were collected which could have provided us with additional information regarding the growth/survival of our yeast. Nevertheless, despite the limited cell growth, we did observe survival of our yeast for up to 48 hours in the artificial colon.

In preliminary studies we evaluated the loss of viable, or rather countable, cells during the freezing process of the concentrated yeast stocks in 15% (v/v) glycerol and found that this amount can be close to 50% (data not shown). We therefore hypothesized that the presence of non-viable cells in the culture might hinder yeast growth. However, we did not find any evidence to support this theory since these cells behaved similar to the freshly prepared cells.

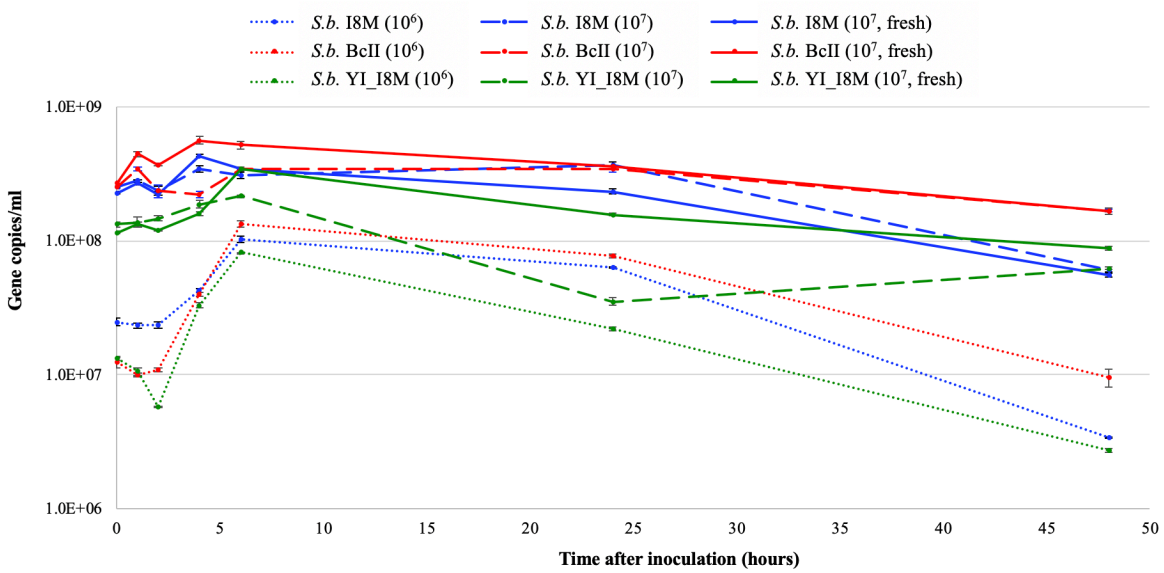

Figure 4.9.2.1: Survival (gene copies/mL) of our yeast strains (episomal I8M in blue, integrated I8M in green and episomal BcII in red) in the short-term colon model over 48 hours with three different inoculum preparations (CFU/mL between brackets). Data points represent an average of a triplicate measurement and error bars represent the standard deviation.

β-lactamase stability in short-term colon model

The stability of purified I8M and BcII was evaluated in the challenging conditions of the colon model at a starting concentration of 10 mg/L. Considering that the activity assays were performed by ProDigest in Belgium in a 96-well set-up, after implementation of our protocol, a number of samples were additionally measured in our laboratory, both in a 96-well set-up and a 1-cm cuvette. Overall, the activity data measured by ProDigest was similar to that measured in our laboratory (Tables 4.9.2.3 and 4.9.2.4), confirming stability of both enzymes in the simulated colon. I8M was stable for up to 6 hours, whereas BcII was active for up to 48 hours.

Table 4.9.2.3: Stability of purified I8M in short-term colon model over time. Activity data (average of triplicate measurement) was determined at ProDigest or at the University of Siena (limited number of samples) from flash-frozen samples in a 96-well format or a 1-cm cuvette, with imipenem as substrate.

Time after inc. (hours)	[I8M] mg/L ProDigest (96-well)	[I8M] mg/L UniSi (96-well)	[I8M] mg/L UniSi (1 cm cuvette)
0	10.6 ± 0.2	10.7 ± 0.7	12.1 ± 0.1
1	9.2 ± 0.4	nd[a]	nd
2	10.4 ± 0.1	nd	nd
4	9.8 ± 0.5	nd	nd
6	9.4 ± 0.4	9.3 ± 0.1	8.4 ± 0.1
24	bdl[b]	bdl	bdl
48	bdl	nd	nd

[a] Not determined
[b] Below detection limit

Table 4.9.2.4: Stability of purified BcII in short-term colon model over time. Activity data (average of triplicate measurement) was determined at ProDigest or at the University of Siena (limited number of samples) from flash-frozen samples in a 96-well format or a 1-cm cuvette, with imipenem as substrate.

Time after inc. (hours)	[BcII] mg/L ProDigest (96-well)	[BcII] mg/L UniSi (96-well)	[BcII] mg/L UniSi (1 cm cuvette)
0	10.7 ± 0.3	9.5 ± 0.1	10.3 ± 0.4
1	10.1 ± 0.7	nd[a]	nd
2	11.5 ± 0.6	nd	nd
4	10.5 ± 0.8	nd	nd
6	12.2 ± 0.9	9.7 ± 0.1	10.3 ± 0.1
24	6.4 ± 1.7	3.6 ± 0.2	6.1 ± 0.1
48	9.1 ± 0.3	nd	nd

[a] Not determined

β-lactamase production in short-term colon model

β-lactamase production in the reactors was evaluated in the clarified supernatants 0, 1, 2, 4, 6, 24 and 48 hours after inoculation. Analysis by ProDigest and our laboratory confirmed that, as with the negative controls, no β-lactamase was detected in any of the reactors containing yeast, except for the reactor containing freshly prepared *S. boulardii* [pSRD-I-K1-I8M-PRE3-I]

(Figure 4.9.2.2). In this reactor, however, we observed immediate activity that slowly decreased over 6 hours and eventually disappeared after 24 hours. Considering the immediate activity observed at time point 0 and the disappearance of activity after the 6th time point, we believe that the initial I8M activity originated from the cells that were freshly collected from plate and inoculated into the reactor without prior wash step. This activity, however, was only observed for the episomal I8M strain and not for the episomal BcII or chromosomal I8M strains, suggesting the episomal I8M construct as the most efficient extracellular β-lactamase producer on agar.

Potential β-lactamase production was additionally evaluated with a meropenem-inactivation model. Meropenem was added to the reactor containing the integrated I8M construct 24 hours after incubation and after an additional 24 hours (time point 48) culture sample was collected, spiked with 5 mM EDTA, to inactivate the potential presence of the MBL enzyme, and flash-frozen as described above. Residual meropenem activity was evaluated using *B. subtilis* as indicator strain. Table 4.9.2.5 shows the estimated meropenem concentrations in the reactors with and without (negative control) the yeast strain. While degradation of meropenem was detected after 24 hours (residual activity of 30%), there was no significant difference in the activity detected in the negative control containing no yeast, or the reactor with our integrated I8M construct.

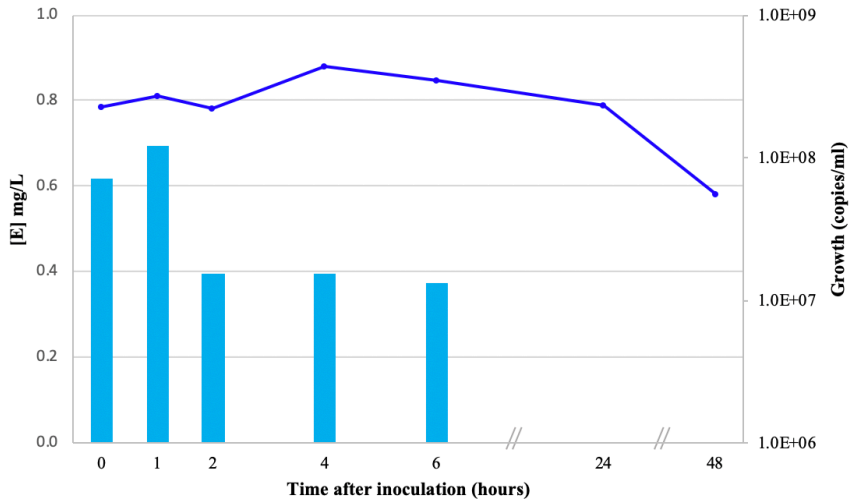

Figure 4.9.2.2: I8M activity (left y-axis) and yeast growth (with PMA-qPCR, right x-axis)) over time in the reactor containing freshly prepared S. boulardii [pSRD-I-K1-I8M-PRE3]. Activity represents an average of two dilutions measured in triplicate with imipenem as substrate and growth represents an average of a triplicate measurement.

Table 4.9.2.5: Meropenem degradation in the short-term colon reactors containing no yeast or YI_I8M. Data represents an average of a biological duplicate, measured in triplicate.

Time point	Meropenem concentration (mg/mL)	
	No yeast (NC)	*S.b.* YI_I8M
24	0.36 ± 0.07	0.33 ± 0.05
48	0.10 ± 0.03	0.10 ± 0.02

4.9.3 Conclusion

For the first time, we evaluated the growth and production of three LBP candidates outside of our laboratory setting, in a colon simulation model. The main conclusions drawn from this preliminary experiment is that our experimental set-up was not designed in an optimal manner. Our observations suggest that the quantity of yeast cells that were inoculated in the reactors was too high. The largest increase in cell number, about one log, was observed with our lowest yeast dose of 10^6 CFU/mL in the reactor. At 10^7 CFU/mL, we merely observed survival, regardless of the inoculum preparation. This indicates that the colon model might have been too occupied to allow for the growth of our yeast, Future experiments should inlcude lower starting inoculums to validate this theory. Furthermore, since limited or no cell growth was observed, it was not surprising that we did not detect any enzyme activity in any of the conditions tested. The limited activity detected in one of the reactors was most likely present due to the lack of a washing step in the fresh inoculum prepared from plate. Nevertheless, these results are encouraging as they confirm the stability of I8M produced by yeast to that of purified I8M in the colon model (*i.e.* stability for up to six hours). Furthermore, we determined a higher stability of purified BcII in the colon model, compared to I8M. Nevertheless, if a continued enzyme production can be achieved through multiple LBP administrations a day, the prolonged stability of BcII does not necessarily provide an advantage over I8M. Furthermore, the absence of protein production was also confirmed by the meropenem degradation assay in which the degradation of meropenem was attributed by the physical conditions in the reactor rather than carbapenemase production by the yeast. Overall, the preliminary short-term colon experiments leave us inconclusive on the functionality of our LBPs and needs further investigation and/or optimization with the SHIME® model(s).

4.10 Enzyme production with probiotic yeast in caecal *ex vivo* medium

4.10.1 Background

In the previous subchapter, we found that it can be challenging to design a suitable SHIME® experiment. The lack of full understanding of the patented and artificial intestinal model limits us in our rational experimental design and interpretation of the data. Therefore, we opted for a different experimental approach in our laboratory, under *ex vivo* conditions. To this end, we evaluated the production of our LBP in extracts of pig caecal samples. Pig models are widely excepted models in gastrointestinal research as they share a great deal of anatomic and physiological similarities with humans (Lunney *et al.* 2021). Their natural omnivorious diet contributes to the many macroscopic and microscopic resemblances between the pig's and human's gastrointestinal tract. Furthermore, just as humans, pigs are colon fermenters for example, in contrast to rodents that ferment within their caecum (Rose *et al*., 2022). In addition, several studies have reported the beneficial impact of *S. boulardii* supplementation in pigs (Bontempo *et al*., 2006, Collier *et al*., 2011 and Zhang *et al*., 2020).

The caecum content of seven pigs was pooled and homogenized, prior to storage at -80°C (Phatophy, Marcy-l'Étoile, France). The piglets were 22 weeks old and on a vegetarian non-medicated (without antibiotic and/or antiparasitic treatment) diet. The pH of the pooled caecal samples, measured on site, was 5.6. Aliquots of these samples were subjected to an extraction process in which the growth and β-lactamase production of yeast was evaluated.

4.10.2 Work

Prior to growth and production assessments of our yeasts with these caecal samples, the presence of endogenous β-lactamases was determined in the individual caecal samples (n=7, Da Volterra, France). Amoxicillin degradation assays revealed the presence of significant levels amoxicillin degrading enzymes in all samples: almost complete degradation of amoxicillin was observed within an hour of incubation with caecal material (1:1 (v/v) with 0.2 mg/mL amoxicillin, data not shown). However, we did not detect carbapenamase activity in our assays with the caecal extracts (CE). CE were prepared from the frozen pooled caecal samples by incubation with sterile Milli-Q water (1:1 dilution, 1 g/mL), clarification and filter-

sterilization (see Materials & Methods section). A ceacal aliquot of 6 mg would typically yield about 5.5 mL of sterile CE. The resulting *ex vivo* medium was measured for acidity, using pH strips, and conductivity, using the conductivity detector of a Fast Protein Liquid Chromatograph (FPLC, Amersham Pharmacia Biotech, GE Healthcare, Chicago, Illinois, U.S.) and had the following characteristics: pH ≈ 6 and conductivity = 7.2 mS/cm, equal to about 100 mM NaCl. The CE was further characterized by assessing enzyme stability (purified I8M) in aliquots stored at 4°C or -80°C (Table 4.10.2.1). Although the difference in enzyme stability between the differently stored CE aliquots was neglectable, we did observe better activity after four hours of incubation in the CE stored at -80°C. Therefore, all CE aliquots were stored at -80°C directly after preparation.

Table 4.10.2.1: Stability of purified I8M in caecal extract (CE) stored at 4°C or -80°C, reported as % residual activity from baseline with % error between brackets. Activity data was measured in triplicate with imipenem as substrate.

Incubation time (hours)	**HZn + BSA (control)**	**CE (4°C)**	**CE (-80°C)**
0	100 (6%)	100 (4%)	100 (5%)
1	106 (3%)	93 (11%)	92 (3%)
4	108 (5%)	72 (2%)	85 (1%)

We assessed growth and enzyme production of the *S. boulardii* [pSRD-I-K1-I8M-PRE3] strain for the first time under anaerobic conditions in our laboratory. As controls, we also included rich buffered YP7 medium, the colon SHIME medium from the previous subchapter (provided by ProDigest without any supplementation) and SHIME medium supplemented with 5% CE to combine the colon simulation medium with physiological properties of the pig caecal samples. Anaerobiosis was created in an Oxoid anaerobic jar (3.5 L, Thermo Scientific) with Oxoid AnaeroGen sachet (3.5 L, Thermo Scientific) and anaerobiosis was confirmed using Oxoid resazurin anaerobic indicators (Thermo Scientific). In order to understand the requirements of our yeast in the abovementioned media, we additionally tested the following variables in the presence or absence of 10 mg/L ergosterol:

- No supplementation
- 50 µM $ZnSO_4$
- 2% (w/v) D-glucose
- $ZnSO_4$ + D-glucose

Contamination controls, containing medium only, or medium with supplementation of ergosterol, zinc and glucose, were included for all media tested. Wells (except for the contamination controls) were seeded at 10^5 CFU/mL in a total volume of 200 µL in a round-bottom 96-well plate and yeast was grown statically at 37°C under anaerobiosis. After 48 hours of incubation, the cell suspension was used for colony counting and the clarified supernatants (through sedimentation) were assessed for β-lactamase production using imipenem as substrate. Cell growth was estimated by colony counting: 5 µL spots of a dilution series of the cell suspension were incubated on YPD agar plates at 30°C for 48 hours. Table 4.10.2.2 shows the CFU counts of one experiment only and Table 4.10.2.3 the enzyme activity data of two independent experiments measured in triplicate. Although the CFU counts are solely estimative, it does give reason to believe that our initial inoculum size was ~5×10^4 CFU/mL rather than 10^5 CFU/mL since no visual growth nor enzyme production was observed in the wells containing YP7 or SHIME medium without glucose. Indeed, in these media growth was only observed (colony counting) in the wells containing glucose. In the wells containing CE medium, a minimal amount of growth, about one log more than the initial inoculum size, was observed with all conditions. Furthermore, yeast grew to minimal extent in the SHIME+CE medium without glucose, whereas the best growth in all test conditions was observed in the cells containing glucose: about two logs increase from initial inoculum size. The supplementation of ergosterol or zinc did not have a significant beneficial impact on yeast growth. Furthermore, we should note that since the colonies were spotted on non-selective medium, the estimated CFU counts likely include plasmid-containing and plasmid-less yeasts.

Table 4.10.2.2: Estimated yeast growth (CFU/ml) in the culture suspension extracted from countable dilutions on plate.

Ergosterol	$ZnSO_4$	D-glucose	CE	SHIME	SHIME+CE	YP7
			7×10^5	5×10^4	10^6	5×10^4
			7×10^5	4×10^4	2×10^6	3×10^4
			9×10^5	7×10^6	7×10^6	7×10^5
			10^6	7×10^6	10^7	4×10^5
			6×10^5	5×10^4	2×10^6	4×10^4
			7×10^5	4×10^4	10^6	4×10^4
			8×10^5	10^7	2×10^7	3×10^5
			8×10^5	2×10^7	2×10^7	3×10^5

The activity data of the experimental replicates showed similar enzyme activity, with an average standard error of 6.2% (median of 6.6%). Overall, measurable activity was detected in the wells containing glucose. In the CE, the production levels of the yeast were borderline and could only be detected in the wells containing glucose and zinc. I8M production was found similar for the wells containing only glucose or glucose and zinc in the SHIME and YP7 medium. In the SHIME+CE medium, I8M production was detected in all wells, of which the wells containing both glucose and zinc showed the best yield. The effect of ergosterol on I8M production was very limited with the highest increase of about 15% observed in the SHIME medium. In the SHIME+CE medium, however, there was no effect of ergosterol on I8M production. Surprisingly, I8M production was found lower in the SHIME+CE medium compared to the SHIME medium alone (~20%), while no activity was observed in the wells without glucose in latter.

Table 4.10.2.3: I8M activity in mg/L in the clarified culture supernatants. Average value of two independent experiments measured in triplicate with imipenem as substrate.

Ergosterol	$ZnSO_4$	D-glucose	CE	SHIME	SHIME+CE	YP7
			<[a]	<	0.02	<
	■		<	<	0.02	<
		■	<	0.98	0.79	0.11
	■	■	0.02	0.99	0.85	0.11
■			<	<	0.02	<
■	■		<	<	0.02	<
■		■	<	1.16	0.78	0.10
■	■	■	0.02	1.13	0.89	0.08

[a] Below detection limit, < 0.01 mg/L

To investigate whether the lower activity in the SHIME+CE can be explained by the presence of proteases, heavily present in the gut, we reassessed the stability of I8M in the presence of a new batch of CE (pH ≈ 6) that was heat-treated (30 min at 100°C) before incubation (Table 4.10.2.4). BcII was also included in the stability assay, prior the evaluation of its yeast construct under anaerobiosis (Table 4.10.2.5). After heating of the CE, we observed some extent of precipitation and therefore briefly centrifuged (15,000 × g) the sample and used the clarified

supernatant for analysis. Surprisingly, both enzymes were highly unstable in the heat-treated CE, losing >80% of their activity after five hours of incubation. However, both enzymes were considerably stable in the CE, maintaining 40-50% of residual activity after 24 hours of incubation at RT. Future experiments were therefore carried out in non-heated CE.

Table 4.10.2.4: Stability of purified I8M in (heat-treated) caecal extract (CE), reported as % residual activity from baseline with % error between brackets. Activity data was measured in triplicate with imipenem as substrate.

Incubation time (hours)	HZn + BSA (control)	CE	Heat-treated CE
0	100 (2%)	100 (2%)	100 (14%)
5	93 (5%)	71 (2%)	18 (16%)
24	93 (9%)	41 (4%)	bdl[a]

[a] Below detection limit

Table 4.10.2.5: Stability of purified I8M in (heat-treated) caecal extract (CE) stored at 4°C or -80°C, reported as % residual activity from baseline with % error between brackets. Activity data was measured in triplicate with imipenem as substrate.

Incubation time (hours)	HZn + BSA (control)	CE	Heat-treated CE
0	100 (16%)	100 (2%)	100 (15%)
5	96 (12%)	88 (8%)	19 (16%)
24	106 (3%)	47 (6%)	17 (18%)

Since we observed no or limited yeast growth and/or enzyme production, we assessed the usability of a different carbon source, mucin, naturally available in the human gut. We made use of the commercially available mucin type II Mucin from porcine stomach (Sigma). Despite the poor solubility of mucin in water, a stock solution of 5% (w/v) was prepared in water, autoclaved and resuspended before use. Using a robotic platform (liquid handling Janus Integrator system, Perkin Elmer, Waltham, Massachusetts, US), we tested 144 different conditions with seven different yeast strains[5] (or negative control without yeast), no or two carbon sources and three different media, with or without ergosterol 10 mg/L. All wells were, additionally, supplemented with 50 µM $ZnSO_4$. The yeast strains were all calculated to have a starting inoculum size of 10^5 CFU/mL in a volume of 200 µL in each well and actual yeast

[5] Yeast strains included *S. boulardii* or *S. cerevisiae* INVSc1/S150-2B [pSRD-I-K1-I8M-PRE3-I], *S. boulardii* [YIp_SRD-I-K1-I8M-PRE3-I] and *S. boulardii* or *S. cerevisiae* INVSc1/S150-2B [pSRD-I-K1-BcII-PRE3-I].

inoculum size was determined at start by colony counting on selective medium agar plates. The actual inoculum size of the viable and plasmid-containing cells varied between 10^4 - 4×10^4 CFU/ml (Tables 4.10.2.6 and 4.10.2.7). After 44 hours of growth under anaerobiosis, enzyme activity was measured spectrophotometrically (single measurement) for a number of samples with imipenem as substrate, using a 1-cm cuvette. Data are reported in Table 4.10.2.6 for the growth without ergosterol and Table 4.10.2.7 for the growth in the presence of ergosterol. Overall, we observed significantly better production of BcII compared to I8M of a 3-8-fold, depending on the type of yeast strain in the SHIME or SHIME+CE medium. Indeed, significant BcII production was detected in the CE medium, with or without glucose. Moreover, the *S. boulardii* strain was the best enzyme producer among the three different yeast strains for both I8M and BcII under these growth conditions. Between the two *S. cerevisiae* strains, the S150-2B variant produced best. Mucin type II could not be used as a carbon source by the yeast since no activity was detected in these wells, or the activity was similar to that in the wells without any carbon source. Furthermore, we only observed a beneficial impact (with an almost 2-fold difference in episomal *S. boulardii* carrying BcII) of ergosterol supplementation in the SHIME medium but not in the SHIME + CE medium. Therefore, we once more evaluated growth under these conditions using type III Mucin from porcine stomach (Sigma).

Table 4.10.2.6: β-lactamase production (mg/L) in the clarified culture supernatants with seven I8M or BcII producing yeast strains in CE, SHIME, SHIME or SHIME + 5% CE medium, without a carbon source (blue shading) or with 2% (w/v) D-glucose ("g", yellow shading) or 0.5% (w/v) mucin type II ("mII", orange shading). Data represents one measurement with imipenem as substrate.

		CE			SHIME			SHIME+CE		
Strain	**Inoculum**	**w/o**	**g**	**mII**	**w/o**	**g**	**mII**	**w/o**	**g**	**mII**
S.b. I8M	1.8×10^4		0.03	<[a]	<	0.42	<	0.04	0.56	0.05
S.b YI_I8M	3.6×10^4		<	<		0.29	<	<	0.26	<
S.c. INVSc1 I8M	1.0×10^4		<	<		0.16	<		0.04	<
S.c. S150-2B I8M	2.9×10^4		<	<		0.12	<		0.10	0.03
S.b. BcII	2.8×10^4	<	0.15	<	<	2.07	<	0.08	2.67	0.14
S.c. INVSc1 BcII	1.5×10^4		<	<		0.48	<		0.24	<
S.c. S150-2B BcII	4.2×10^4	0.11	0.40	0.13		0.91	<		0.73	0.29

[a] Below detection limit, <0.01 mg/mL

Table 4.10.2.7: β-lactamase production (mg/L) in the clarified culture supernatants with seven I8M or BcII producing yeast strains in CE, SHIME, SHIME or SHIME + 5% CE medium, supplemented with ergosterol 10 mg/L, without a carbon source (blue shading) or with 2% (w/v) D-glucose ("g", yellow shading) or 0.5% (w/v) mucin type II ("mII", orange shading). Data represent one measurement with imipenem as substrate.

		CE + ergosterol			SHIME + ergosterol			SHIME+CE + ergosterol		
Strain	**Inoculum**	**w/o**	**g**	**mII**	**w/o**	**g**	**mII**	**w/o**	**g**	**mII**
S.b. I8M	1.8×10^4		0.02	<[a]	<	1.20	<	0.04	0.47	0.05
S.b YI_I8M	3.6×10^4		0.02	<		0.36	<	<	0.28	<
S.c. INVSc1 I8M	1.0×10^4		<	<		0.16		<	0.06	<
S.c. S150-2B I8M	2.9×10^4		<	<		0.19		0.03	0.14	0.03
S.b. BcII	2.8×10^4	<	0.20	<		3.93		0.10	2.64	0.18
S.c. INVSc1 BcII	1.5×10^4		0.07			0.62		<	0.32	<
S.c. S150-2B BcII	4.2×10^4	0.10	0.35	0.15	<	1.28	<	0.21	0.88	0.26

[a] Below detection limit, <0.01 mg/mL

The types of mucin offered by Sigma differ in their purification processes, in which mucin type III is partially purified and contains ≤1.2% bound sialic acid, whereas mucin type II contains 0.5-1.5% sialic acid. As with mucin type II, mucin type III was also poorly soluble in water but autoclaved and resuspended before use nonetheless. We evaluated the β-lactamase production of the episomal and chromosomal I8M and BcII constructs in *S. boulardii* in CE, supplemented with zinc and one of the carbon sources: D-glucose, mucin type II or mucin type III. Contamination controls included medium with or without supplementation and in the absence of yeast cells. Viable and plasmid-containing cells at start were counted on selective medium plates and yeast production was spectrophotometrically (1 cm cuvette) determined in the clarified culture supernatant with imipenem as substrate after 44 hours of growth (Table 4.10.2.8). In the absence of a carbon source, we only observed activity for the episomal BcII construct. This activity was almost tripled in the presence of glucose and doubled in the presence of mucin type III. This yeast strain showed activity in all conditions tested, with the exception of mucin type II. For the episomal I8M construct, the (limited) activity observed with mucin type III was almost half of what was observed with glucose. Furthermore, no activity was observed with the chromosomal integrated constructs, despite the double inoculum dosage for the I8M integrated yeast cells.

Table 4.10.2.8: β-lactamase production in the clarified culture supernatants with S. boulardii strains carrying the episomal or chromosomal integrated I8M or BcII in CE, supplemented with or without 50 µM $ZnSO_4$, 2% (w/v) D-glucose, 0.5% (w/v) mucin type II or 0.5% (w/v) mucin type III. Data represent an average of three measurements with imipenem as substrate and starting inoculum counts are reported between brackets.

$ZnSO_4$	D-glucose	Mucin II	Mucin III	***S.b* I8M** (1.7×10^4 CFU/ml)	***S.b* YI_I8M** (3.5×10^4 CFU/ml)	***S.b* BcII** (2.3×10^4 CFU/ml)	***S.b* YI_BcII** [a] (? CFU/ml)
				<[b]	<	0.07	<
				<	<	0.20	<
				0.03	<	0.20	<
				<	<	<	<
				0.02	<	0.12	<

[a] Colonies could not be counted due to contamination on plate
[b] Below detection limit, < 0.01 mg/L for I8M and <0.05 mg/L for BcII

In order to estimate how our enzyme secretion yields relate with *in vivo* efficacy, we computed the minimal amount of secreted enzyme necessary to effectively degrade antibiotic residues during therapy in the caecum based on well-known pharmacokinetic/pharmacodynamic (PK/PD) data and the integrated equation of Henri-Michaelis-Menten. We calculated that with 1 mg/L of secreted enzyme BcII could reach effective degradation (from residual concentrations in the caecum during antibiotic therapy to the minimal inhibitory concentration of *E. coli*) of imipenem and piperacillin within 10 minutes and I8M within 2 minutes.

4.10.3 Conclusion

Here, we investigated the performance of our transformed yeasts in *ex vivo* conditions with caecal contents of pigs. We developed a reproducible extraction method that can be used for the assessment of yeast growth and enzyme production in sterility. We demonstrated that purified MBLs I8M and BcII are relatively stable in these CE, retaining ~50% of activity after 24 hours incubation at RT. After observing a decrease in enzyme production in SHIME medium supplemented with 5% CE *versus* SHIME medium alone, we evaluated the stability of our enzymes in heat-treated CE. This treatment was most likely too harsh, affecting the composition of the medium in a way that destabilizes our enzymes. Moreover, glucose, or a usable carbon source, seems to be essential for yeast growth and production. Although minimal

growth was observed in CE alone, measurable levels of production could only be found in the presence of glucose. In addition, yeast could not grow nor produce in the presence of SHIME medium alone. This gives reason to believe that the supplementation of a microbiota in the SHIME study somehow contributed to the minimal growth observed in the short-time colon model (previous subchapter). Indeed, when we supplemented the SHIME medium with CE (5% (v/v)) we observed minimal growth and production in the absence of glucose. Nevertheless, the most significant increase of activity was observed in the presence of glucose. Since glucose supplementation would not be beneficial in a clinical setting due to its absorption in the intestine, we explored the impact of mucin. Mucins are membrane-bound glycoproteins that are naturally present in the intestine where they provide mucosal protection and communication with the external environment (Corfield, 2015). While porcine-originating mucin type II did not have a beneficial impact on enzyme production in yeast, we did observe a slight increase in production with mucin type III. While the differences between these types of mucins are not well-documented, the usefulness of mucin type III as a carbon source by yeast under *ex vivo* conditions, is encouraging. With the current 0.2 mg/L BcII production observed with mucin type III, efficient antibiotic degradation in the human caecum during antibiotic therapy is estimated to take place within an hour. Nevertheless, further experiments will be necessary to understand the potential value of mucin supplementation with our antibiotic degrading yeast probiotics.

5. CONCLUSIONS & PERSPECTIVES

In this PhD study we aimed to develop and validate a yeast probiotic with antibiotic-degrading activity, therefore able to eliminate antibiotic residues in the gut during antibiotic treatment. Although our research is not complete, data from our different studies did shed light on the potential of a yeast LBP as an innovative approach to prevent antibiotic-induced intestinal dysbiosis.

First, we evaluated the endogenous β-lactamase production in healthy subjects and confirmed its presence in the majority of subjects tested, a factor potentially explaining the various susceptibility of individuals to develop intestinal dysbiosis during an antibacterial therapy. In one study these β-lactamases mainly belonged to the group of serine β-lactamase although the presence of a combination of enzymes could not be excluded. These endogenous activities highlight the risk of dysbiosis during antibiotic treatment as the outgrowth of antibiotic resistant commensals is likely to occur. Furthermore, the findings emphasize the importance of protecting the gut microbiota from antibiotic resistance genes used in our LBPs. Thus, these results support the utility of an antibiotic degrading probiotic with containment properties, as was sought to obtain with our current study.

Using molecular cloning, we designed a number of different plasmid variants (named pSRD) to evaluate the production of a protein of interest by the yeast host, allowing a comparison of the different constructs. Many molecular factors are involved in the successful production of heterologous proteins and, therefore, we evaluated a number of these in our initial studies. To start, we made use of the strong *S. cerevisae* TEF1 promoter and ADH1 terminator that are well-described in literature. Although these regions worked adequately in our systems, we did not evaluate the performance of other regions. A set of different promoter(s) and terminator(s) (combinations) could additionally be tested to explore their potential impact on yeast production in general and with different enzymes. Additionally, the loss of activity (generally around 50%) with chromosomal integration could be improved. Different chromosomal integration strategies such as chromosomal integration into multiple genes or multi-copy genes should be explored for their efficient increase in protein expression.

Codon optimization is another element that has shown to be of great value in the enhancement of protein production. In the case of the P3A enzyme, the non-optimized gene performed poorly in our yeast, as well as the manually optimized gene. When using an established optimization algorithm from an online tool, however, satisfactory levels of cytoplasmic production (reaching

10 mg/L early in cell growth) could be obtained. Secretion of the same enzyme, however, was, although significant, less successful. The secretion with the K1 signal peptide from *K. lactis* worked more efficient than the commonly used α-factor pre-pro leader sequence of *S. cerevisiae*. Additional genetic constructs could be designed in the future with other or modified signal peptides, to further improve protein secretion. Optimization of this aspect is subject to many potential bottlenecks, due to the involvement of many cross-reacting factors such as co- or post-translational translocation into the ER, protein folding and quality control in the ER, intracellular protein trafficking, proteolytic degradation and, not to forget, stress response due to protein overproduction or accumulation of misfolded peptides (Idiris *et al*., 2010). Different strategies have been investigated for their beneficiary impact on the yeast secretion pathways. Of these, strain engineering by genetic modification has proven especially useful and should therefore be considered in our future studies. Nevertheless, despite the limited secretion yields we did obtain significant and impactful levels of production for three different β-lactamases and a macrolide esterase, in challenging conditions. For the enzyme candidates tested, different secretion levels were observed, which will need to be evaluated in regards to their clinical relevance (substrate profiles) in future studies.

The presence of an artificially inserted intron was shown to have minimal impact on the production of our heterologous proteins. In addition, we have demonstrated that out of the two yeast introns tested, the PRE3 intron was associated with the highest production yields. Furthermore, we have evidence to support the flexibility of the intron insertion position, at least regarding the secondary structure of the intron-exon junction. This is especially beneficial when designing genes in which the intron is positioned in a specific region to induce a loss of function of the protein product without adequate splicing. This loss of function in a prokaryotic host (*E. coli* in our case) was demonstrated with different enzymes, different introns and different insertion positions, thus limiting the risk of acquisition of functional antibiotic resistance genes in prokaryotes, and ensuring the safety of a potential LBP. Although not yet in the development pipeline, recently an engineered live biotherapeutic with antibiotic degrading capabilities using a different containment strategy has been described (Cubillos-Ruiz *et al*., 2022). Here, the authors describe an engineered probiotic strain of *Lactococcus lactis* capable of the secretion and extracellular assembly of the TEM-1 β-lactamase through two separated fragments. Although the authors provided promising *in vivo* data in mice, so far, the functionality of such a strategy has only been demonstrated with the class A β-lactamase and not with other relevant and complex antibiotic-degrading enzymes. The application of such

an approach with MBLs would require much more sophistication as the system would demand perfect positioning of the zinc ligands in order to achieve proper enzymatic activity. In addition, the pH in the gut might hinder the stability of such protein complexes. By contrast, our antibiotic insensitive LBP relies on the production of a single active polypeptide. Compared to the biological drugs currently developed for the prevention of intestinal dysbiosis (and besides fecal microbiota transplantation), our system may represent a cost-effective approach equally leading to active degradation of the antibiotics in the gut. Indeed, the manufacturing costs of such an LBP are expected to be much lower than that of a functional purified enzyme (*e. g.* ribaxamase) whose production relies on sophisticated and sensitive steps such as purification and formulation, and shall not alter the structural and/or functional integrity of the protein.

In this study, we established the design and paved the way for the development of an antibiotic-degrading LBP, although *in vivo* proof-of-concept remains to be established. However, we observed encouraging levels of β-lactamase activity in *ex vivo* experiments mimicking, to some extent, the gut environment (*e. g.* in pig caecal extracts supplemented with artificial colon medium under anaerobiosis). However, future and parallel studies should focus on improving these levels further, including the evaluation of usable carbon sources for yeast *in situ*, in order to reach the level of true clinical potential.

An international patent, according to the Patent Cooperation Treaty (PCT), titled "AN ENGINEERED YEAST CELL FOR THE DELIVERY OF ANTIBIOTIC INACTIVATING ENZYMES", with inventors Jean-Denis Docquier & Savannah Devente, has been filed on September 8th 2022 (patent application number PCT/EP2022/075025). See Appendix 8.4 for generic patent application information.

6. REFERENCES

Alakomi, H. L., Skyttä, E., Saarela, M., Mattila-Sandholm, T., Latva-Kala, K., & Helander, I. M. (2000). Lactic acid permeabilizes gram-negative bacteria by disrupting the outer membrane. Appl. Environ. Microbiol., 66(5), 2001-2005.

Ambler, R. P., Coulson, A. F., Frère, J. M., Ghuysen, J. M., Joris, B., Forsman, M., ... & Waley, S. G. (1991). A standard numbering scheme for the class A beta-lactamases. Biochemical Journal, 276(Pt 1), 269.

Andremont, A., Cervesi, J., Bandinelli, P. A., Vitry, F., & de Gunzburg, J. (2021). Spare and repair the gut microbiota from antibiotic-induced dysbiosis: state-of-the-art. Drug Discovery Today, 26(9), 2159-2163.

Baldari, C., Murray, J. A., Ghiara, P., Cesareni, G., & Galeotti, C. L. (1987). A novel leader peptide which allows efficient secretion of a fragment of human interleukin 1 beta in Saccharomyces cerevisiae. The EMBO Journal, 6(1), 229-234.

Bassis, C. M., Theriot, C. M., & Young, V. B. (2014). Alteration of the murine gastrointestinal microbiota by tigecycline leads to increased susceptibility to Clostridium difficile infection. Antimicrobial agents and chemotherapy, 58(5), 2767-2774.

Bertani, G. (1951). Studies on lysogenesis I: the mode of phage liberation by lysogenic Escherichia coli. Journal of bacteriology, 62(3), 293-300.

Bontempo, V., Di Giancamillo, A., Savoini, G., Dell'Orto, V., & Domeneghini, C. (2006). Live yeast dietary supplementation acts upon intestinal morpho-functional aspects and growth in weanling piglets. Animal Feed Science and Technology, 129(3-4), 224-236.

Bourriaud, C., Akoka, S., Goupry, S., Robins, R., Cherbut, C., & Michel, C. (2002). Butyrate production from lactate by human colonic microflora. Reproduction Nutrition Development, 42(1), S55-S55.

Bradford, M. M. (1976). A rapid and sensitive method for the quantitation of microgram quantities of protein utilizing the principle of protein-dye binding. Analytical biochemistry, 72(1-2), 248-254.

Brake, A. J., Merryweather, J. P., Coit, D. G., Heberlein, U. A., Masiarz, F. R., Mullenbach, G. T., ... & Barr, P. J. (1984). Alpha-factor-directed synthesis and secretion of mature foreign proteins in Saccharomyces cerevisiae. Proceedings of the National Academy of Sciences, 81(15), 4642-4646.

Brandt, C., Braun, S. D., Stein, C., Slickers, P., Ehricht, R., Pletz, M. W., & Makarewicz, O. (2017). In silico serine β-lactamases analysis reveals a huge potential resistome in environmental and pathogenic species. Scientific reports, 7(1), 1-13.

Britton, R. A., & Cani, P. D. (Eds.). (2018). Bugs as Drugs: Therapeutic Microbes for Prevention and Treatment of Disease. John Wiley & Sons.

Buffie, C. G., Bucci, V., Stein, R. R., McKenney, P. T., Ling, L., Gobourne, A., ... & Pamer, E. G. (2015). Precision microbiome reconstitution restores bile acid mediated resistance to Clostridium difficile. Nature, 517(7533), 205-208.

Buffie, C. G., Jarchum, I., Equinda, M., Lipuma, L., Gobourne, A., Viale, A., ... & Pamer, E. G. (2012). Profound alterations of intestinal microbiota following a single dose of clindamycin results in sustained susceptibility to Clostridium difficile-induced colitis. Infection and immunity, 80(1), 62-73.

Burdet, C., Sayah-Jeanne, S., Nguyen, T. T., Hugon, P., Sablier-Gallis, F., Saint-Lu, N., ... & De Gunzburg, J. (2018). Antibiotic-induced dysbiosis predicts mortality in an animal model of Clostridium difficile infection. Antimicrobial agents and chemotherapy, 62(10), e00925-18.

Burdet, C., Sayah-Jeanne, S., Nguyen, T. T., Miossec, C., Saint-Lu, N., Pulse, M., ... & De Gunzburg, J. (2017). Protection of hamsters from mortality by reducing fecal moxifloxacin concentration with DAV131A in a model of moxifloxacin-induced Clostridium difficile colitis. Antimicrobial agents and chemotherapy, 61(10), e00543-17.

Bush, K. (2013). Proliferation and significance of clinically relevant β-lactamases. Annals of the New York Academy of Sciences, 1277(1), 84-90.

Bush, K., & Bradford, P. A. (2016). β-Lactams and β-lactamase inhibitors: an overview. Cold Spring Harbor perspectives in medicine, 6(8), a025247.

Busti, S., Coccetti, P., Alberghina, L., & Vanoni, M. (2010). Glucose signaling-mediated coordination of cell growth and cell cycle in Saccharomyces cerevisiae. Sensors, 10(6), 6195-6240.

Cao, Z., Sugimura, N., Burgermeister, E., Ebert, M. P., Zuo, T., & Lan, P. (2022). The gut virome: A new microbiome component in health and disease. EBioMedicine, 81, 104113.

Carfi, A., S. Pares, E. Duee, Moreno Galleni, Colette Duez, Jean-Marie Frère, and Otto Dideberg. "The 3-D structure of a zinc metallo-beta-lactamase from Bacillus cereus reveals a new type of protein fold." The EMBO journal 14, no. 20 (1995): 4914-4921.

Carvalho, F. A., Aitken, J. D., Vijay-Kumar, M., & Gewirtz, A. T. (2012). Toll-like receptor–gut microbiota interactions: perturb at your own risk!. Annual review of physiology, 74, 177-198.

Cash, H. L., Whitham, C. V., Behrendt, C. L., & Hooper, L. V. (2006). Symbiotic bacteria direct expression of an intestinal bactericidal lectin. Science, 313(5790), 1126-1130.

CDC. Clostridioides difficile [Internet]. [cited 2022 October 14]. Available from https://www.cdc.gov/HAI/organisms/cdiff/Cdiff_infect.html Centers for Disease Control and Prevention (CDC. (2006). Community-associated methicillin-resistant Staphylococcus aureus infection among healthy newborns--Chicago and Los Angeles County, 2004. MMWR. Morbidity and mortality weekly report, 55(12), 329-332.

Centers for Disease Control and Prevention: Antibiotic Resistance Threats in the United States, 2019. Atlanta, GA: Centers for Disease Control and Prevention.

Chachaty, E., Depitre, C., Mario, N., Bourneix, C., Saulnier, P., Corthier, G., & Andremont, A. (1992). Presence of Clostridium difficile and antibiotic and beta-lactamase activities in feces of volunteers treated with oral cefixime, oral cefpodoxime proxetil, or placebo. Antimicrobial agents and chemotherapy, 36(9), 2009-2013.

Chang, H. W., Nam, Y. D., Sung, Y., Kim, K. H., Roh, S. W., Yoon, J. H., ... & Bae, J. W. (2007). Quantitative real time PCR assays for the enumeration of Saccharomyces cerevisiae and the Saccharomyces sensu stricto complex in human feces. Journal of microbiological methods, 71(3), 191-201.

Chang, J. Y., Antonopoulos, D. A., Kalra, A., Tonelli, A., Khalife, W. T., Schmidt, T. M., & Young, V. B. (2008). Decreased diversity of the fecal microbiome in recurrent Clostridium difficile—associated diarrhea. The Journal of infectious diseases, 197(3), 435-438.

Chin, J. X., Chung, B. K. S., & Lee, D. Y. (2014). Codon Optimization OnLine (COOL): a web-based multi-objective optimization platform for synthetic gene design. Bioinformatics, 30(15), 2210-2212.

Chorev, M., & Carmel, L. (2012). The function of introns. Frontiers in genetics, 3, 55.

Collier, C. T., Carroll, J. A., Ballou, M. A., Starkey, J. D., & Sparks, J. C. (2011). Oral administration of Saccharomyces cerevisiae boulardii reduces mortality associated with immune and cortisol responses to Escherichia coli endotoxin in pigs. Journal of Animal Science, 89(1), 52-58.

Corfield, A. P. (2015). Mucins: a biologically relevant glycan barrier in mucosal protection. Biochimica et Biophysica Acta (BBA)-General Subjects, 1850(1), 236-252.

Cosovanu, C., & Neumann, C. (2020). The many functions of Foxp3+ regulatory T cells in the intestine. Frontiers in Immunology, 11, 600973.

Cubillos-Ruiz, A., Alcantar, M. A., Donghia, N. M., Cárdenas, P., Avila-Pacheco, J., & Collins, J. J. (2022). An engineered live biotherapeutic for the prevention of antibiotic-induced dysbiosis. Nature Biomedical Engineering, 1-12.

Czerucka, D., & Rampal, P. (2019). Diversity of Saccharomyces boulardii CNCM I-745 mechanisms of action against intestinal infections. World Journal of Gastroenterology, 25(18), 2188.
Da Volterra. (2022, April 28). Da Volterra Announces Positive Preclinical Results in Immuno-Oncology with DAV132, a Revolutionary Gut Protector "Press release". https://davolterra.com/wp-content/uploads/2022/04/2022-04-28-press-release-preclinical-results.pdf. Accessed on October 31, 2022

Da Volterra. (2022). DAV361. https://davolterra.com/dav361/. Accessed on October 31, 2022

De Gunzburg, J., & Docquier, J. D. (2021). U.S. Patent No. 10,982,205. Washington, DC: U.S. Patent and Trademark Office.

De Gunzburg, J., & Docquier, J. D. (2021). U.S. Patent No. 10,988,749. Washington, DC: U.S. Patent and Trademark Office.

De Gunzburg, J., & Docquier, J. D. (2022). U.S. Patent No. 11,365,403. Washington, DC: U.S. Patent and Trademark Office.

De Gunzburg, J., Ghozlane, A., Ducher, A., Le Chatelier, E., Duval, X., Ruppé, E., ... & Andremont, A. (2018). Protection of the human gut microbiome from antibiotics. The Journal of infectious diseases, 217(4), 628-636.

d'Humières, C., Delavy, M., Alla, L., Ichou, F., Gauliard, E., Ghozlane, A., … & Burdet, C. (manuscript in preparation). Perturbation and resilience of the gut microbiome three months after β-lactams exposure in healthy volunteers suggest an important role of endogenous β-lactamases.

Delavy, M., Burdet, C., Sertour, N., Devente, S., Docquier, J. D., Grall, N., ... & Bougnoux, M. E. (2022). A Clinical Study Provides the First Direct Evidence That Interindividual Variations in Fecal β-Lactamase Activity Affect the Gut Mycobiota Dynamics in Response to β-Lactam Antibiotics. Mbio, 13(6), e02880-22.

De Luca, F., Benvenuti, M., Carboni, F., Pozzi, C., Rossolini, G. M., Mangani, S., & Docquier, J. D. (2011). Evolution to carbapenem-hydrolyzing activity in noncarbapenemase class D β-lactamase OXA-10 by rational protein design. Proceedings of the National Academy of Sciences, 108(45), 18424-18429.

Devillard, E., McIntosh, F. M., Duncan, S. H., & Wallace, R. J. (2007). Metabolism of linoleic acid by human gut bacteria: different routes for biosynthesis of conjugated linoleic acid. Journal of bacteriology, 189(6), 2566-2570.

Devillard, E., McIntosh, F. M., Paillard, D., Thomas, N. A., Shingfield, K. J., & Wallace, R. J. (2009). Differences between human subjects in the composition of the faecal bacterial community and faecal metabolism of linoleic acid. Microbiology, 155(2), 513-520.

Docquier, J. D., Lamotte-Brasseur, J., Galleni, M., Amicosante, G., Frère, J. M., & Rossolini, G. M. (2003). On functional and structural heterogeneity of VIM-type metallo-β-lactamases. Journal of Antimicrobial Chemotherapy, 51(2), 257-266.

Dominguez-Bello, M. G., Costello, E. K., Contreras, M., Magris, M., Hidalgo, G., Fierer, N., & Knight, R. (2010). Delivery mode shapes the acquisition and structure of the initial microbiota across multiple body habitats in newborns. Proceedings of the National Academy of Sciences, 107(26), 11971-11975.

Drissi, F., Buffet, S., Raoult, D., & Merhej, V. (2015). Common occurrence of antibacterial agents in human intestinal microbiota. Frontiers in Microbiology, 6, 441.

Ducher, A., Vehreschild, M. J., Vehreschild, M. J., Louie, T. J., Cornely, O. A., Féger, C., ... & Mentré, F. (2020, October). LB-5. DAV132 Protects Intestinal Microbiota of Patients Treated with Quinolones, a European Phase II Randomized Controlled Trial (SHIELD). In Open Forum Infectious Diseases (Vol. 7, No. Supplement_1, pp. S845-S846). US: Oxford University Press.

Durkin, H. G., Bazin, H., & Waksman, B. H. (1981). Origin and fate of IgE-bearing lymphocytes. I. Peyer's patches as differentiation site of cells. Simultaneously bearing IgA and IgE. The Journal of experimental medicine, 154(3), 640-648.

Durmusoglu, D., Al'Abri, I., Collins, S. P., Beisel, C., & Crook, N. (2020). Establishing Probiotic Saccharomyces boulardii as a Model Organism for Synthesis and Delivery of Biomolecules. bioRxiv.

Duysburgh, C., Van den Abbeele, P., Morera, M., & Marzorati, M. (2021). Lacticaseibacillus rhamnosus GG and Saccharomyces cerevisiae boulardii supplementation exert protective effects on human gut microbiome following antibiotic administration in vitro. Beneficial Microbes, 12(4), 365-379.

Edwards-Ingram, L., Gitsham, P., Burton, N., Warhurst, G., Clarke, I., Hoyle, D., ... & Stateva, L. (2007). Genotypic and physiological characterization of Saccharomyces boulardii, the probiotic strain of Saccharomyces cerevisiae. Applied and environmental microbiology, 73(8), 2458-2467.

Ehmann, D. E., Jahić, H., Ross, P. L., Gu, R. F., Hu, J., Durand-Réville, T. F., ... & Fisher, S. L. (2013). Kinetics of avibactam inhibition against class A, C, and D β-lactamases. Journal of Biological Chemistry, 288(39), 27960-27971.
European Commission. EU Action on Antimicrobial Resistance [Internet]. [cited 2022 Jun 8]. Available from https://health.ec.europa.eu/antimicrobial-resistance/eu-action-antimicrobial-resistance_en

Feitoza, A. B., Pereira, A. F., da Costa, N. F., & Ribeiro, B. G. (2009). Conjugated linoleic acid (CLA): effect modulation of body composition and lipid profile. Nutricion hospitalaria, 24(4), 422-428.
Fietto, J. L., Araújo, R. S., Valadão, F. N., Fietto, L. G., Brandão, R. L., Neves, M. J., ... & Castro, I. M. (2004). Molecular and physiological comparisons between Saccharomyces cerevisiae and Saccharomyces boulardii. Canadian journal of microbiology, 50(8), 615-621.

Freter, R., Brickner, H., Botney, M., Cleven, D., & Aranki, A. (1983). Mechanisms that control bacterial populations in continuous-flow culture models of mouse large intestinal flora. Infection and immunity, 39(2), 676-685.

Fukiya, S., Arata, M., Kawashima, H., Yoshida, D., Kaneko, M., Minamida, K., ... & Wada, M. (2009). Conversion of cholic acid and chenodeoxycholic acid into their 7-oxo derivatives by Bacteroides intestinalis AM-1 isolated from human feces. FEMS microbiology letters, 293(2), 263-270.

Gatignol, A., Dassain, M., & Tiraby, G. (1990). Cloning of Saccharomyces cerevisiae promoters using a probe vector based on phleomycin resistance. Gene, 91(1), 35-41.

Gietz, R. D., & Schiestl, R. H. (2007). High-efficiency yeast transformation using the LiAc/SS carrier DNA/PEG method. Nature protocols, 2(1), 31-34.

Gnügge, R., Liphardt, T., & Rudolf, F. (2016). A shuttle vector series for precise genetic engineering of Saccharomyces cerevisiae. Yeast, 33(3), 83-98.

Grall, N., Massias, L., Nguyen, T. T., Sayah-Jeanne, S., Ducrot, N., Chachaty, E., ... & Andremont, A. (2013). Oral DAV131, a charcoal-based adsorbent, inhibits intestinal colonization by β-lactam-resistant Klebsiella pneumoniae in cefotaxime-treated mice. Antimicrobial agents and chemotherapy, 57(11), 5423-5425.

Grote, A., Hiller, K., Scheer, M., Münch, R., Nörtemann, B., Hempel, D. C., & Jahn, D. (2005). JCat: a novel tool to adapt codon usage of a target gene to its potential expression host. Nucleic acids research, 33(suppl_2), W526-W531.

Gruber, A. R., Lorenz, R., Bernhart, S. H., Neuböck, R., & Hofacker, I. L. (2008). The vienna RNA websuite. Nucleic acids research, 36(suppl_2), W70-W74.

Hanahan, D., and D. M. Glover. "DNA cloning: a practical approach." DNA cloning: a practical approach 1 (1985): 109-135.

He, B., Xu, W., Santini, P. A., Polydorides, A. D., Chiu, A., Estrella, J., ... & Knowles, D. M. (2007). Intestinal bacteria trigger T cell-independent immunoglobulin A2 class switching by inducing epithelial-cell secretion of the cytokine APRIL. Immunity, 26(6), 812-826.

Hernandez Valladares, M., Felici, A., Weber, G., Adolph, H. W., Zeppezauer, M., Rossolini, G. M., ... & Galleni, M. (1997). Zn (II) dependence of the Aeromonas hydrophila AE036 metallo-β-lactamase activity and stability. Biochemistry, 36(38), 11534-11541.

Higa, J. T., & Kelly, C. P. (2014). New drugs and strategies for management of Clostridium difficile colitis. Journal of intensive care medicine, 29(4), 190-199.

Hill, C., Guarner, F., Reid, G., Gibson, G. R., Merenstein, D. J., Pot, B., ... & Sanders, M. E. (2014). Expert consensus document: The International Scientific Association for Probiotics and Prebiotics consensus statement on the scope and appropriate use of the term probiotic. Nature reviews Gastroenterology & hepatology.

Hooper, L. V., Wong, M. H., Thelin, A., Hansson, L., Falk, P. G., & Gordon, J. I. (2001). Molecular analysis of commensal host-microbial relationships in the intestine. Science, 291(5505), 881-884.

Hudson, L. E., Fasken, M. B., McDermott, C. D., McBride, S. M., Kuiper, E. G., Guiliano, D. B., ... & Lamb, T. J. (2014). Functional heterologous protein expression by genetically engineered probiotic yeast Saccharomyces boulardii. PloS one, 9(11), e112660.

Hudson, L. E., Stewart, T. P., Fasken, M. B., Corbett, A. H., & Lamb, T. J. (2016). Transformation of probiotic yeast and their recovery from gastrointestinal immune tissues following oral gavage in mice. JoVE (Journal of Visualized Experiments), (108), e53453.
Idiris, A., Tohda, H., Kumagai, H., & Takegawa, K. (2010). Engineering of protein secretion in yeast: strategies and impact on protein production. Applied microbiology and biotechnology, 86(2), 403-417.

Ito, H., Fukuda, Y. A. S. U. K. I., Murata, K., & Kimura, A. (1983). Transformation of intact yeast cells treated with alkali cations. Journal of bacteriology, 153(1), 163-168.

Jakobsson, H. E., Jernberg, C., Andersson, A. F., Sjölund-Karlsson, M., Jansson, J. K., & Engstrand, L. (2010). Short-term antibiotic treatment has differing long-term impacts on the human throat and gut microbiome. PloS one, 5(3), e9836.

Jandhyala, S. M., Talukdar, R., Subramanyam, C., Vuyyuru, H., Sasikala, M., & Reddy, D. N. (2015). Role of the normal gut microbiota. World journal of gastroenterology: WJG, 21(29), 8787.

Jaramillo, V. D. A., Sukno, S. A., & Thon, M. R. (2015). Identification of horizontally transferred genes in the genus Colletotrichum reveals a steady tempo of bacterial to fungal gene transfer. BMC genomics, 16(1), 1-16.
Jernberg, C., Löfmark, S., Edlund, C., & Jansson, J. K. (2007). Long-term ecological impacts of antibiotic administration on the human intestinal microbiota. The ISME journal, 1(1), 56-66.

Johansson, M. E., Larsson, J. M. H., & Hansson, G. C. (2011). The two mucus layers of colon are organized by the MUC2 mucin, whereas the outer layer is a legislator of host–microbial interactions. Proceedings of the national academy of sciences, 108(Supplement 1), 4659-4665.

Jump, R. L., Polinkovsky, A., Hurless, K., Sitzlar, B., Eckart, K., Tomas, M., ... & Donskey, C. J. (2014). Metabolomics analysis identifies intestinal microbiota-derived biomarkers of colonization resistance in clindamycin-treated mice. PLoS One, 9(7), e101267.

Jumpertz, R., Le, D. S., Turnbaugh, P. J., Trinidad, C., Bogardus, C., Gordon, J. I., & Krakoff, J. (2011). Energy-balance studies reveal associations between gut microbes, caloric load, and nutrient absorption in humans. The American journal of clinical nutrition, 94(1), 58-65.

Juneau, K., Miranda, M., Hillenmeyer, M. E., Nislow, C., & Davis, R. W. (2006). Introns regulate RNA and protein abundance in yeast. Genetics, 174(1), 511-518.

Jung, S. K., & McDonald, K. (2011). Visual gene developer: a fully programmable bioinformatics software for synthetic gene optimization. Bmc Bioinformatics, 12(1), 1-13.

Kamada, N., Kim, Y. G., Sham, H. P., Vallance, B. A., Puente, J. L., Martens, E. C., & Núñez, G. (2012). Regulated virulence controls the ability of a pathogen to compete with the gut microbiota. Science, 336(6086), 1325-1329.

Kamada, N., Chen, G. Y., Inohara, N., & Núñez, G. (2013). Control of pathogens and pathobionts by the gut microbiota. Nature immunology, 14(7), 685-690.

Khatri, I., Tomar, R., Ganesan, K., Prasad, G. S., & Subramanian, S. (2017). Complete genome sequence and comparative genomics of the probiotic yeast Saccharomyces boulardii. Scientific reports, 7(1), 1-12.

Klaassen, C. D., & Cui, J. Y. (2015). Mechanisms of how the intestinal microbiota alters the effects of drugs and bile acids. Drug Metabolism and Disposition, 43(10), 1505-1521.

Knoop, K. A., Gustafsson, J. K., McDonald, K. G., Kulkarni, D. H., Coughlin, P. E., McCrate, S., ... & Newberry, R. D. (2017). Microbial antigen encounter during a preweaning interval is critical for tolerance to gut bacteria. Science immunology, 2(18), eaao1314.

Knoop, K. A., McDonald, K. G., Kulkarni, D. H., & Newberry, R. D. (2016). Antibiotics promote inflammation through the translocation of native commensal colonic bacteria. Gut, 65(7), 1100-1109.

Kokai-Kun, J. F., Roberts, T., Coughlin, O., Le, C., Whalen, H., Stevenson, R., ... & Sliman, J. (2019). Use of ribaxamase (SYN-004), a β-lactamase, to prevent Clostridium difficile infection in β-lactam-treated patients: a double-blind, phase 2b, randomised placebo-controlled trial. The Lancet infectious diseases, 19(5), 487-496.

Kokai-Kun, J. F., Roberts, T., Coughlin, O., Sicard, E., Rufiange, M., Fedorak, R., ... & Sliman, J. (2017). The oral β-lactamase SYN-004 (ribaxamase) degrades ceftriaxone excreted into the intestine in phase 2a clinical studies. Antimicrobial agents and chemotherapy, 61(3), e02197-16.
Langdon, A., Crook, N., & Dantas, G. (2016). The effects of antibiotics on the microbiome throughout development and alternative approaches for therapeutic modulation. Genome medicine, 8(1), 1-16.

Lee, S. M., Donaldson, G. P., Mikulski, Z., Boyajian, S., Ley, K., & Mazmanian, S. K. (2013). Bacterial colonization factors control specificity and stability of the gut microbiota. Nature, 501(7467), 426-429.

Léonard, F., Andremont, A., Leclerq, B., Labia, R., & Tancrède, C. (1989). Use of β-lactamase-producing anaerobes to prevent ceftriaxone from degrading intestinal resistance to colonization. Journal of Infectious Diseases, 160(2), 274-280.

Lerner, A., Matthias, T., & Aminov, R. (2017). Potential effects of horizontal gene exchange in the human gut. Frontiers in immunology, 8, 1630.

Losurdo, G., Iannone, A., Contaldo, A., Ierardi, E., Di Leo, A., & Principi, M. (2015). Escherichia coli Nissle 1917 in ulcerative colitis treatment: systematic review and meta-analysis. J Gastrointestin Liver Dis, 24(4), 499-505.

Lunney, J. K., Van Goor, A., Walker, K. E., Hailstock, T., Franklin, J., & Dai, C. (2021). Importance of the pig as a human biomedical model. Science Translational Medicine, 13(621), eabd5758.

Macfarlane, S., & Macfarlane, G. T. (2003). Regulation of short-chain fatty acid production. Proceedings of the Nutrition Society, 62(1), 67-72.

Magwira, C. A., Kullin, B., Lewandowski, S., Rodgers, A., Reid, S. J., & Abratt, V. R. (2012). Diversity of faecal oxalate-degrading bacteria in black and white South African study groups: insights into understanding the rarity of urolithiasis in the black group. Journal of applied microbiology, 113(2), 418-428.

Maldonado-Gómez, M. X., Martínez, I., Bottacini, F., O'Callaghan, A., Ventura, M., van Sinderen, D., ... & Walter, J. (2016). Stable engraftment of Bifidobacterium longum AH1206 in the human gut depends on individualized features of the resident microbiome. Cell host & microbe, 20(4), 515-526.

Marín, L., Miguélez, E. M., Villar, C. J., & Lombó, F. (2015). Bioavailability of dietary polyphenols and gut microbiota metabolism: antimicrobial properties. BioMed research international, 2015.

Mellor, J., Dobson, M. J., Roberts, N. A., Kingsman, A. J., & Kingsman, S. M. (1985). Factors affecting heterologous gene expression in Saccharomyces cerevisiae. Gene, 33(2), 215-226.

Moens, F., Duysburgh, C., van den Abbeele, P., Morera, M., & Marzorati, M. (2019). Lactobacillus rhamnosus GG and Saccharomyces cerevisiae boulardii exert synergistic antipathogenic activity in vitro against enterotoxigenic Escherichia coli. Beneficial microbes, 10(8), 923-935.

Morar, M., Pengelly, K., Koteva, K., & Wright, G. D. (2012). Mechanism and diversity of the erythromycin esterase family of enzymes. Biochemistry, 51(8), 1740-1751.

Moriguchi, K., Yamamoto, S., Tanaka, K., Kurata, N., & Suzuki, K. (2013). Trans-kingdom horizontal DNA transfer from bacteria to yeast is highly plastic due to natural polymorphisms in auxiliary nonessential recipient genes. PLoS One, 8(9), e74590.

Moya, A., & Ferrer, M. (2016). Functional redundancy-induced stability of gut microbiota subjected to disturbance. Trends in microbiology, 24(5), 402-413.

Navarro, Y., Torija, M. J., Mas, A., & Beltran, G. (2020). Viability-PCR allows monitoring yeast population dynamics in mixed fermentations including viable but non-culturable yeasts. Foods, 9(10), 1373.

Ng, K. M., Ferreyra, J. A., Higginbottom, S. K., Lynch, J. B., Kashyap, P. C., Gopinath, S., ... & Sonnenburg, J. L. (2013). Microbiota-liberated host sugars facilitate post-antibiotic expansion of enteric pathogens. Nature, 502(7469), 96-99.

Ng, K. M., Ferreyra, J. A., Higginbottom, S. K., Lynch, J. B., Kashyap, P. C., Gopinath, S., ... & Sonnenburg, J. L. (2013). Microbiota-liberated host sugars facilitate post-antibiotic expansion of enteric pathogens. Nature, 502(7469), 96-99.
O'Callaghan, C. H., Morris, A., Kirby, S. M., & Shingler, A. H. (1972). Novel method for detection of β-lactamases by using a chromogenic cephalosporin substrate. Antimicrobial agents and chemotherapy, 1(4), 283-288.

Pickard, J. M., Zeng, M. Y., Caruso, R., & Núñez, G. (2017). Gut microbiota: Role in pathogen colonization, immune responses, and inflammatory disease. Immunological reviews, 279(1), 70-89

Pinquier, J. L., Varastet, M., Meyers, D., Sayah-Jeanne, S., Féger, C., Gaumétou, O., ... & Ducher, A. (2021). A Colon-Targeted Adsorbent (DAV132) Does Not Affect the Pharmacokinetics of Warfarin or Clonazepam in Healthy Subjects. Clinical Pharmacology in Drug Development, 10(8), 908-917.

Pitout, J. D. (2009). IPSAT P1A, a class A beta-lactamase therapy for the prevention of penicillin-induced disruption to the intestinal microflora. Current opinion in investigational drugs (London, England: 2000), 10(8), 838-844.

Podolsky, D. K., Lynch-Devaney, K., Stow, J. L., Oates, P., Murgue, B., DeBeaumont, M., ... & Mahida, Y. R. (1993). Identification of human intestinal trefoil factor. Goblet cell-specific expression of a peptide targeted for apical secretion. Journal of Biological Chemistry, 268(9), 6694-6702.

Reyes, A., Semenkovich, N. P., Whiteson, K., Rohwer, F., & Gordon, J. I. (2012). Going viral: next-generation sequencing applied to phage populations in the human gut. Nature Reviews Microbiology, 10(9), 607-617.

Roldán, M. D., Pérez-Reinado, E., Castillo, F., & Moreno-Vivián, C. (2008). Reduction of polynitroaromatic compounds: the bacterial nitroreductases. FEMS microbiology reviews, 32(3), 474-500.

Romick-Rosendale, L. E., Goodpaster, A. M., Hanwright, P. J., Patel, N. B., Wheeler, E. T., Chona, D. L., & Kennedy, M. A. (2009). NMR-based metabonomics analysis of mouse urine and fecal extracts following oral treatment with the broad-spectrum antibiotic enrofloxacin (Baytril). Magnetic resonance in chemistry, 47(S1), S36-S46.

Rose, E. C., Blikslager, A. T., & Ziegler, A. L. (2022). Porcine Models of the Intestinal Microbiota: The Translational Key to Understanding How Gut Commensals Contribute to Gastrointestinal Disease. Frontiers in Veterinary Science, 9.

Roussel, C., De Paepe, K., Galia, W., De Bodt, J., Chalancon, S., Denis, S., ... & Van de Wiele, T. (2021). Multi-targeted properties of the probiotic saccharomyces cerevisiae CNCM I-3856 against enterotoxigenic escherichia coli (ETEC) H10407 pathogenesis across human gut models. Gut microbes, 13(1), 1953246.

Saint-Lu, N., Burdet, C., Sablier-Gallis, F., Corbel, T., Nevière, A., Sayah-Jeanne, S., ... & de Gunzburg, J. (2019). DAV131A protects hamsters from lethal Clostridioides difficile infection induced by fluoroquinolones. Antimicrobial agents and chemotherapy, 64(1), e01196-19.

Sakurai, A., Fujimori, S., Kochiwa, H., Kitamura-Abe, S., Washio, T., Saito, R., ... & RIKEN Genome Exploration Research Group Phase II Team. (2002). On biased distribution of introns in various eukaryotes. Gene, 300(1-2), 89-95.

Salzman, N. H., Underwood, M. A., & Bevins, C. L. (2007, April). Paneth cells, defensins, and the commensal microbiota: a hypothesis on intimate interplay at the intestinal mucosa. In Seminars in immunology (Vol. 19, No. 2, pp. 70-83). Academic Press.

Sambrook, J., Russell, D. W., & Sambrook, J. (2006). The condensed protocols: from molecular cloning: a laboratory manual (No. Sirsi) i9780879697723). Cold Spring Harbor, NY: Cold spring harbor laboratory press.

Sanders, M. E., Merenstein, D. J., Reid, G., Gibson, G. R., & Rastall, R. A. (2019). Probiotics and prebiotics in intestinal health and disease: from biology to the clinic. Nature reviews Gastroenterology & hepatology, 16(10), 605-616.

Segel, I. H. (1975). Rapid equilibrium partial and mixed-type inhibition. Enzyme kinetics, behavior and analysis of rapid equilibrium and steady-state enzyme systems.

Sekirov, I., Russell, S. L., Antunes, L. C. M., & Finlay, B. B. (2010). Gut microbiota in health and disease. Physiological reviews, 90(3), 859-904.
Sharp, P. M., & Li, W. H. (1987). The codon adaptation index-a measure of directional synonymous codon usage bias, and its potential applications. Nucleic acids research, 15(3), 1281-1295.

Sidhu, H., Hoppe, B., Hesse, A., Tenbrock, K., Bromme, S., Rietschel, E., &Peck, A. B. (1998). Absence of Oxalobacter formigenes in cystic fibrosis patients: a risk factor for hyperoxaluria. The Lancet, 352(9133), 1026-1029.

Sousa, T., Paterson, R., Moore, V., Carlsson, A., Abrahamsson, B., & Basit, A. W. (2008). The gastrointestinal microbiota as a site for the biotransformation of drugs. International journal of pharmaceutics, 363(1-2), 1-25.

Spingola, M., Grate, L., Haussler, D., & Ares, M. (1999). Genome-wide bioinformatic and molecular analysis of introns in Saccharomyces cerevisiae. Rna, 5(2), 221-234.

Stiefel, U., Tima, M. A., & Nerandzic, M. M. (2015). Metallo-β-lactamase-producing Bacteroides species can shield other members of the gut microbiota from antibiotics. Antimicrobial Agents and Chemotherapy, 59(1), 650-653.

Studier, F. W. (2005). Protein production by auto-induction in high-density shaking cultures. Protein expression and purification, 41(1), 207-234.

Suez, J., Zmora, N., Zilberman-Schapira, G., Mor, U., Dori-Bachash, M., Bashiardes, S., ... & Elinav, E. (2018). Post-antibiotic gut mucosal microbiome reconstitution is impaired by probiotics and improved by autologous FMT. Cell, 174(6), 1406-1423.

Suzuki, K., Maruya, M., Kawamoto, S., Sitnik, K., Kitamura, H., Agace, W. W., & Fagarasan, S. (2010). The sensing of environmental stimuli by follicular dendritic cells promotes immunoglobulin A generation in the gut. Immunity, 33(1), 71-83.

Swanson, H. I. (2015). Drug metabolism by the host and gut microbiota: a partnership or rivalry?. Drug Metabolism and Disposition, 43(10), 1499-1504.

Sweeney, N. J., Klemm, P., McCormick, B. A., Moller-Nielsen, E., Utley, M., Schembri, M. A., ... & Cohen, P. S. (1996). The Escherichia coli K-12 gntP gene allows E. coli F-18 to occupy a distinct nutritional niche in the streptomycin-treated mouse large intestine. Infection and immunity, 64(9), 3497-3503.

Takeuchi, O., & Akira, S. (2010). Pattern recognition receptors and inflammation. Cell, 140(6), 805-820.

Tarkkanen, A. M., Heinonen, T., Jõgi, R., Mentula, S., van der Rest, M. E., Donskey, C. J., ... & Nord, C. E. (2009). P1A recombinant β-lactamase prevents emergence of antimicrobial resistance in gut microflora of healthy subjects during intravenous administration of ampicillin. Antimicrobial agents and chemotherapy, 53(6), 2455-2462.

Theriot, C. M., Koenigsknecht, M. J., Carlson, P. E., Hatton, G. E., Nelson, A. M., Li, B., ... & Young, V. B. (2014). Antibiotic-induced shifts in the mouse gut microbiome and metabolome increase susceptibility to Clostridium difficile infection. Nature communications, 5(1), 1-10.

Van de Wiele, T., Van den Abbeele, P., Ossieur, W., Possemiers, S., & Marzorati, M. (2015). The simulator of the human intestinal microbial ecosystem (SHIME®). The Impact of Food Bioactives on Health: in vitro and ex vivo models, 305-317.

Van Schaik, W. (2015). The human gut resistome. Philosophical Transactions of the Royal Society B: Biological Sciences, 370(1670), 20140087.

Vehreschild, M. J., Ducher, A., Louie, T., Cornely, O. A., Feger, C., Dane, A., ... & Wilcox, M. H. (2022). An open randomized multicentre Phase 2 trial to assess the safety of DAV132 and its efficacy to protect gut microbiota diversity in hospitalized patients treated with fluoroquinolones. Journal of Antimicrobial Chemotherapy, 77(4), 1155-1165.

Velculescu, V. E., Zhang, L., Zhou, W., Vogelstein, J., Basrai, M. A., Bassett Jr, D. E., ... & Kinzler, K. W. (1997). Characterization of the yeast transcriptome. Cell, 88(2), 243-251.
Wallace, B. D., Wang, H., Lane, K. T., Scott, J. E., Orans, J., Koo, J. S., ... & Redinbo, M. R. (2010). Alleviating cancer drug toxicity by inhibiting a bacterial enzyme. Science, 330(6005), 831-835.

Washington II, J. A., & Wilson, W. R. (1985, March). Erythromycin: a microbial and clinical perspective after 30 years of clinical use (first of two parts). In Mayo Clinic Proceedings (Vol. 60, No. 3, pp. 189-203). Elsevier.

Wieërs, G., Belkhir, L., Enaud, R., Leclercq, S., Philippart de Foy, J. M., Dequenne, I., ... & Cani, P. D. (2020). How probiotics affect the microbiota. Frontiers in cellular and infection microbiology, 454.

Yap, I. K., Li, J. V., Saric, J., Martin, F. P., Davies, H., Wang, Y., ... & Holmes, E. (2008). Metabonomic and microbiological analysis of the dynamic effect of vancomycin-induced gut microbiota modification in the mouse. Journal of proteome research, 7(9), 3718-3728.

Yatsunenko, T., Rey, F. E., Manary, M. J., Trehan, I., Dominguez-Bello, M. G., Contreras, M., ... & Gordon, J. I. (2012). Human gut microbiome viewed across age and geography. nature, 486(7402), 222-227.

Yofe, I., Zafrir, Z., Blau, R., Schuldiner, M., Tuller, T., Shapiro, E., & Ben-Yehezkel, T. (2014). Accurate, model-based tuning of synthetic gene expression using introns in S. cerevisiae. PLoS genetics, 10(6), e1004407.

Zafrir, Z., & Tuller, T. (2015). Nucleotide sequence composition adjacent to intronic splice sites improves splicing efficiency via its effect on pre-mRNA local folding in fungi. RNA, 21(10), 1704-1718.

Zaura, E., Brandt, B. W., Teixeira de Mattos, M. J., Buijs, M. J., Caspers, M. P., Rashid, M. U., ... & Crielaard, W. (2015). Same exposure but two radically different responses to antibiotics: resilience of the salivary microbiome versus long-term microbial shifts in feces. MBio, 6(6), e01693-15.

Zhang, W., Bao, C., Wang, J., Zang, J., & Cao, Y. (2020). Administration of Saccharomyces boulardii mafic-1701 improves feed conversion ratio, promotes antioxidant capacity, alleviates intestinal inflammation and modulates gut microbiota in weaned piglets. Journal of Animal Science and Biotechnology, 11(1), 1-11.

Zhao, Y., Wu, J., Li, J. V., Zhou, N. Y., Tang, H., & Wang, Y. (2013). Gut microbiota composition modifies fecal metabolic profiles in mice. Journal of proteome research, 12(6), 2987-2999.

Zuker, M., & Stiegler, P. (1981). Optimal computer folding of large RNA sequences using thermodynamics and auxiliary information. Nucleic acids research, 9(1), 133-148.

7. ACKNOWLEDGEMENTS

To my husband, Viktor. I do not know where to start because I could write pages full with gratefulness for your daily support and pep-talks, your pitstop help in the morning in order to get me out of the house as soon as possible with backpack, poncho, hat, helmet, lunch, warm tea, phone and electric roller to make my 07:15 bus to Siena, your incredible creative cooking every (single!) day, your patience when I would not make it home on time and, finally, your willingness to endure just until I managed to finished my PhD. Words could never compare. Thank you for enduring me as well during this period, as I know that I was not my best self.

To my supervisor Jean-Denis, thank you for having given me an opportunity. I learned the most resulting from your trust and challenges. You showed me that too much is never too much and you can never think big enough.

To my fellow PhD-ers and other laboratory or department members, Filomena, Federica, Giusi, Selene, Maria, Felice, Tiziana and Gianni, thank you for your support, technically (especially Giusi), but foremost mentally, during these last 4+ years. All the gestures and jokes, as insignificant as may have seemed, made the whole experience that much more durable.

To the students I got to guide during their Master's thesis, Leonardo and Ilenia, thank you for allowing me to share some of my knowledge with you and for making me grow more.

To Da Volterra, thank you for the insightful collaboration with industry and inspirational minds in general. Tatiana, thank you for your input and for having been a bridge between these two worlds.

To the external reviewers of my thesis, Antoine Andremont, Emeritus Professor at the Paris Diderot University Medical School and founder of Da Volterra and Serena Schippa, Associate Professor at the Sapienza University of Rome, thank you for your time, interest and valuable insights.

To my family and friends who did not understand what I was doing and why it could be worth it. Thank you for supporting and believing in me, nevertheless.

To past supervisors and teachers that once believed in me, I still manage to get strength from your words and encouragements to this day.

8. APPENDICES

8.1 CAI profiles of *S. cerevisiae* optimized genes

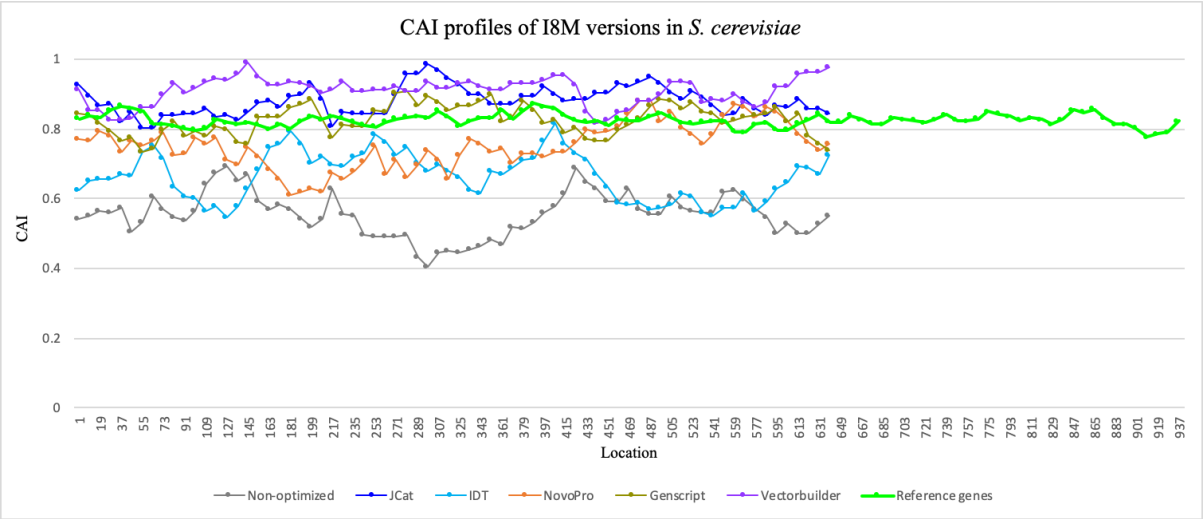

Figure 8.1.1: Comparison of CAI profiles obtained with different online optimization for I8M gene. The y-axis reports the CAI score 0-1 and the x-axis the location of the sequence, with each point representing an average of 3 CAI values.

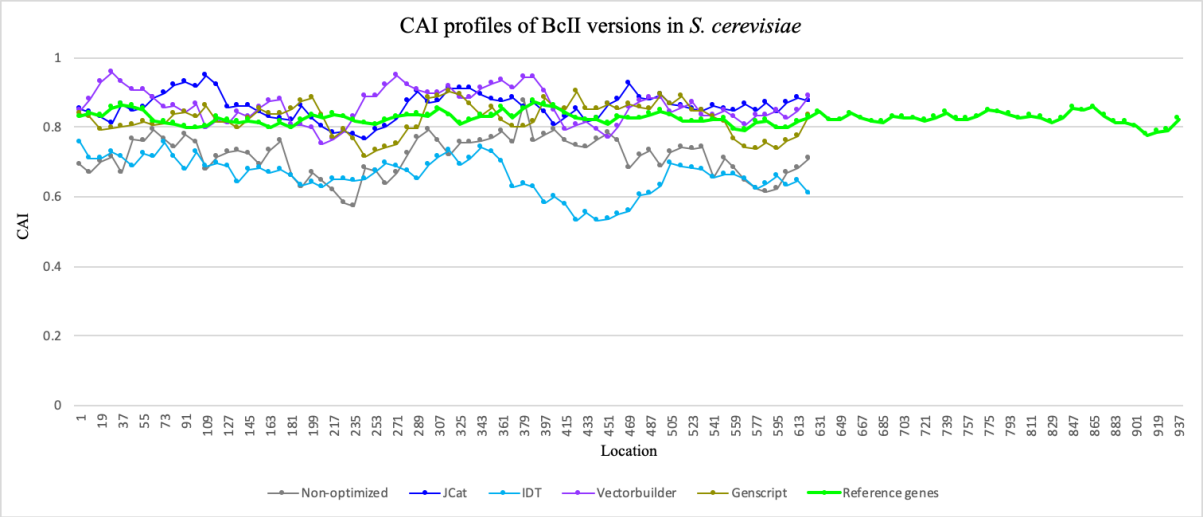

Figure 8.1.2: Comparison of CAI profiles obtained with different online optimization for BcII gene. The y-axis reports the CAI score 0-1 and the x-axis the location of the sequence, with each point representing an average of 3 CAI values.

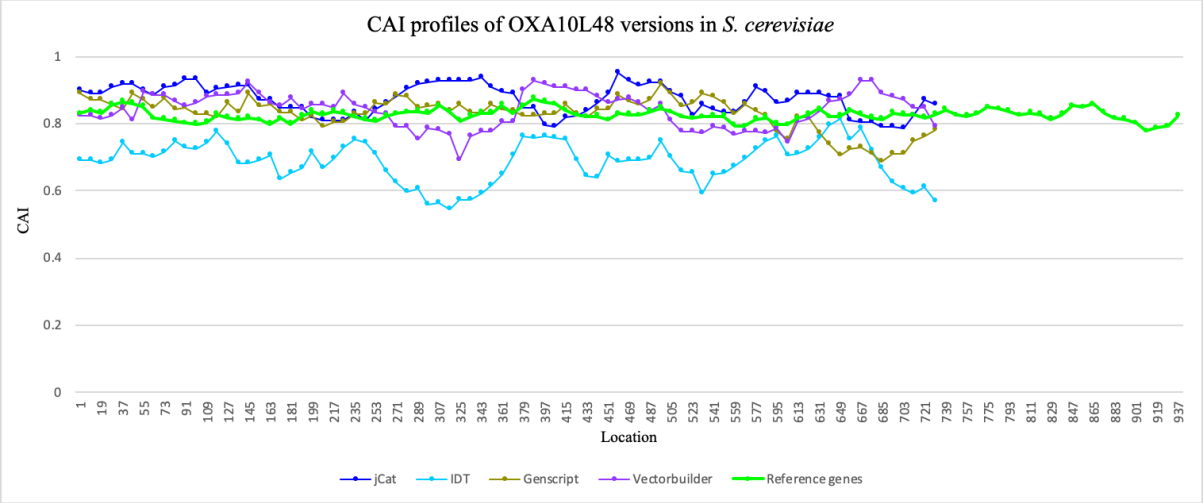

Figure 8.1.3: Comparison of CAI profiles obtained with different online optimization for OXAL48 gene. The y-axis reports the CAI score 0-1 and the x-axis the location of the sequence, with each point representing an average of 3 CAI values.

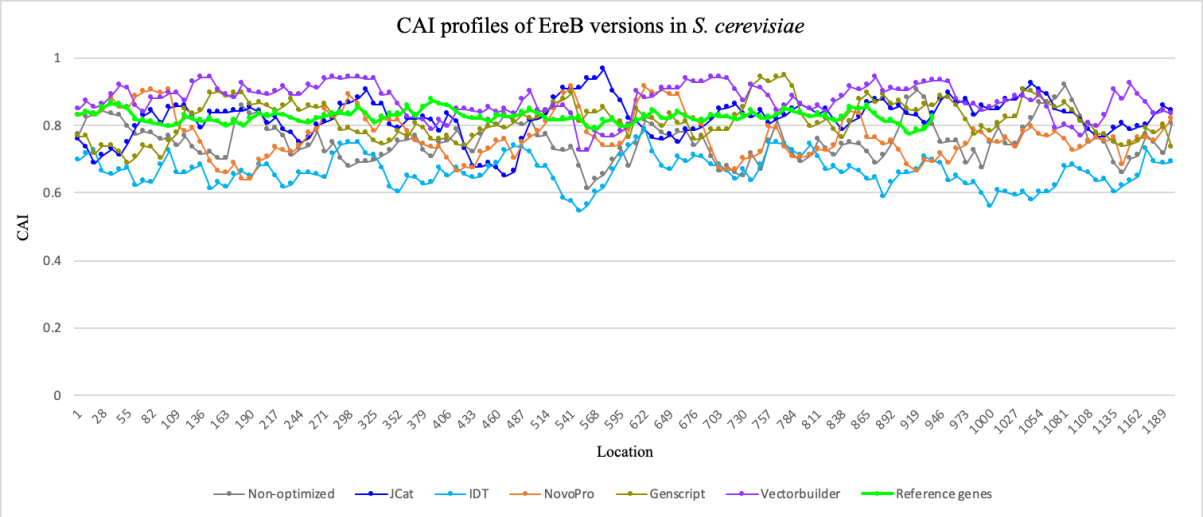

Figure 8.1.4: Comparison of CAI profiles obtained with different online optimization for EreB gene. The y-axis reports the CAI score 0-1 and the x-axis the location of the sequence, with each point representing an average of 3 CAI values.

8.2 MFE profiles of intron-exon junctions

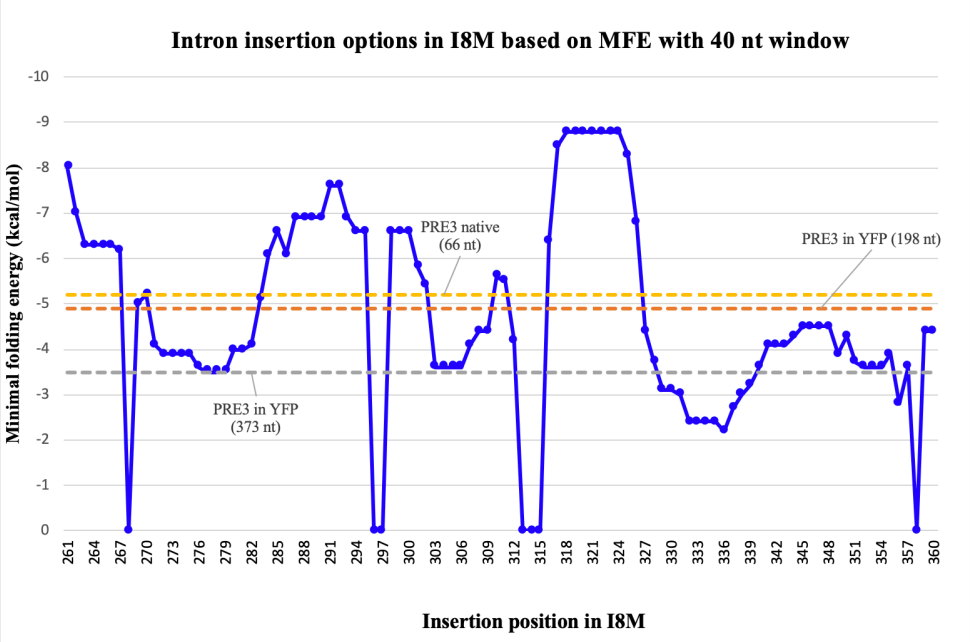

Figure 8.2.1: MFE analysis of potential intron-exon junctions in the yI8M-I gene with a 40 nt window with on the x-axis the nucleotide insertion position and on the y-axis the inverted display of the calculated MFE values. Baseline MFE values are depicted as reference for the MFE of the PRE3 intron in the PRE3 gene of S. cerevisiae or artificially in the YFP gene on position 198 or 373 (Yofe et al., 2014). Corresponding amino acid sequence was not disclosed due to confidentiality.

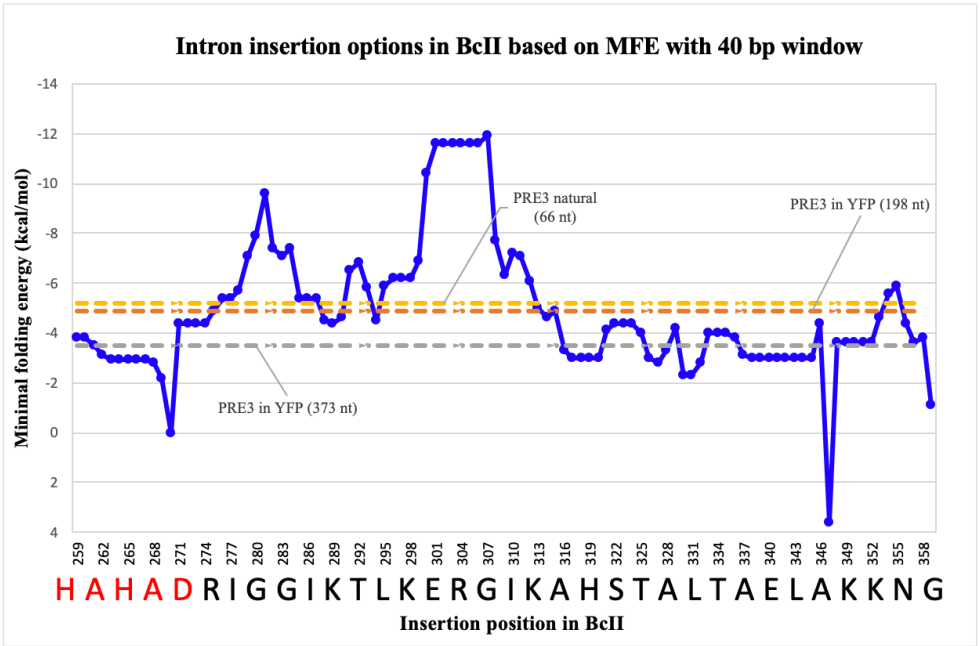

Figure 8.2.2: MFE analysis of potential intron-exon junctions in the yBcII-I gene with a 40 nt window with on the x-axis the nucleotide insertion position and the corresponding amino acid sequence (with conserved motif in red) and on the y-axis the inverted display of the calculated MFE values. Baseline MFE values are depicted as reference for the MFE of the PRE3 intron in the PRE3 gene of S. cerevisiae or artificially in the YFP gene on position 198 or 373 (Yofe et al., 2014).

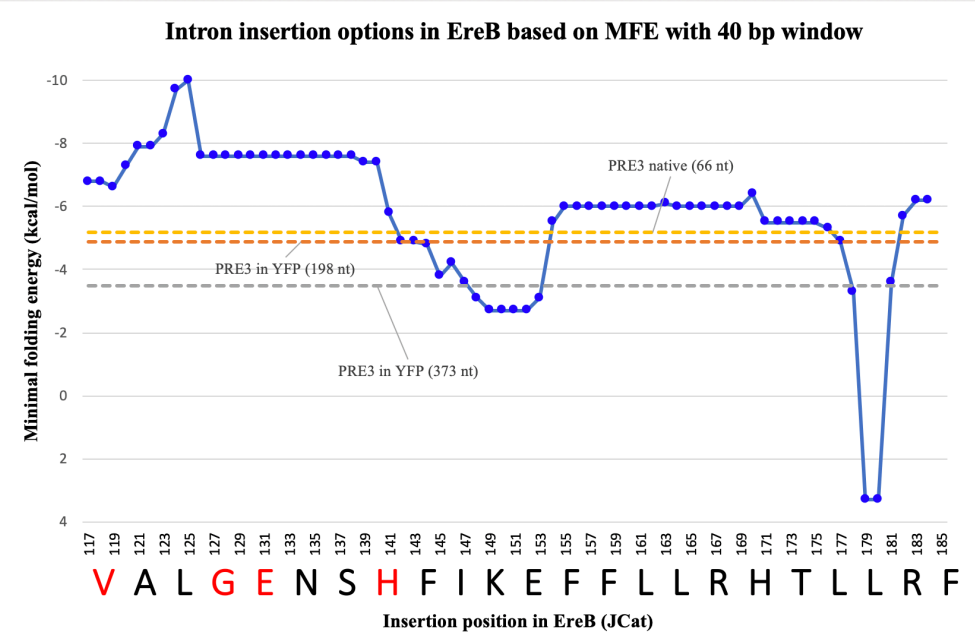

Figure 8.2.3: MFE analysis of potential intron-exon junctions in the yEreB-I gene with a 40 nt window with on the x-axis the nucleotide insertion position and the corresponding amino acid sequence (with strictly conserved residues in red) and on the y-axis the inverted display of the calculated MFE values. Baseline MFE values are depicted as reference for the MFE of the PRE3 intron in the PRE3 gene of S. cerevisiae or artificially in the YFP gene on position 198 or 373 (Yofe et al., 2014).

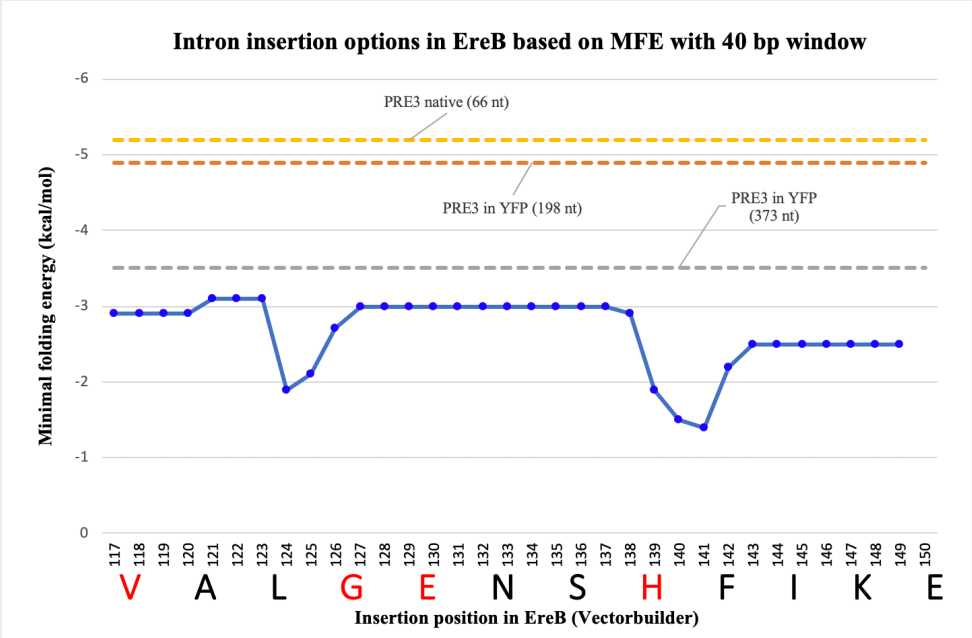

Figure 8.2.4: MFE analysis of potential intron-exon junctions in the yEreB-II gene with a 40 nt window with on the x-axis the nucleotide insertion position and the corresponding amino acid sequence (with strictly conserved residues in red) and on the y-axis the inverted display of the calculated MFE values. Baseline MFE values are depicted as reference for the MFE of the PRE3 intron in the PRE3 gene of S. cerevisiae or artificially in the YFP gene on position 198 or 373 (Yofe et al., 2014).

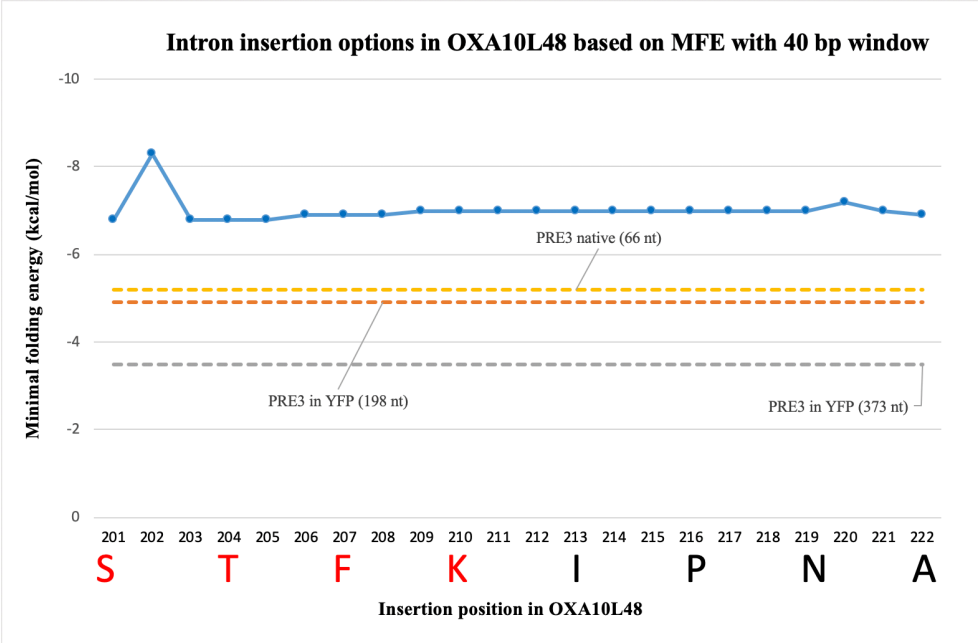

Figure 8.2.5: MFE analysis of potential intron-exon junctions in the yOXA10L48-I gene with a 40 nt window with on the x-axis the nucleotide insertion position and the corresponding amino acid sequence (with strictly conserved residues in red) and on the y-axis the inverted display of the calculated MFE values. Baseline MFE values are depicted as reference for the MFE of the PRE3 intron in the PRE3 gene of S. cerevisiae or artificially in the YFP gene on position 198 or 373 (Yofe et al., 2014).

8.3 Kinetic parameters

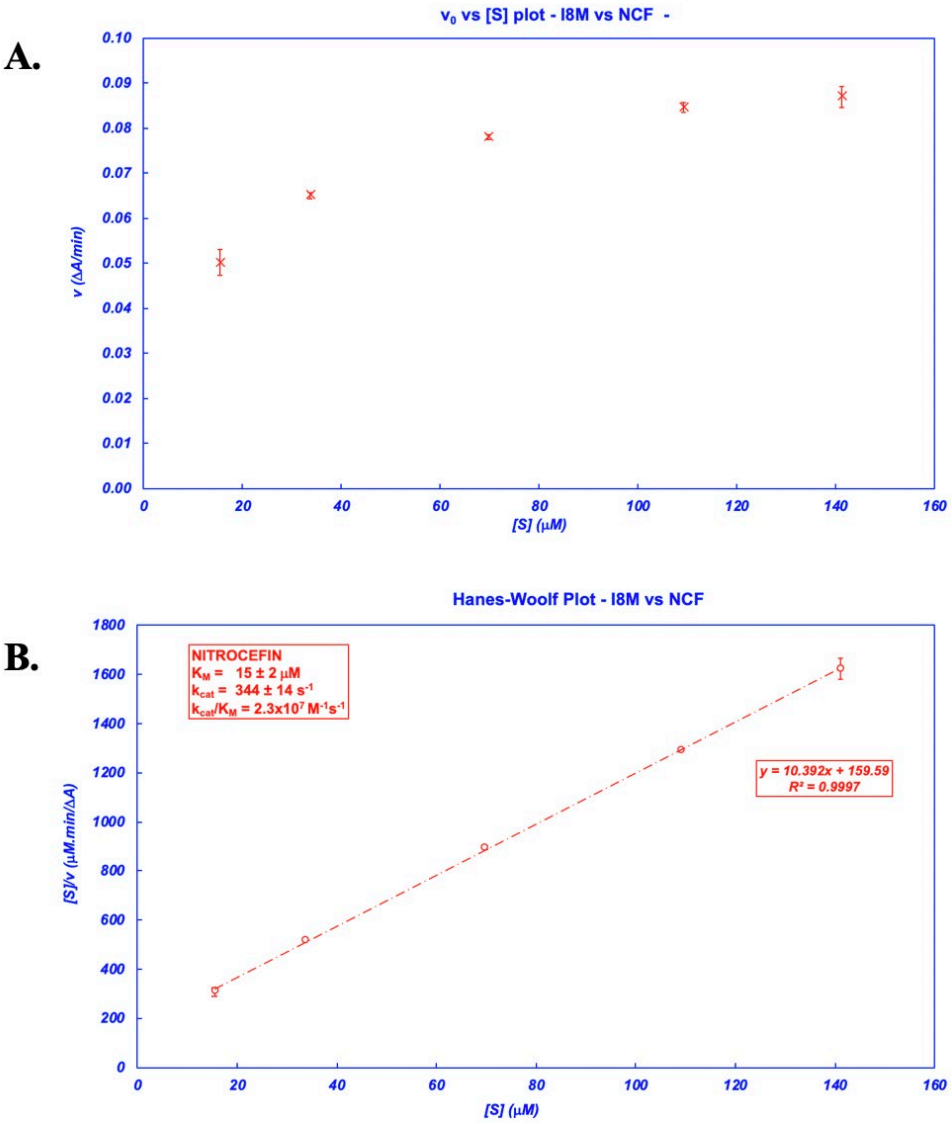

Figure 8.3.1: Determination of the kinetic parameters of I8M for nitrocefin hydrolysis. (A) reaction rate vs substrate concentration (Henri-Michaelis-Menten) plot and (B) the Hanes-Woolf plot.

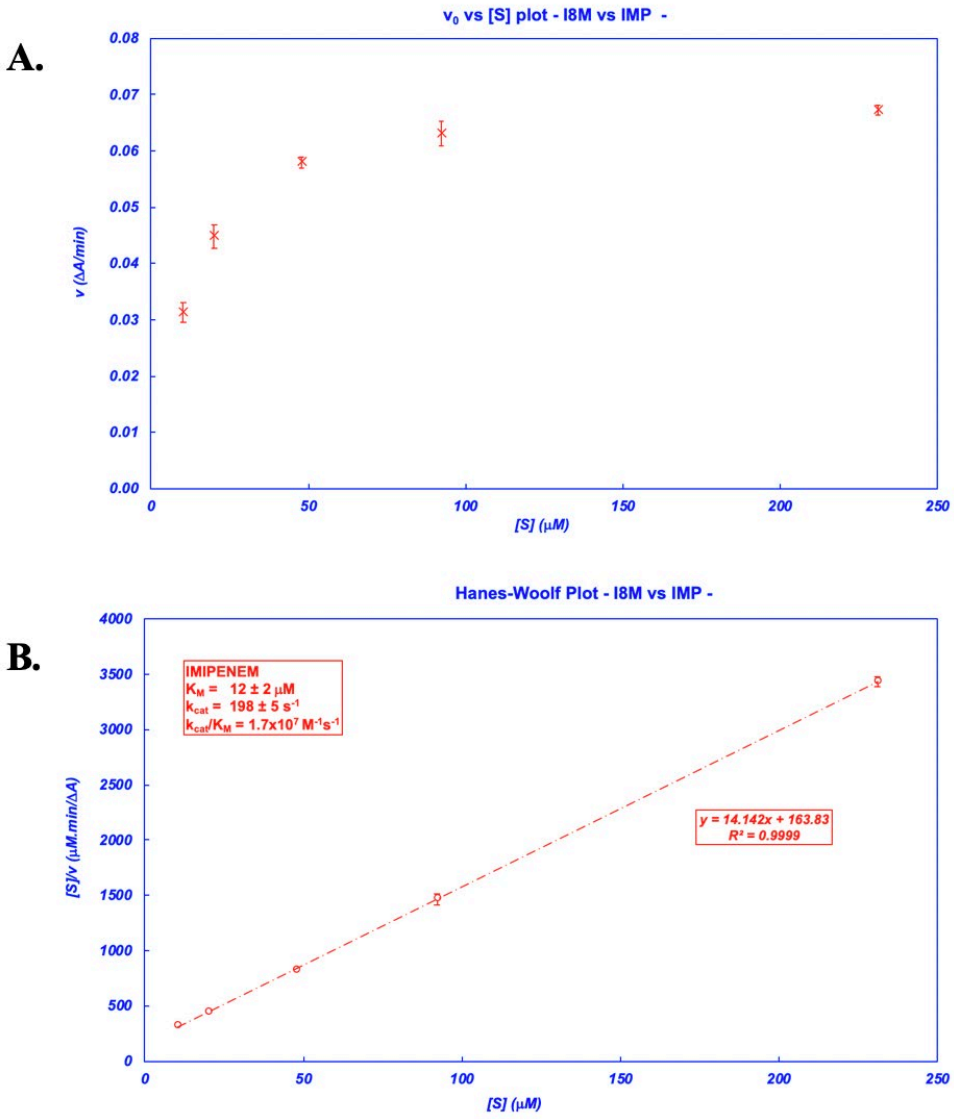

Figure 8.3.2: Determination of the kinetic parameters of I8M for imipenem hydrolysis. (A) reaction rate vs substrate concentration (Henri-Michaelis-Menten) plot and (B) the Hanes-Woolf plot.

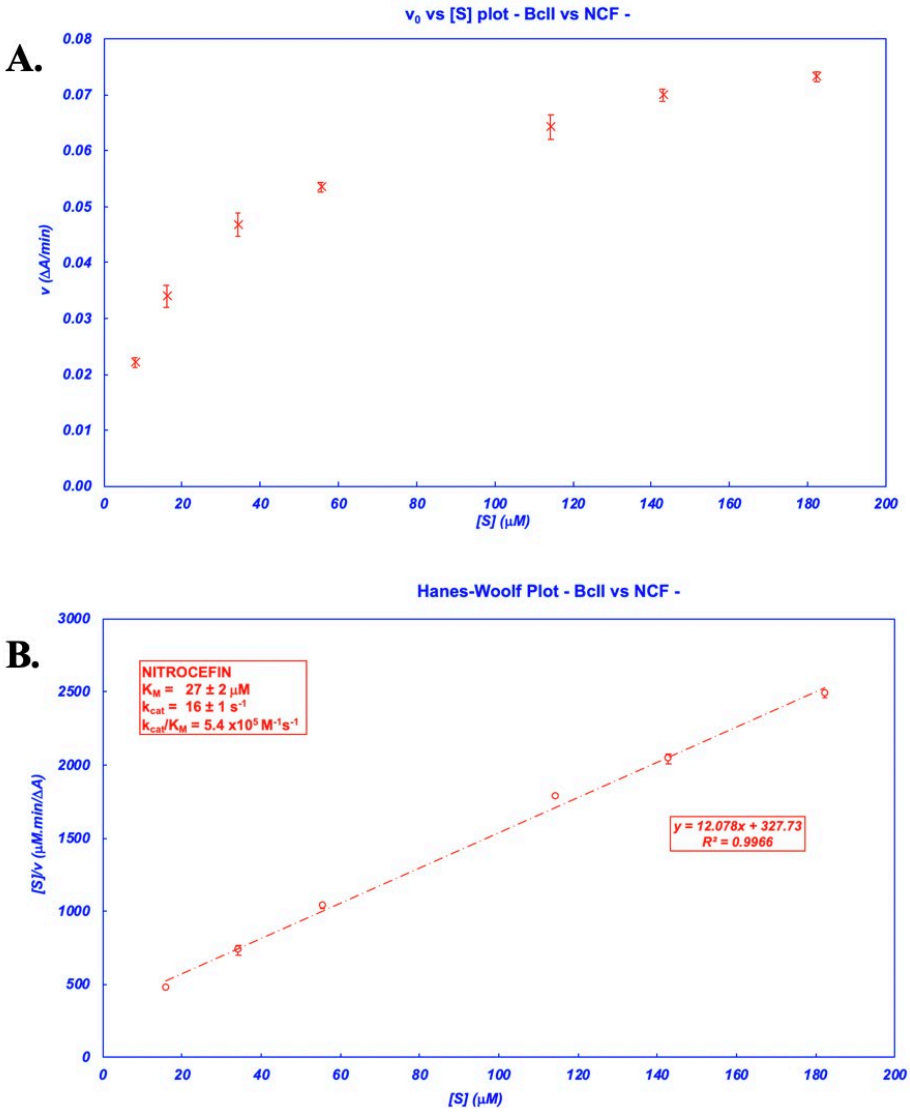

Figure 8.3.3: Determination of the kinetic parameters of BcII for nitrocefin hydrolysis. (A) reaction rate vs substrate concentration (Henri-Michaelis-Menten) plot and (B) the Hanes-Woolf plot.

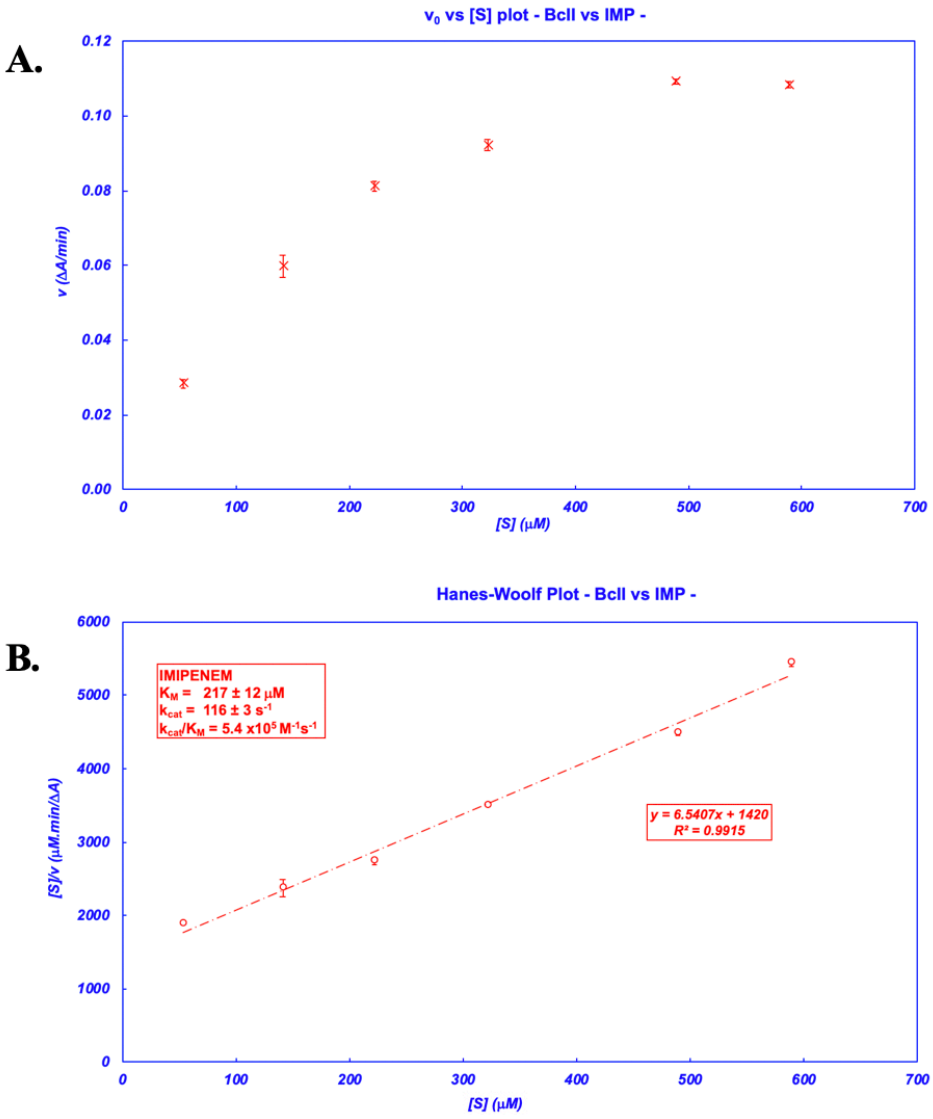

Figure 8.3.4: Determination of the kinetic parameters of BcII for imipenem hydrolysis. (A) reaction rate vs substrate concentration (Henri-Michaelis-Menten) plot and (B) the Hanes-Woolf plot.

8.4 Patent application

Acknowledgement of receipt

We hereby acknowledge receipt of your request for the processing of an international application according to the Patent Cooperation Treaty as follows:

Submission number	11288143
PCT application number	PCT/EP2022/075025
Date of receipt	08 September 2022
Receiving Office	European Patent Office, The Hague

AN ENGINEERED YEAST CELL FOR THE DELIVERY OF ANTIBIOTIC-INACTIVATING ENZYMES

Abstract

The present invention relates to a yeast cell producing a functional antibiotic-inactivating enzyme. The yeast cell of the invention comprises an exogenous nucleic acid encoding the antibiotic-inactivating enzyme, wherein the exogenous nucleic acid comprises an intron able to prevent the production of a functional antibiotic-inactivating enzyme in a bacterial host cell.

FIELD OF THE INVENTION

The present invention relates to a yeast cell producing a functional antibiotic-inactivating enzyme. The yeast cell of the invention comprises an exogenous nucleic acid encoding the antibiotic-inactivating enzyme, wherein the exogenous nucleic acid comprises an intron able to prevent the production of a functional antibiotic-inactivating enzyme in a bacterial host cell.

8.5 Published article on endogenous fecal β-lactamase activity

AMERICAN SOCIETY FOR MICROBIOLOGY | mBio®

RESEARCH ARTICLE

A Clinical Study Provides the First Direct Evidence That Interindividual Variations in Fecal β-Lactamase Activity Affect the Gut Mycobiota Dynamics in Response to β-Lactam Antibiotics

Margot Delavy,[a] Charles Burdet,[b,c] Natacha Sertour,[a] Savannah Devente,[d] Jean-Denis Docquier,[d] Nathalie Grall,[b] Stevenn Volant,[e] Amine Ghozlane,[e] Xavier Duval,[b,f] France Mentré,[b,c] Christophe d'Enfert,[a] Marie-Elisabeth Bougnoux,[a,g] on behalf of the PrediRes Study Group

[a]Institut Pasteur, Université Paris Cité, INRAE USC2019, Unité Biologie et Pathogénicité Fongiques, Paris, France
[b]Université Paris Cité, IAME, INSERM, Paris, France
[c]AP-HP, Département d'Epidémiologie, Biostatistique et Recherche Clinique, Hôpital Bichat, Paris, France
[d]Università di Siena, Dipartimento di Biotecnologie Mediche, Siena, Italy
[e]Institut Pasteur, Université Paris Cité, Bioinformatics and Biostatistics Hub, Paris, France
[f]Clinical investigation center, INSERM 1425, IAME, Hôpital Bichat, Assistance Publique des Hôpitaux de Paris (APHP), Université Paris Cité, Paris, France
[g]Unité de Parasitologie-Mycologie, Service de Microbiologie Clinique, Hôpital Necker-Enfants-Malades, Assistance Publique des Hôpitaux de Paris (APHP), Paris, France

ABSTRACT Antibiotics disturb the intestinal bacterial microbiota, leading to gut dysbiosis and an increased risk for the overgrowth of opportunistic pathogens. It is not fully understood to what extent antibiotics affect the fungal fraction of the intestinal microbiota, the mycobiota. There is no report of the direct role of antibiotics in the overgrowth in healthy humans of the opportunistic pathogenic yeast *Candida albicans*. Here, we have explored the gut mycobiota of 22 healthy subjects before, during, and up to 6 months after a 3-day regimen of third-generation cephalosporins (3GCs). Using ITS1-targeted metagenomics, we highlighted the strong intra- and interindividual diversity of the healthy gut mycobiota. With a specific quantitative approach, we showed that *C. albicans* prevalence was much higher than previously reported, with all subjects but one being carriers of *C. albicans*, although with highly variable burdens. 3GCs significantly altered the mycobiota composition and the fungal load was increased both at short and long term. Both *C. albicans* relative and absolute abundances were increased but 3GCs did not reduce intersubject variability. Variations in *C. albicans* burden in response to 3GC treatment could be partly explained by changes in the levels of endogenous fecal β-lactamase activity, with subjects characterized by a high increase of β-lactamase activity displaying a lower increase of *C. albicans* levels. A same antibiotic treatment might thus affect differentially the gut mycobiota and *C. albicans* carriage, depending on the treated subject, suggesting a need to adjust the current risk factors for *C. albicans* overgrowth after a β-lactam treatment.

IMPORTANCE Fungal infections are redoubtable healthcare-associated complications in immunocompromised patients. Particularly, the commensal intestinal yeast *Candida albicans* causes invasive infections in intensive care patients and is, therefore, associated with high mortality. These infections are preceded by an intestinal expansion of *C. albicans* before its translocation into the bloodstream. Antibiotics are a well-known risk factor for *C. albicans* overgrowth but the impact of antibiotic-induced dysbiosis on the human gut mycobiota—the fungal microbiota—and the understanding of the mechanisms involved in *C. albicans* overgrowth in humans are very limited. Our study shows that antibiotics increase the fungal proportion in the gut and disturb the fungal composition, especially *C. albicans*, in a subject-dependent manner. Indeed, variations across subjects in *C. albicans*

Editor Joseph Heitman, Duke University

Address correspondence to Marie-Elisabeth Bougnoux, bougnoux@pasteur.fr.

The authors declare no conflict of interest.

This article is a direct contribution from Christophe d'Enfert, a Fellow of the American Academy of Microbiology, who arranged for and secured reviews by Scott Filler, UCLA, and Iliyan Iliev, Cornell University.

Received 17 October 2022
Accepted 21 October 2022

burden in response to β-lactam treatment could be partly explained by changes in the levels of endogenous fecal β-lactamase activity. This highlighted a potential new key factor for *C. albicans* overgrowth. Thus, the significance of our research is in providing a better understanding of the factors behind *C. albicans* intestinal overgrowth, which might lead to new means to prevent life-threatening secondary infections.

KEYWORDS antibiotics, *Candida albicans*, gut mycobiota, healthy individuals, beta-lactamases

Interest in the role of the gut microbiota in health and disease is rising (1–4) and the role of antibiotics as major disturbers of the microbiota healthy state has been largely studied (5–8). By killing the resident bacteria of the gut, broad-spectrum antibiotics reduce bacterial diversity in the gastrointestinal (GI) tract and decrease the abundance of beneficial bacteria (5, 7). They also alter the gut microbiota interaction network, thus contributing to the overgrowth of opportunistic pathogens (6, 9). More alarmingly, the prolonged use of antibiotics may promote antibiotic resistance (10). For example, β-lactam exposure can lead to the selection of specific gut bacteria able to produce β-lactamases, enzymes that can hydrolyze β-lactam antibiotics, leading to an overall increase in antibiotic resistance (11, 12).

While the bacterial microbiota is extensively studied, less attention has been paid to the mycobiota—the fungal part of the microbiota—and to the consequences that antibiotic-induced dysbiosis may have on the fungal communities of the gut. It is now well established that fungi can rapidly proliferate in the GI tract of mice after removal of gut bacteria by antibiotics (13). The GI tract of mice is not naturally colonized by the opportunistic pathogen *Candida albicans* and antibiotics have been used to trigger such colonization (14), suggesting that they clear specific bacteria able to inhibit *C. albicans* growth in the mouse GI tract (15). Yet, we need more information about the impact of an antibiotic-induced dysbiosis on the healthy human gut mycobiota and specifically *C. albicans*. Because *C. albicans* systemic infections are responsible for thousands of deaths each year (16) and antibiotics are a well-known risk factor for these infections (17), we need to better understand the mechanisms of *C. albicans* overgrowth in the human gut, upon antibiotic treatment.

In this work, we prospectively followed two parallel groups of 11 healthy subjects each, before, during, and after they were treated intravenously with either cefotaxime or ceftriaxone, two third-generation cephalosporin (3GC) antibiotics that share a similar activity spectrum (8). We quantified the levels of *C. albicans* carriage in all subjects and characterized their healthy mycobiota and its variability during the 2-week period preceding antibiotic administration. Then, we analyzed the changes in terms of fungal diversity, fungal burden, community profile, and *C. albicans* levels, occurring in the mycobiota after antibiotics were administered, both at short and long term. Finally, we monitored the level of fecal β-lactamase activity, which is known to modulate the intensity of the post-3GC intestinal dysbiosis, and we correlated the changes in β-lactamase activity with the impact of 3GCs on *C. albicans* carriage.

RESULTS

The gut mycobiota of healthy subjects is highly dynamic and variable. To study the healthy mycobiota, we used fecal samples collected from each of 22 healthy volunteers at day −15 (−D15), −D7, and −D1, before antibiotic administration (see Materials and Methods). In total, 54 fecal samples (one to three available per subject) were available for analyses.

First, we assessed the fungal load, i.e., the ratio between the fungal DNA concentration and the total fecal DNA (see Materials and Methods). The mycobiota represented a very small fraction of the total microbiota in healthy subjects (median fungal load: 7.9×10^{-6}, min: 6.7×10^{-10}, max: 1.5×10^{-3}, Fig. S1A).

Using ITS1 sequencing, we further characterized the mycobiota composition of the 22 subjects during the 2 weeks preceding 3GC exposure. We identified 233 different

TABLE 1 Prevalence of the main fungal species in healthy subjects and in their fecal samples, estimated by ITS1 sequencing

Main fungal species	Prevalence[a]	
	Fecal samples (%) (*N* = 54)	Healthy subjects (%) (*N* = 22)
Vanrija humicola	98.2	100.0
Galactomyces candidus	92.6	95.5
Saccharomyces cerevisiae	88.9	95.5
Candida parapsilosis	88.9	95.5
Penicillium roqueforti	72.2	90.9
Cutaneotrichosporon curvatum	87.0	86.4
Malassezia restricta	88.8	77.3
Candida albicans	75.9	72.7
Debaryomyces hansenii	68.5	59.1

[a]A species is considered present in a sample if its relative abundance is above 0.1%. A species is considered present in a subject if it is present in at least one sample between −D15 and −D1.

OTUs, 182 OTUs (78.1%) being annotated at the phylum level, 167 (71.7%) at the genus level, and 123 (52.8%) at the species level. Overall, the 167 OTUs annotated at the genus level and the 123 OTUs annotated at the species level represented 99.7% and 91.2% of the total number of sequences, respectively.

Ascomycota was the most abundant phylum (mean relative abundance of 77.9%), followed by Basidiomycota (21.9%; Fig. S1B). Sixty-two fungal genera were identified in at least two samples, with eight reaching a mean relative abundance across subjects above 1% (Fig. S1C). Ninety-five species were identified in at least two samples, nine reaching a mean relative abundance across subjects above 1% (Table 1). The taxa relative abundances were highly variable between individuals and across time (Fig. 1A), with *Galactomyces candidus* being the most disparately represented taxa, with a relative abundance varying from 0% to 99.2% depending on the sample.

We identified a median of only 25 OTUs per sample (min: 5, max: 55, Fig. 1B), corresponding to a median Shannon Index of 1.18 (min: 0.18, max: 2.26, Fig. 1B), reflecting a low richness and evenness within each sample. Unlike this low α-diversity, we observed a high β-diversity, which quantifies the level of dissimilarity between samples, with a median Bray-Curtis dissimilarity index of 0.87 between the subjects (min: 0.02 max: 1.00, Fig. 1C). We also followed the variations occurring overtime during the 2-week period preceding 3GC exposure. The within subjects' diversity, measured between the samples collected from the same subject at different time, was almost as high as the between subject diversity, with a Bray-Curtis dissimilarity index of 0.75 (min: 0.08, max: 0.99, Fig. 1C; Fig. S2).

We quantified the levels of fecal *C. albicans* in these volunteers by determining the absolute abundance of *C. albicans* using specific qPCR. We detected *C. albicans* DNA at least once between −D15 and −D1 in 20/21 subjects (95.2%) before 3GC administration. In total, 42/51 samples analyzed were positive for *C. albicans* (82.4%). In these samples, *C. albicans* DNA levels ranged from 2.8×10^{-4} to 1.26 ng/g of stool, with a median of 9.4×10^{-3} ng/g of stool (Fig. 1D). In comparison, by using ITS1 sequencing data and culture methods, we could detect *C. albicans* in only 16/22 (72.7%; Table 1) and in 7/22 (15.8%) subjects, respectively.

Cefotaxime and ceftriaxone exposure increases the fungal load and disturbs the gut mycobiota composition. To measure how much the antibiotic treatment affected the gut mycobiota, we compared its features, including the fungal load, genera and species composition, and *C. albicans* absolute levels, at baseline (D0) with those during and after antibiotics (Fig. 2A). Data collected at −D1 were used as baseline. If missing, −D7 data were used instead (see Fig. S3).

We used two metrics to estimate changes during and after antibiotic administration: the areas under the curve (AUCs) of the mycobiota characteristics' changes from D0, and the changes from D0 of the mycobiota characteristics, for each subject, at

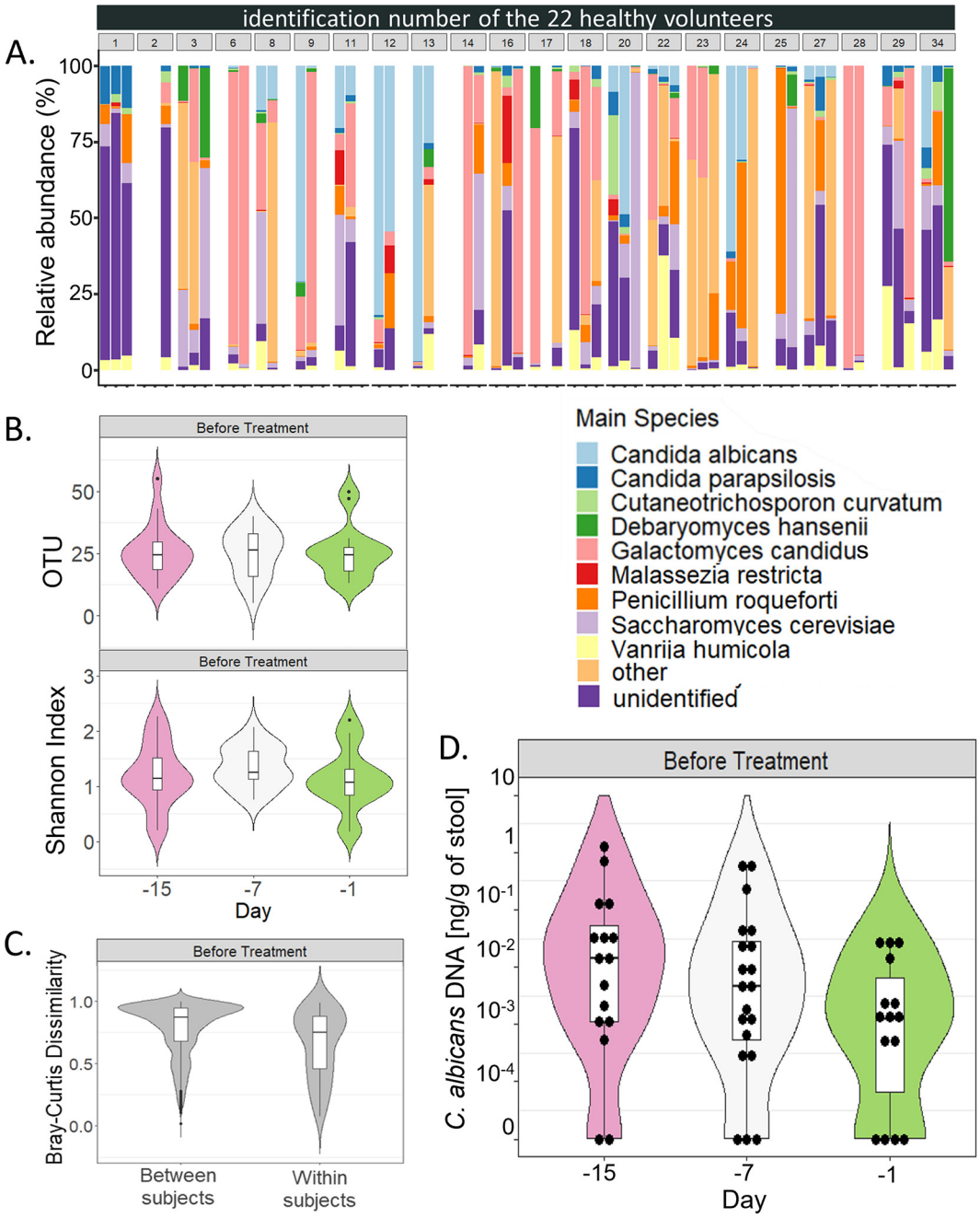

FIG 1 Dynamic of the mycobiota characteristics in 22 healthy individuals during a 2-week period. (A) Fungal species relative abundances at 1-week apart time points for 22 healthy subjects. For each subject, barplot are ordered by time (−D15, −D7, −D1 before antibiotics). Represented species reached a mean relative abundance across subjects above 1%. (B) Alpha diversity: violin plot of the number of OTUs and of the Shannon index values at 1-week apart time points for 22 healthy subjects. (C) Beta diversity: Bray-Curtis dissimilarity values between samples donated by different subjects (between subjects) and between samples donated by the same subjects (within subjects) for ITS1 sequencing data. Values range from 0 to 1, with 0 being the least dissimilar and 1 being the most dissimilar. (D) Violin and boxplots of the *C. albicans* DNA levels at 1-week apart time points for 22 healthy subjects. Each dot represents a sample. For all panels, the upper whiskers extend from the hinge to the largest value below 1.5× the interquartile range, and the lower whiskers extend from the hinge to the smallest value above 1.5× the interquartile range.

different time points between D1 and D180. The first metric allows the aggregation of both the duration of the changes and their amplitude whereas the second allows the detection of more punctual variations.

We observed a general long-term increase of the fungal load in the 22 subjects early after the start of the antibiotic treatment. The fungal load significantly increased

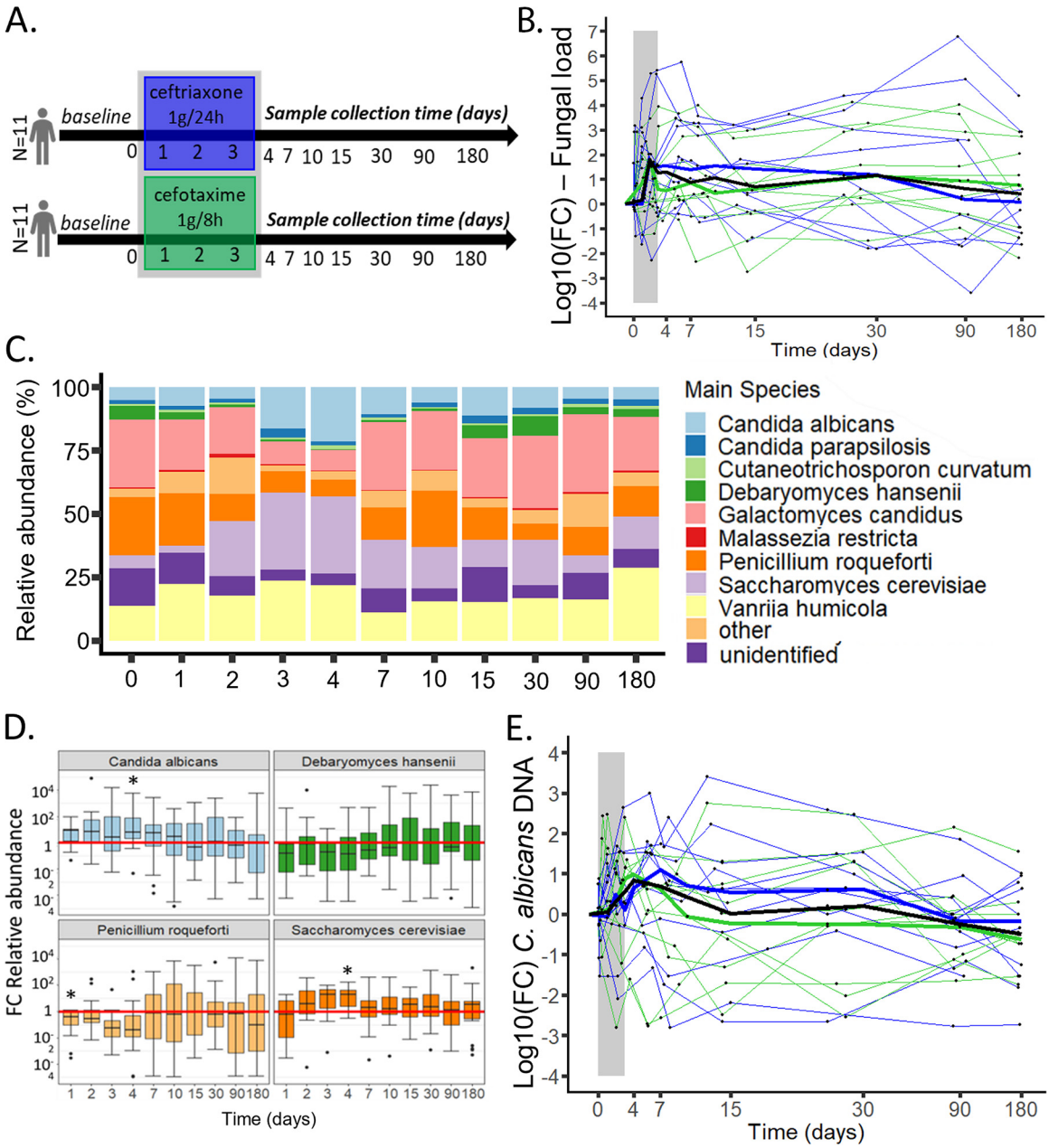

FIG 2 Impact of 3-day cefotaxime and ceftriaxone IV treatment on the gut mycobiota of 22 healthy subjects followed for a 6-month period. (A) Study design. (B) Log_{10} (foldchange [FC]) of the fungal load following ceftriaxone and cefotaxime treatment (gray area). Thin lines represent the subjects, thicker lines represent the medians at each day for each treatment group (blue and green) and for all subjects (black). (C) Main fungal species distribution following ceftriaxone and cefotaxime treatment. (D) Distribution of the relative abundance log_{10} (FC) AUCs for *Candida albicans*, *Debaryomyces hansenii*, *Penicillium roqueforti*, and *Saccharomyces cerevisiae*, highlighting the duration and the amplitude of the perturbations *q value $<$ 0.05, Wilcoxon t-test, false-discovery rate correction. Upper whiskers extend from the hinge to the largest value below 1.5× the interquartile range, and the lower whiskers extend from the hinge to the smallest value above 1.5× the interquartile range. (E) Log_{10} (FC) of *C. albicans* DNA levels following ceftriaxone and cefotaxime treatment (gray area). Thin lines represent the subjects, thicker lines represent the medians at each day for each treatment group (blue and green) and for all subjects (black).

immediately after the start of antibiotics, independently of the antibiotic used, with a positive AUCs for all calculated periods between D0 and D2, and D0 and D90 (Wilcoxon test; *P* values of 0.008, 0.017, 0.040, 0.014, 0.009, 0.005, 0.006, and 0.048, respectively) with a maximal 62.3-fold increase at D2 (min: 0.02, max: 1.8 $\times 10^4$; Wilcoxon test; *P* value of 0.007; Fig. 2B; Fig. S4B; Table S1). No difference was observed between the subjects treated with ceftriaxone and those treated with cefotaxime (Fig. 2B; Table S2).

At D15, we observed a slight increase of the number of fungal OTUs, compared with D0 (Wilcoxon test; *P* value of 0.030; Table S1) but not of the Shannon Index (Wilcoxon test; *P* value of 0.47), suggesting that the fungal α-diversity is not strongly impacted by the antibiotics. No difference was observed between the subjects treated with ceftriaxone or those treated with cefotaxime, and this for all fungal diversity indices studied (Table S2).

Three genera were significantly impacted by the antibiotics *Debaryomyces* sp., *Penicillium* sp., and *Saccharomyces* sp. (Fig. S4A and B; Table S1). *Debaryomyces* sp. were significantly decreased immediately after the start of the treatment, with negative AUCs between D0 and D3 (Wilcoxon test; *q* value of 0.02) and a maximal but not significant 12.5-fold drop at D3 (min: 0.09, max: 1.7×10^5, Wilcoxon test; *q* value of 0.08). *Penicillium* sp. were also decreased immediately after the start of the treatment, with negative AUCs between D0 and D2 and up to D0 and D7 (Wilcoxon test; *q* values of 0.01, 0.005, 0.003, and 0.0002, respectively) with a maximal 21.4-fold decrease at D4 (min: 0.81, max: 776.2; Wilcoxon test; *q* value of 0.0008). On the contrary, *Saccharomyces* sp. relative abundance was punctually increased at D4 (median: 19.5-fold increase, min: 0.32, max: 169.8), compared with baseline (Wilcoxon test; *q* value of 0.01), before returning to basal levels. No significant difference between the subjects of the two treatment groups was observed at any day, for all genera tested (Table S2).

In addition, at the species level, four taxa were significantly affected by 3GC treatment: *S. cerevisiae*, *D. hansenii*, *P. roqueforti*, and *C. albicans* (Fig. 2C; Table S1). *D. hansenii* was decreased for the period D0 to D3, with a corresponding negative AUC (Wilcoxon test; *q* value of 0.047; Fig. S4C) and *P. roqueforti* was punctually reduced after the treatment with a 2.4-fold drop at D1 (min: 0.74, max: 3.3×10^3; Wilcoxon test; *q* value of 0.026; Fig. 2D). In contrast, *C. albicans* and *S. cerevisiae* relative abundance displayed a 9.8-fold and 19.5-fold raise at D4, respectively (*C. albicans:* max: 1.1×10^5, min: 0.004; Wilcoxon test; *q* value of 0.04, *S. cerevisiae:* max: 169.8, min: 0.32 Wilcoxon test; *q* value of 0.026; Fig. S4C). As for the genera, no significant difference between the subjects of the two groups was observed for any species (Table S2).

Not only *C. albicans* relative abundance but also its absolute abundance was punctually increased after antibiotics. Indeed, 3GC administration led to a punctual raise of *C. albicans* DNA levels on the D0 to D4 period (Wilcoxon test, *q* value of 0.047) with a maximal 2.1-fold increase at D2 (min: 0.03, max: 288.4; Wilcoxon test; *P* value of 0.02; Fig. 2E), when measured by qPCR. However, this increase of *C. albicans* DNA levels was subject-dependent. For example, subject 1 displayed an impressive increase of *C. albicans* DNA, with a maximal 2,521.3-fold raise at D15 whereas *C. albicans* DNA levels were reduced in subject 12 after the treatment. No difference was observed between the two groups of treatment at any days (Fig. 2E; Table S2).

Change in β-lactamase activity levels as a key parameter for *C. albicans* overgrowth in the GI tract after third-generation cephalosporin administration. β-lactamase activity was measured in each fecal sample by dosing the NFC-hydrolyzing activity. This activity was heterogenous between subjects before antibiotics, ranging from 2.40 to 1,240 nmol/min·g of stool, with no difference between the two groups that received either ceftriaxone or cefotaxime (Wilcoxon test, *P* value: 0.78). Globally, β-lactamase activity was significantly increased after 3GC administration for all the periods calculated between D0 to D3 and D0 to D180 (Wilcoxon test; *P* values of 0.040, 0.006, 0.002, 0.0008, 0.0003, 0.0006, 0.0007, and 0.03, respectively), with a maximal 2.25-fold increase at D7 (Fig. 3A). However, we observed two types of behavior in the D0 to D10 AUC of the change in β-lactamase activity, with some subjects displaying a high increase of the β-lactamase activity after antibiotic treatment (up to a 28-fold rise) whereas others showed no change or even a decrease of this activity (up to a 7-fold decrease). Therefore, we split the 22 subjects in two groups; the "high" group was characterized by a strong increase of the fecal β-lactamase activity (AUC D0 to D10 $\geq$ 2.36), whereas the "low" group had a lower increase or even a decrease of this activity (AUC D0 to D10 $<$ 2.36; Fig. 3B). Changes of *C. albicans* DNA levels were significantly different between subjects of the "low" and "high" groups, both for the D0 to D10 period and at D4 and D30 (Wilcoxon test; *P* value of 0.02, 0.02, and 0.007, respectively). At D4 and D30,

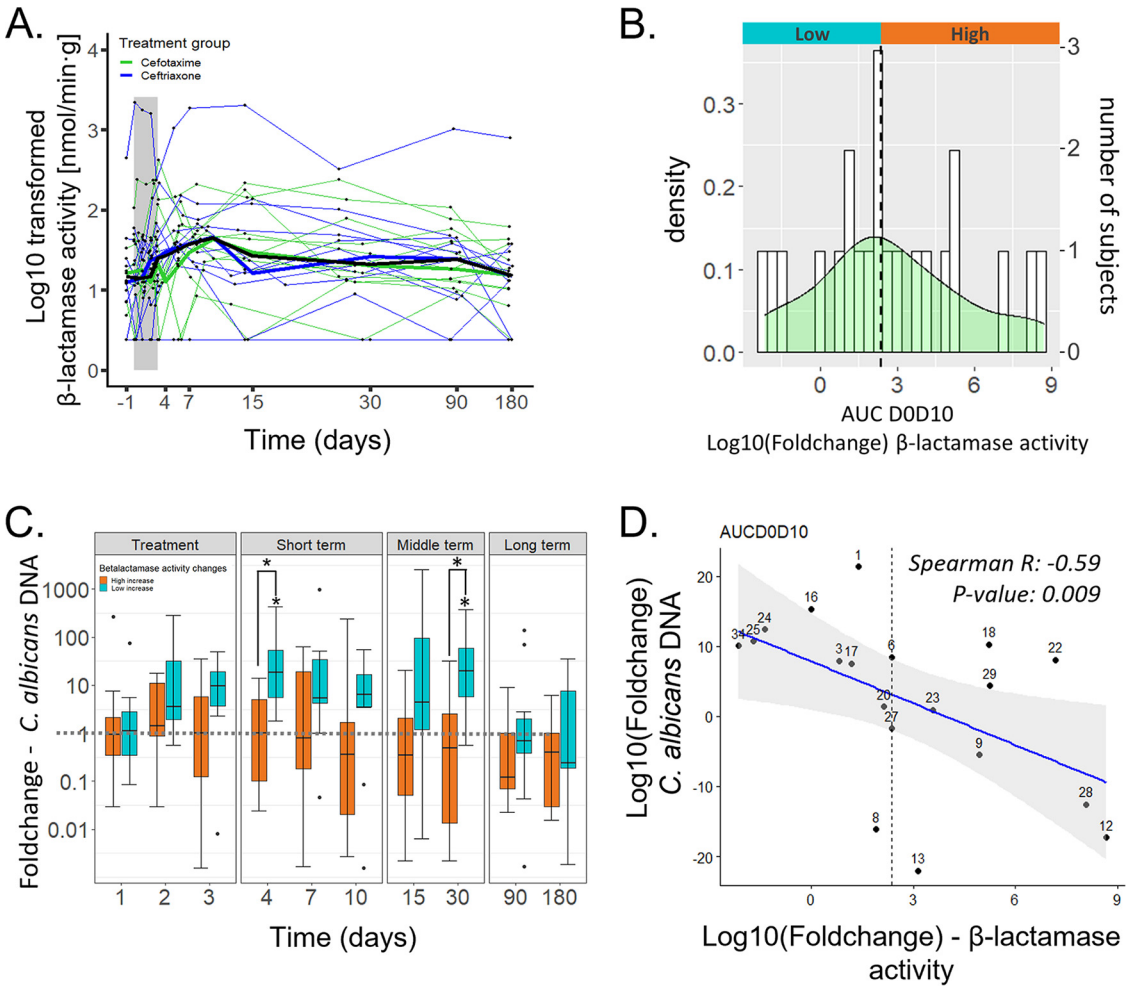

FIG 3 Change in β-lactamases activity levels as a key parameter for *C. albicans* proliferation in the gut after third-generation cephalosporin administration. (A) β-lactamases activity before, during, and after the antibiotic treatment. Thin lines represent the subjects; thicker lines represent the medians at each day for each treatment group (ceftriaxone, blue; cefotaxime, green) and for all subjects (black). (B) Distribution of the D0 to D10 AUCs of the change of β-lactamases activity in 22 healthy subjects. The density distribution is represented by the green curve and the number of subjects for each range of AUC values are represented by the white histogram. The group "high" (orange) regroups the subjects with a D0 to D10 AUC above the median (black dashed line) and the group "low" (blue) regroups the subjects with a D0 to D10 AUC below the median. (C) Boxplots of *C. albicans* DNA levels $\log_{10}$ (FC) following ceftriaxone and cefotaxime treatment. Orange boxplots indicates values for the subjects from the group "high" of and blue boxplots represents the values for the subjects from the group "low." Upper whiskers extend from the hinge to the largest value below 1.5× the interquartile range, and the lower whiskers extend from the hinge to the smallest value above 1.5× the interquartile range. (D) Correlation plot of the $\log_{10}$ (FC) AUCs of *C. albicans* DNA levels and β-lactamases activity for the D0 to D10 period. Regression is represented by a blue line and the confidence interval by the gray area. Subjects are designated by their ID number.

C. albicans DNA levels were significantly increased in the group "low," whereas no change was detected in the group "high" (D4: Wilcoxon test; *P* value of 0.008 and 0.84, respectively; D30: Wilcoxon test; *P* value of 0.023 and 0.26, respectively; Fig. 3C).

Finally, we showed a highly significant negative interaction between the D0 to D10 AUC of the change in β-lactamase activity and the D0 to D10 AUC of the change in *C. albicans* DNA levels (Spearman correlation; R: −0.59, *P* value: 0.009; Fig. 3D). No such correlation could be found between the D0 to D10 AUC of the fungal load and the D0 to D10 AUC of the change in β-lactamase activity (Spearman correlation; R: −0.25, *P* value: 0.3).

DISCUSSION

In this study, we explored the impact of β-lactam antibiotics on the human gut mycobiota by performing a targeted metagenomic analysis of the mycobiota of healthy subjects before, during, and after 3GC exposure. 3GC strongly affected the

mycobiota, especially *C. albicans* carriage, with wide intersubject variations that were not related to the type of 3CG they received. We identified the changes of fecal β-lactamase activity after treatment as a potential key factor regulating *C. albicans* overgrowth, with subjects characterized by a low increase of β-lactamase activity displaying a stronger increase of *C. albicans* levels following antibiotics. This regulation is likely mediated by a differential impact of antibiotics on the endogenous gut bacteria, according to differences in the occurrence of β-lactamase-producing bacteria in the microbiota. Briefly, a microbiota rich in β-lactamase-producing bacteria would favor 3GC hydrolysis, reduced antibiotic-induced microbiota dysbiosis, and reduced *C. albicans* overgrowth. In contrast, a microbiota poor in β-lactamase-producing bacteria would allow 3GC maintenance, high antibiotic-induced microbiota dysbiosis, and high *C. albicans* overgrowth. This phenomenon may explain the so-called *C. albicans* colonization resistance experienced by some individuals. Such colonization resistance has been the subject of an old and preliminary report (11) but has not been further explored until this present study. Overall, these results are coherent with the hypothesis stating that specific intestinal bacteria or their metabolites regulate *C. albicans* overgrowth (6, 14, 15, 18, 19). Our results attest that the same antibiotic regimen may affect differentially the microbiota and consequently lead to different risks of *C. albicans* overgrowth depending on the subject that receives it. The current paradigm stating that antibiotics are systematically a risk factor for *C. albicans* overgrowth should thus be adjusted for treatments based on β-lactams antibiotics. Monitoring fecal β-lactamase activity during and after a β-lactams antibiotic treatment could be an accurate predictor of the actual risk of a later increase of *C. albicans* burden.

As importantly, we found that *C. albicans* was present, in varying quantity, in the gut of almost every healthy subject. This study is the first to use a qPCR method to quantify and follow *C. albicans* carriage, allowing an increasingly specific detection. Using more traditional assays, the prevalence of *C. albicans* in these subjects was much lower and close to what has been previously reported (20–22). This suggests that our results reflect the reality of what is the true presence of *C. albicans* in the gut of healthy humans. If confirmed in a larger study, this might indicate that *C. albicans* is not a facultative commensal as previously thought, but that it is able to maintain itself in the gut of most individuals, even at very low concentration.

That almost all subjects in this study were colonized by *C. albicans* renders our cohort particularly adapted to follow the effects of antibiotic treatment on *C. albicans* carriage. Moreover, contrary to what has been done in other studies (6), our focus on a single antibiotic family allows a precise understanding on how 3GC, a largely used antibiotics family, acts on the human gut mycobiota. This allowed us to show that 3GC strongly affect the gut mycobiota, with a global increase of the fungal load, as well as a punctual perturbation of several fungal species and genera, including *C. albicans*. Indeed, both *C. albicans* relative and absolute abundances were increased after the start of antibiotics. This is particularly concerning since a recent report showed that the administration of β-lactam antibiotics leads to increased virulence of *C. albicans* (23). By killing Gram-negative commensal bacteria, β-lactams cause the release of a large amount of peptidoglycans, which can then induce *C. albicans* hyphal growth, an essential virulence factor of this species (23). Moreover, a recent study showed that exposure to non-3GC broad-spectrum antibiotics not only promotes susceptibility to *C. albicans* systemic infection in mice, but also increases the mortality, through an impairment of the lymphocyte-dependent IL-17A- and GM-CSF-mediated response (24). Therefore, *C. albicans* cannot only growth in patients treated with 3GCs, but its disruptive abilities might also be increased. This can be particularly problematic, not only for immunosuppressed patients, but also for those with inflammatory bowel disease that are already carrying higher levels of *C. albicans* (25, 26) in their gut.

Overall, most of the mycobiota perturbations following 3GC treatment were subject-dependent, with some subjects more impacted than others. This is not particularly surprising considering the within- and between-subjects Bray-Curtis dissimilarity observed

pretreatment. This has already been reported (21) and suggests that the largest part of the fecal mycobiota is made of transient species brought by the diet, such as *D. hansenii*, which is commonly found in cheese (27), or potentially by the respiration of spores of filamentous fungi, which can then be swallowed, such as *Penicillium* sp. This hypothesis is supported by a recent study showing that diet-associated fungi are recovered with low relative abundances in mucosal surgical-recovered samples, highlighting the differences observed in the gut mycobiota depending on its spatial organization across the GI tract (28). Moreover, associated fungi strongly contribute to the fungal biomass of the fecal microbiota (29). Our results would also indicate that contrary to *Penicillium* sp. or *D. hansenii*, *C. albicans* main reservoir is indeed humans, which would explain why an environmental reservoir for this species has yet to be found (18, 30, 31).

Finally, fungi represented only a small fraction of the total microbiota based on total and fungal DNA quantification. This underrepresentation of the fungal community in the human gut has already been reported (32), but the authors did not quantify the exact proportion of the mycobiota. More recently, the fungal load of 24 healthy subjects was estimated, with results very similar to ours (33). Finally, Doron et al. confirmed that the fungal biomass was low within the gut microbiota, representing only 1% to 2% of the microbial biomass of the gut (29). However, to our knowledge, this present study is the first to assess the day-to-day variation of the fungal load in healthy individuals.

Taken together, this study offers a better understanding of the factors behind *C. albicans* overgrowth after antibiotics. We showed that a same antibiotic treatment may disturb differentially the gut microbiota, depending on the subject that receives it. This highlights the importance of a more personalized use of antifungal prophylaxis, and helps limiting the selection of fungi resistant to antifungal drugs in patients at high risk of invasive candidiasis, such as intensive care unit or haemato-oncology patients.

MATERIALS AND METHODS

CEREMI cohort. In this study, we used fecal samples from the CEREMI study, a prospective, open-label, and randomized clinical trial conducted from March 2016 to August 2017 in healthy adult subjects at the Clinical Investigation Center at Bichat-Claude Bernard Hospital (Paris, France) (8). Participants were given oral and written information and had to return signed consent before inclusion in the trial. For more information about the clinical trial, see Burdet et al. (8).

The 22 included subjects were randomized in a 1:1 ratio and were treated for 3 days with either ceftriaxone (1 g/24 h) or cefotaxime (1 g/8 h). 3GC were administered as a 30-min intravenous infusion using an automatic high-precision infusion pump.

Fecal samples were collected before treatment at −D15, −D7, and −D1; during treatment at D1, D2, and D3; and after treatment at D4, D7, D10, D15, D30, D90, and D180. Fecal samples were stored at −80°C.

Fungal DNA extraction from fecal samples. For each sample, 250 mg of stool was processed following the repeated bead beating plus column method described by Yu and Morrison (34), except than a FastPrep-24 device (MP Biomedicals, Belgium) was used instead of a Mini-Beadbeater.

Total fecal DNA levels were measured by Qubit (Invitrogen, USA) using the dsDNA Broad Range Kit (Invitrogen, USA). Samples for which this concentration was below 50 ng/μL were excluded from the analysis.

ITS1 sequencing. We prepared amplicon libraries, targeting the ITS1 region, using ITS1F and ITS2 primers (35, 36). Amplicon were generated by PCR using a 96-well thermal cycler in the following conditions: 95°C for 3 min, 25 cycles of 95°C for 30 s, 55°C for 30 s, 72°C for 30 s, and 72°C for 5 min, and cooling at 4°C. Amplicons were purified with AMPure XP (Beckman Coulter, USA) as described in the 16S Metagenomic Sequencing Library Preparation guide (37). Adapter were attached using Nextera XT Index Kit (Illumina, France) and the index PCRs were performed in the following conditions: 95°C for 3 min, eight cycles of 95°C for 30 s, 55°C for 30 s, 72°C for 30 s, and 72°C for 5 min, and cooling at 4°C. Barcoded PCR products were purified with AMPure XP (Beckman Coulter, USA) and verified and quantified on a Bioanalyzer DNA 1000 chip (Agilent, USA). Samples were normalized at 4 nM and pooled into a library, using 5 μL of each diluted sample. A PhiX sequencing control was prepared following the manufacturer's instructions. The libraries were sequenced in 300-bp paired-end using the MiSeq reagent kit V3 on Illumina MiSeq platform (Illumina, Evry, France).

OTU building process and taxonomic assignment. We recovered 8,819,635 amplicons from ITS1 region. After removal of singletons and chimera amplicons using the SHAMAN pipeline (38), we clustered the 56,634 remaining amplicons in OTUs using a cut-off value of 97% similarity. Thus, 4,648 OTUs were obtained and 551 of them could be aligned against fungal sequences of the UNITE database. On

these 551 fungal OTUs, 340 were present in at least two fecal samples and were conserved for the downstream analyses. We performed a first round of annotation on SHAMAN against the UNITE database (rev. 8.0) and then a second round against a more recent release of UNITE (rev. 8.2). The OTUs we could not annotate were submitted to a classic BLASTN. Only hits matched with a similarity above 97% to reference genomes were conserved. The abundances and weighted non-null normalized counts tables were generated with SHAMAN (38).

Quantitative PCR for detection of total fungal load in human DNA samples. Fungal DNA was quantified by TaqMan qPCR as described by Liu et al. (39) using a double dye MGB 5′ 6-FAM-labeled probe (Eurogentec, Belgium). All reactions were performed on a CFX96 real-time PCR system (Bio-Rad, USA) with the following conditions: 2 min at 50°C, 10 min at 95°C, 15 s at 95°C, and 1 min at 65°C, the last two steps repeated for 45 cycles. All samples were tested in two independent rounds, each time in duplicates.

The fungal load was estimated by dividing the fungal DNA concentration by the total DNA concentration of the sample (33), obtained by Qubit Broad Range protocol.

Quantitative PCR for detection of *C. albicans* DNA in human DNA samples. At 1:10 dilution, 7.5 μL of the extracted total fecal DNA were used as a template for TaqMan qPCR analysis, using probe and primers described by Guiver et al. (40), at 0.1 μM and 0.2 μM, respectively. All reactions were performed on a CFX96 real-time PCR system (Bio-Rad, USA) with the following conditions: 2 min at 50°C, 10 min at 95°C, 15 s at 95°C, and 1 min at 62°C; the last two steps repeated for 45 cycles. All samples were tested in two independent rounds, each time in duplicates.

Quantitative PCR amplification control. To exclude the presence of qPCR inhibitors, samples diluted at 1:10, were submitted to the Universal Exogenous qPCR Positive Control for TaqMan Assay (Eurogentec, Belgium), using a Cy5-QXL 670 Probe system (Eurogentec, Belgium). Manufacturer's recommendations were followed.

Culture of the fecal samples. A 10-μL loop of fecal samples was mixed with 100 μL H_2O and plated on a *Candida* CHROMAGAR medium plate (bioMérieux, France). Potential *C. albicans* colonies were further tested by MALDI-TOF MS (Brucker, USA) to confirm the identification.

Measure of the β-lactamase activity. Fecal β-lactamase activity was quantified by measuring the hydrolysis of nitrocephin, a chromogenic cephalosporin. Activity was measured at least in duplicate.

Fecal samples (stored at 65°C) were thawed 30 min on ice. Then, 140 mg to 380 mg of each fecal sample was mixed with 5 mL/g of stool HZn buffer (50 mM (2-hydroxyethyl)-1-piperazineethanesulfonic acid (HEPES) buffer, pH 7.5, supplemented with 50 μM ZnSO4) and agitated for 1 h. Samples were centrifuged twice at 4°C (15 min and 30 min). Then, 3 to 20μL of the obtained supernatant were mixed with 100 μM nitrocefin (Cayman Chemical, USA) and HZn buffer to reach a final volume of 200 μL. Samples were incubated 20 min at room temperature in a 1:1 ratio with HZn buffer. Nitrocefin hydrolysis was monitored in EnVision microplate reader (Perkin Elmer, USA) at a 482-nm wavelength. SpectraPlate-96 (Perkin-Elmer, USA) using an automated liquid handling Janus Integrator system (Perkin Elmer, USA) was used to conduct the assays.

β-lactamase activity was normalized to one gram of fecal sample and to 1-cm pathlength. Detection threshold was set at a cut-off value of 4.8 nmol/min·g of fecal sample.

Biostatistical analyses. All analyses were performed on R (version 4.0.2 [41]). We used the vegan package (v.2.5-6 [42]) to compute diversity indexes and ggplot2 package to generate the figures (v. 3.3.5 [43]).

We used samples collected at −D1 before treatment as baseline, called D0. If this sample was missing for a subject, sample collected at −D7 before treatment was used instead. If both samples were missing, sample collected at −D15 before treatment was used as D0 sample.

We calculated the change from baseline of the fungal load, *C. albicans* DNA absolute abundance, the relative abundance of the fungal genera, and species and β-lactamase activity. Null values were replaced by the minimal non-null value of the given variables divided by two, to allow a $\log_{10}$ transformation. Only the fungal genera and species reaching a maximal relative abundance superior to 1% for at least half of the subjects were analyzed. We calculated the AUCs using the R package MESS (v. 0.5.7, [44]) for each period from D0 to D2 up to D0 to D180 based on the normalized changes from baseline and the actual time and date of stool collection.

For all analyses, we used bilateral nonparametric Wilcoxon exact tests. We used a type I error of 0.05 and corrected the *P* values for multitesting using false discovery rate correction.

Data availability. The data sets generated during and/or analyzed during the current study are available from the corresponding author on reasonable request.

SUPPLEMENTAL MATERIAL

Supplemental material is available online only.

FIG S1, TIF file, 1.6 MB.

FIG S2, TIF file, 1 MB.

FIG S3, TIF file, 0.9 MB.

FIG S4, TIF file, 2 MB.

TABLE S1, XLSX file, 0.02 MB.

TABLE S2, XLSX file, 0.02 MB.

ACKNOWLEDGMENTS

This work was supported by grants from Agence Nationale de la Recherche (FunComPath ANR-14-IFEC-0004 and PrediRes ANR-16-CE15-0022); the French Government's Investissement d'Avenir program (Laboratoire d'Excellence Integrative Biology of Emerging Infectious Diseases [ANR10-LABX-62-IBEID]); the European Union's Horizon 2020 research and innovation program under the Marie Sklodowska-Curie action, Innovative Training Network (FunHoMic; Grant No. 812969) and Assistance Publique – Hôpitaux de Paris (CEREMI CRC13-179).

We thank Antoine Andremont and David Skurnik for the fruitful discussions.

We thank the Institut Pasteur Biomics platform (Marc Monot and Laurence Motreff) and the Institut Pasteur Bioinformatics and Biostatistics Hub for their help for generating and analyzing the sequencing data.

For the PrediRes study group: Charles Burdet (INSERM, Université de Paris APHP-Bichat Hospital), Erick Denamur (INSERM, Université de Paris), Xavier Duval (INSERM, Université de Paris, APHP-Bichat Hospital), Dusko Ehrlich (INRA Metagenopolis), France Mentré (INSERM, Université de Paris, APHP-Bichat Hospital), Eduardo P. C. Rocha (Institut Pasteur), Laurie Alla (INRA Metagenopolis), Emmanuelle Lechatelier (INRA Metagenopolis), Florence Levenez (INRA Metagenopolis), Nicolas Pons (INRA Metagenopolis), Benoît Quinquis (INRA Metagenopolis), Khadija Bourabha (INSERM), Antoine Bridier Nahmias (INSERM, Université de Paris), Olivier Clermont (INSERM, Université de Paris), Mélanie Magnan (INSERM, Université de Paris), Olivier Tenaillon (INSERM, Université de Paris), Camille d'Humières (INSERM, Université de Paris, APHP-Bichat Hospital, Institut Pasteur), Amandine Perrin (Institut Pasteur), Marie Touchon (Institut Pasteur), Dominique Rainteau (INSERM, Université Pierre et Marie Curie, APHP – Saint Antoine Hospital), Farid Ichou (ICAN), Philippe Lesnik (ICAN), Jimmy Mullaert (INSERM, Université de Paris, APHP – Bichat Hospital), Thu Thuy Nguyen (INSERM).

REFERENCES

1. Krajmalnik-Brown R, Lozupone C, Kang D-W, Adams JB. 2015. Gut bacteria in children with autism spectrum disorders: challenges and promise of studying how a complex community influences a complex disease. Microb Ecol Heal Dis 26.
2. Milani C, Ticinesi A, Gerritsen J, Nouvenne A, Lugli GA, Mancabelli L, Turroni F, Duranti S, Mangifesta M, Viappiani A, Ferrario C, Maggio M, Lauretani F, De Vos W, van Sinderen D, Meschi T, Ventura M. 2016. Gut microbiota composition and Clostridium difficile infection in hospitalized elderly individuals: a metagenomic study. Sci Rep 6:25945. https://doi.org/10.1038/srep25945.
3. Zuo T, Zhang F, Lui GCY, Yeoh YK, Li AYL, Zhan H, Wan Y, Chung ACK, Cheung CP, Chen N, Lai CKC, Chen Z, Tso EYK, Fung KSC, Chan V, Ling L, Joynt G, Hui DSC, Chan FKL, Chan PKS, Ng SC. 2020. Alterations in gut microbiota of patients with COVID-19 during time of hospitalization. Gastroenterology 159:944–955.e8. https://doi.org/10.1053/j.gastro.2020.05.048.
4. Turnbaugh PJ, Ley RE, Hamady M, Fraser-Liggett CM, Knight R, Gordon JI. 2007. The Human Microbiome Project. Nat 449:804–810. https://doi.org/10.1038/nature06244.
5. Burdet C, Nguyen TT, Duval X, Ferreira S, Andremont A, Guedj J, Mentré F, Ait-Ilalne B, Alavoine L, Duval X, Ecobichon JL, Ilic-Habensus E, Laparra A, Nisus ME, Ralaimazava P, Raine S, Tubiana S, Vignali V, Chachaty E, the DAV132-CL-1002 Study Group. 2019. Impact of antibiotic gut exposure on the temporal changes in microbiome diversity. Antimicrob Agents Chemother 63. https://doi.org/10.1128/AAC.00820-19.
6. Seelbinder B, Chen J, Brunke S, Vazquez-Uribe R, Santhaman R, Meyer AC, De Oliveira Lino FS, Chan KF, Loos D, Imamovic L, Tsang CC, Lam RPK, Sridhar S, Kang K, Hube B, Woo PCY, Sommer MOA, Panagiotou G. 2020. Antibiotics create a shift from mutualism to competition in human gut communities with a longer-lasting impact on fungi than bacteria. Microbiome 8:133. https://doi.org/10.1186/s40168-020-00899-6.
7. Fouhy F, Guinane CM, Hussey S, Wall R, Ryan CA, Dempsey EM, Murphy B, Ross RP, Fitzgerald GF, Stanton C, Cotter PD. 2012. High-throughput sequencing reveals the incomplete, short-term recovery of infant gut microbiota following parenteral antibiotic treatment with ampicillin and gentamicin. Antimicrob Agents Chemother 56:5811–5820. https://doi.org/10.1128/AAC.00789-12.
8. Burdet C, Grall N, Linard M, Bridier-Nahmias A, Benhayoun M, Bourabha K, Magnan M, Clermont O, d'Humières C, Tenaillon O, Denamur E, Massias L, Tubiana S, Alavoine L, Andremont A, Mentré F, Duval X, Andremont A, Burdet C, Duval X, Fantin B, Grall N, Marcault E, Massias L, Mentré F, Tubiana S, Alavoine L, Benhayoun M, Djerdjour F, Ecobichon J-L, Ilic-Habensus E, Laparra A, Mandic M, Nisus ME, Raine S, Ralaimazava P, Vignali V, Andremont A, d'Humières C, Grall N, Riberty J, Bourabha K, Nahmias AB, Clermont O, Denamur E, Magnan M, Tenaillon O, Massias L, Marcault E, Schneider M, for the CEREMI Group, et al. 2019. Ceftriaxone and cefotaxime have similar effects on the intestinal microbiota in human volunteers treated by standard-dose regimens. Antimicrob Agents Chemother 63. https://doi.org/10.1128/AAC.02244-18.
9. Smits WK, Lyras D, Lacy DB, Wilcox MH, Kuijper EJ. 2016. Clostridium difficile infection. Nat Rev Dis Primers 2:16020. https://doi.org/10.1038/nrdp.2016.20.
10. Blair JMA, Webber MA, Baylay AJ, Ogbolu DO, Piddock LJV. 2015. Molecular mechanisms of antibiotic resistance. Nat Rev Microbiol 13:42–51. https://doi.org/10.1038/nrmicro3380.
11. Leonard F, Andremont A, Leclerq B, Labia R, Tancrede C. 1989. Use of β-lactamase-producing anaerobes to prevent ceftriaxone from degrading intestinal resistance to colonization. J Infect Dis 160:274–280. https://doi.org/10.1093/infdis/160.2.274.
12. Niehus R, van Kleef E, Mo Y, Turlej-Rogacka A, Lammens C, Carmeli Y, Goossens H, Tacconelli E, Carevic B, Preotescu L, Malhotra-Kumar S, Cooper BS. 2020. Quantifying antibiotic impact on within-patient dynamics of extended-spectrum beta-lactamase resistance. Elife 9:1–20. https://doi.org/10.7554/eLife.49206.
13. Dollive S, Chen Y-Y, Grunberg S, Bittinger K, Hoffmann C, Vandivier L, Cuff C, Lewis JD, Wu GD, Bushman FD. 2013. Fungi of the murine gut: episodic variation and proliferation during antibiotic treatment. PLoS One 8:e71806. https://doi.org/10.1371/journal.pone.0071806.
14. Fan D, Coughlin LA, Neubauer MM, Kim J, Kim MS, Zhan X, Simms-Waldrip TR, Xie Y, Hooper LV, Koh AY. 2015. Activation of HIF-1α and LL-37 by commensal bacteria inhibits Candida albicans colonization. Nat Med 21:808–814. https://doi.org/10.1038/nm.3871.

15. Mirhakkak MH, Schäuble S, Klassert TE, Brunke S, Brandt P, Loos D, Uribe RV, Senne de Oliveira Lino F, Ni Y, Vylkova S, Slevogt H, Hube B, Weiss GJ, Sommer MOA, Panagiotou G. 2021. Metabolic modeling predicts specific gut bacteria as key determinants for Candida albicans colonization levels. ISME J 15:1257–1270. https://doi.org/10.1038/s41396-020-00848-z.
16. Brown GD, Denning DW, Gow NAR, Levitz SM, Netea MG, White TC. 2012. Hidden killers: human fungal infections. Sci Transl Med 4:165rv13.
17. Pappas PG, Lionakis MS, Arendrup MC, Ostrosky-Zeichner L, Kullberg BJ. 2018. Invasive candidiasis. Nat Rev Dis Prim 4.
18. d'Enfert C, Kaune AK, Alaban LR, Chakraborty S, Cole N, Delavy M, Kosmala D, Marsaux B, Fróis-Martins R, Morelli M, Rosati D, Valentine M, Xie Z, Emritloll Y, Warn PA, Bequet F, Bougnoux ME, Bornes S, Gresnigt MS, Hube B, Jacobsen ID, Legrand M, Leibundgut-Landmann S, Manichanh C, Munro CA, Netea MG, Queiroz K, Roget K, Thomas V, Thoral C, Van den Abbeele P, Walker AW, Brown AJP. 2021. The impact of the fungus-host-microbiota interplay upon Candida albicans infections: current knowledge and new perspectives. FEMS Microbiol Rev 45.
19. Leonardi I, Paramsothy S, Doron I, Semon A, Kaakoush NO, Clemente JC, Faith JJ, Borody TJ, Mitchell HM, Colombel JF, Kamm MA, Iliev ID. 2020. Fungal trans-kingdom dynamics linked to responsiveness to fecal microbiota transplantation (FMT) therapy in ulcerative colitis. Cell Host Microbe 27:823–829.e3. https://doi.org/10.1016/j.chom.2020.03.006.
20. Bougnoux M-E, Diogo D, François N, Sendid B, Veirmeire S, Colombel JF, Bouchier C, Van Kruiningen H, d'Enfert C, Poulain D. 2006. Multilocus sequence typing reveals intrafamilial transmission and microevolutions of Candida albicans isolates from the human digestive tract. J Clin Microbiol 44:1810–1820. https://doi.org/10.1128/JCM.44.5.1810-1820.2006.
21. Nash AK, Auchtung TA, Wong MC, Smith DP, Gesell JR, Ross MC, Stewart CJ, Metcalf GA, Muzny DM, Gibbs RA, Ajami NJ, Petrosino JF. 2017. The gut mycobiome of the Human Microbiome Project healthy cohort. Microbiome 5:153. https://doi.org/10.1186/s40168-017-0373-4.
22. da Silva Dantas A, Lee KK, Raziunaite I, Schaefer K, Wagener J, Yadav B, Gow NA. 2016. Cell biology of Candida albicans–host interactions. Curr Opin Microbiol Curr Opin Microbiol 34:111–118. https://doi.org/10.1016/j.mib.2016.08.006.
23. Tan CT, Xu X, Qiao Y, Wang Y. 2021. A peptidoglycan storm caused by β-lactam antibiotic's action on host microbiota drives Candida albicans infection. Nat Commun 12. https://doi.org/10.1038/s41467-021-22845-2.
24. Drummond RA, Desai JV, Ricotta EE, Swamydas M, Deming C, Conlan S, Quinones M, Matei-Rascu V, Sherif L, Lecky D, Lee CCR, Green NM, Collins N, Zelazny AM, Prevots DR, Bending D, Withers D, Belkaid Y, Segre JA, Lionakis MS. 2022. Long-term antibiotic exposure promotes mortality after systemic fungal infection by driving lymphocyte dysfunction and systemic escape of commensal bacteria. Cell Host Microbe 30:1020–1033.e6. https://doi.org/10.1016/j.chom.2022.04.013.
25. Sokol H, Leducq V, Aschard H, Pham HP, Jegou S, Landman C, Cohen D, Liguori G, Bourrier A, Nion-Larmurier I, Cosnes J, Seksik P, Langella P, Skurnik D, Richard ML, Beaugerie L. 2017. Fungal microbiota dysbiosis in IBD. Gut 66:1039–1048. https://doi.org/10.1136/gutjnl-2015-310746.
26. Sendid B, Dotan N, Nseir S, Savaux C, Vandewalle P, Standaert A, Zerimech F, Guery BP, Dukler A, Colombe JF, Poulain D. 2008. Antibodies against glucan, chitin, and Saccharomyces cerevisiae mannan as new biomarkers of Candida albicans infection that complement tests based on C. albicans mannan. Clin Vaccine Immunol 15:1868–1877. https://doi.org/10.1128/CVI.00200-08.
27. Fröhlich-Wyder MT, Arias-Roth E, Jakob E. 2019. Cheese yeasts. Yeast 36:129–141. https://doi.org/10.1002/yea.3368.
28. Leonardi I, Gao IH, Lin WY, Allen M, Li XV, Fiers WD, De Celie MB, Putzel GG, Yantiss RK, Johncilla M, Colak D, Iliev ID. 2022. Mucosal fungi promote gut barrier function and social behavior via Type 17 immunity. Cell 185:831–846.e14. https://doi.org/10.1016/j.cell.2022.01.017.
29. Doron I, Leonardi I, Li XV, Fiers WD, Semon A, Bialt-DeCelie M, Migaud M, Gao IH, Lin WY, Kusakabe T, Puel A, Iliev ID. 2021. Human gut mycobiota tune immunity via CARD9-dependent induction of anti-fungal IgG antibodies. Cell 184:1017–1031.e14. https://doi.org/10.1016/j.cell.2021.01.016.
30. Jabra-Rizk MA, Kong EF, Tsui C, Nguyen MH, Clancy CJ, Fidel PL, Noverr M. 2016. Candida albicans pathogenesis: fitting within the host-microbe damage response framework. Infect Immun 84:2724–2739. https://doi.org/10.1128/IAI.00469-16.
31. Nucci M, Anaissie E. 2001. Revisiting the source of candidemia: skin or gut? Clin Infect Dis 33:1959–1967. https://doi.org/10.1086/323759.
32. Qin J, Li R, Raes J, Arumugam M, Burgdorf KS, Manichanh C, Nielsen T, Pons N, Levenez F, Yamada T, Mende DR, Li J, Xu J, Li S, Li D, Cao J, Wang B, Liang H, Zheng H, Xie Y, Tap J, Lepage P, Bertalan M, Batto JM, Hansen T, Le Paslier D, Linneberg A, Nielsen HB, Pelletier E, Renault P, Sicheritz-Ponten T, Turner K, Zhu H, Yu C, Li S, Jian M, Zhou Y, Li Y, Zhang X, Li S, Qin N, Yang H, Wang J, Brunak S, Doré J, Guarner F, Kristiansen K, Pedersen O, Parkhill J, Weissenbach J, MetaHIT Consortium, et al. 2010. A human gut microbial gene catalogue established by metagenomic sequencing. Nature 464:59–65. https://doi.org/10.1038/nature08821.
33. Zuo T, Wong SH, Cheung CP, Lam K, Lui R, Cheung K, Zhang F, Tang W, Ching JYL, Wu JCY, Chan PKS, Sung JJY, Yu J, Chan FKL, Ng SC. 2018. Gut fungal dysbiosis correlates with reduced efficacy of fecal microbiota transplantation in Clostridium difficile infection. Nat Commun 9. https://doi.org/10.1038/s41467-018-06103-6.
34. Yu Z, Morrison M. 2004. Improved extraction of PCR-quality community DNA from digesta and fecal samples. Biotechniques 36:808–812. https://doi.org/10.2144/04365ST04.
35. Cui L, Morris A, Ghedin E. 2013. The human mycobiome in health and disease. Genome Med 5:63. https://doi.org/10.1186/gm467.
36. Gardes M, Bruns TD. 1993. ITS primers with enhanced specificity for basidiomycetes - application to the identification of mycorrhizae and rusts. Mol Ecol 2:113–118. https://doi.org/10.1111/j.1365-294x.1993.tb00005.x.
37. 16S Metagenomic Sequencing Library Preparation. https://emea.support.illumina.com/downloads/16s_metagenomic_sequencing_library_preparation.html#. Retrieved 25 August 2021.
38. Volant S, Lechat P, Woringer P, Motreff L, Campagne P, Malabat C, Kennedy S, Ghozlane A. 2020. SHAMAN: a user-friendly website for metataxonomic analysis from raw reads to statistical analysis. BMC Bioinformatics 21. https://doi.org/10.1186/s12859-020-03666-4.
39. Liu CM, Kachur S, Dwan MG, Abraham AG, Aziz M, Hsueh PR, Huang YT, Busch JD, Lamit LJ, Gehring CA, Keim P, Price LB. 2012. FungiQuant: a broad-coverage fungal quantitative real-time PCR assay. BMC Microbiol 12. https://doi.org/10.1186/1471-2180-12-56.
40. Guiver M, Levi K, Oppenheim BA. 2001. Rapid identification of candida species by TaqMan PCR. J Clin Pathol 54:362–366. https://doi.org/10.1136/jcp.54.5.362.
41. R Core Team. 2020. R: a language and environment for statistical computing. R Foundation for Statistical Computing, Vienna, Austria.
42. Oksanen AJ, Blanchet FG, Friendly M, Kindt R, Legendre P, Mcglinn D, Minchin PR, Hara RBO, Simpson GL, Solymos P, Stevens MHH, Szoecs E. 2019. Package 'vegan.' R Packag Libr. https://CRAN.R-project.org/package=vegan.
43. Wickham H, Chang W, Henry L, Pedersen TL, Takahashi K, Wilke C, Woo K. 2016. ggplot2: Elegant Graphics for Data Analysis. Springer-Verlag New York. https://ggplot2.tidyverse.org.
44. Ekstrøm CT. 2020. Miscellaneous esoteric statistical scripts [R package MESS version 0.5.7]. https://CRAN.R-project.org/package=MESS.